STUDY OF THE OPTICAL PROPERTIES AND DC ELECTRICAL CARRIER TRANSPORT ON THIN FILMS OF PLASMA POLYMERIZED METHYL ACRYLATE

Sumon Deb Nath

Roll No.: 1014143008 P

Session: October/2014

Department of Physics

Bangladesh University of Engineering and Technology (BUET)

Dhaka-1000, Bangladesh

December, 2017

STUDY OF THE OPTICAL PROPERTIES AND DC ELECTRICAL CARRIER TRANSPORT ON THIN FILMS OF PLASMA POLYMERIZED METHYL ACRYLATE

A dissertation submitted to the Department of Physics, Bangladesh University of Engineering and Technology in partial fulfillment of the requirements for the degree of MASTER OF PHILOSOPHY (M. Phil.) in Physics.

by

Sumon Deb Nath

Roll No.: 1014143008 P

Session: October/2014

Department of Physics

Bangladesh University of Engineering and Technology (BUET)

Dhaka-1000, Bangladesh

December, 2017

CANDIDATE'S DECLARATION

It is hereby declared that this thesis or any part of it has not been submitted elsewhere for the award of any degree of diploma.

Sumon

_____

(Sumon Deb Nath)
Roll No: 1014143008P
Session: October/2014

BANGLADESH UNIVERSITY OF ENGINEERING AND TECHNOLOGY, DHAKA
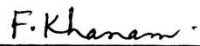
DEPARTMENT OF PHYSICS

CERTIFICATION OF THESIS

The thesis titled **"STUDY OF THE OPTICAL PROPERTIES AND DCELECTRICAL CARRIER TRANSPORT ON THIN FILMS OF PLASMA POLYMERIZED METHYL ACRYLATE"** submitted by **Mr. Sumon Deb Nath**, Roll No.:1014143008P, Session: October/2014 has been accepted as satisfactory in partial fulfillment of the requirement for the degree of **Master of Philosophy (M.Phil.)** in **Physics** on 17 December, 2017.

BOARD OF EXAMINERS

1. _____

   Dr. Md Abu Hashan Bhuiyan (Supervisor)   Chairman
   Professor
   Department of Physics, BUET, Dhaka.

2. _____

   Prof. Fahima Khanam   Member (Ex-Officio)
   Head
   Department of Physics, BUET, Dhaka.

3. _____

   Dr. Jiban Podder   Member
   Professor
   Department of Physics, BUET, Dhaka.

4. _____

   Dr. Mohammad Jellur Rahman   Member
   Assistant Professor
   Department of Physics, BUET, Dhaka.

5. _____

   Dr. Mohammad Mizanur Rahman   Member (External)
   Associate Professor, Department of Physics,
   University of Dhaka, Dhaka-1000.

DEDICATED

TO

MY BELOVED FATHER

<u>CONTENTS</u>

LIST OF FIGURES

LIST OF TABLES

Glossary

α	Absorption Co-efficient	IR	Infrared
d	Thickness	PPMA	Plasma Polymerized Methyl Acrylate
$E_{g(d)}$	Direct Transition Energy Gap	PECVD	Plasma Enhanced Chemical Vapor
$E_{g(i)}$	Indirect Transition Energy Gap	PVD	Plasma Vapor Deposition
F_L	Fermi Level	DSC	Differential Scanning Calorimetry
I	Intensity of radiation	SCLC	Space Charge Limited Conduction
J	Current Density		
k	Boltzmann Constant		
K	Extinction Co-efficient		
T_g	Glass Transition Temperature		
Rf	Radio Frequency		
V	Voltage		
ΔE	Activation Energy		
λ	Wavelength		
μ	Mobility of Charge Carrier		
θ	Trapping Factor		
V	Voltage		
ABS	Absorbance		
AC	Alternating Current		
Cr-Al	Chromel-Alumel		
T_m	Melting Point		
CRT	Cathode-Ray Tube		
Cc	Capactitively Coupled		
DC	Direct Current		
DTA	Differential Thermal Analysis		

ACKNOWLEDGEMENTS

Abstract

Plasma polymerization is a distinctive technique for direct polymeric thin films deposition from different organic monomers. The organic compound methyl acrylate (MA) has been chosen as monomer to deposit plasma polymerized methyl acrylate (PPMA) thin films of different thicknesses. The polymerization is carried out by using a capacitively coupled glow discharge reactor by optimizing the plasma parameters. The thermal, morphological, structural and optical properties of PPMA thin films are ascertained by using different characterization techniques. The DC electrical properties of PPMA thin films are also investigated. DTA/ TGA analysis suggests that PPMA is thermally stable up to about 534 K in air and 543 K in N_2 environments. The weight loss in N_2 environment is lower than air environment. FESEM micrographs show that structures of the films are observed to have clusters/agglomeration structure separated by grain boundaries. The EDX analysis indicates the presence of prominent percentage of carbon and oxygen in PPMA thin films. From the ATR-FTIR analyses, it is found that the PPMA thin films deposited by plasma polymerization technique have partially changed chemical structure owing to reorganization of MA structure due to plasma polymerization. From the UV-Vis analyses, it is observed that the values of direct energy band gap, ($E_{g(d)}$) varies from 3.77 to 3.83 eV and that of the indirect energy band gap, ($E_{g(i)}$) varies from 3.40 to 3.48 eV for the PPMA thin films. The increase of $E_{g(i)}$ values with the increasing thicknesses is due to the increase in fragmentation/cross-linking in the bulk of the material due to the impact of plasma on the surface of the thin films with plasma duration. The values of the Urbach energy, E_u varies from 0.29 to 0.35 eV. So the E_u increases with the variation of thickness due the increase of disorder in the PPMA thin films. The increase of extinction co-efficient, k with the increase of $h\nu$ indicates the probability of electron transfer across the mobility gap rises with $h\nu$. The J-V characteristics revealed that the dependence of J on V is Ohmic is the lower voltage (0.1~10 V) region and in higher voltage (10~75 V) region it is non-Ohmic. J–d and V_{tr}-d curves confirmed that the conduction mechanism is space charge limited conduction (SCLC) type. The activation energy for Ohmic region is observed higher than non-Ohmic region in the lower temperature region whereas the activation energy for Ohmic region is observed lower than non-Ohmic region in the higher temperature region. These findings may facilitate using PPMA in manufacturing optical and electronic devices.

CHAPTER 1

INTRODUCTION

1.1 Introduction

Recently, solid state and material scientists have been given extensive attention to the innovation and characterization of thin films of polymeric materials. Since the last four decades, various synthesis techniques, such as, radiation induced polymerization [1], conventional evaporation method [2], sputtering [3], solution cast techniques [4], etc., have been used for the generating of polymer thin films. Plasma polymerization has been recognized as an attractive modern technique, widely used for direct polymer thin films deposition of varying thickness on various substrates from almost any organic vapor. This technique usually produces polymers of cross-linked, branched and highly insulating materials. It is a very fast technique for direct dry deposition of homogeneous and pinhole free [5-6] thin films. The organic plasma polymer thin films have versatile advantages which include excellent coating adhesion onto a large variety of substrates, thermal, mechanical and chemical stability. The properties of the thin films can be changed by varying the deposition parameters [7] like deposition power, pressure, monomer flow rate, and deposition time. Plasma polymerization for the deposition of thin films has achieved significant importance in several fields of applications such as microelectronics, automobile industries and biomaterials. These films have been extensively investigated in the last few decades for a variety of important applications as follows:

(i)   **Optical Devices:** as optical fibre, optical wave guide, laser and optical window, contact lens , anti-reflection coating, anti-dimming coating, improvement of transparency, etc.

(ii)   **Electrical Devices:** as different layers such as insulating, dielectric and functional insulator etc.

(iii)   **Electronic Devices:** as transistors, diodes, sensors like bio, chemical, and humidity etc., switching elements, photovoltaic devices, capacitors etc. These films are also used as very large scale integration (VLSI) resists and in non-crystalline semiconductor and non-crystalline fine ceramic etching.

(iv)   **Chemical Processing Systems:** as protective coating, anti-creasing and scratching, and adhesion improvement abrasion resistant coating.

(v)   **Biomedical Appliances:** as artificial kidney, blood vessel, blood bag, anti-clotting, immobilized enzymes organelles and cells, sustained release of drugs and pesticides, sterilization and pasteurization,

(vi) **Textile:** Anti-flammability, anti-electrostatic treatment, dying affinity, hydrophilic improvement, and water repellence, shrink-proofing.

(vii) **Filters and Membranes:** as reverse osmosis membrane, ion exchange membranes for reaction microprobes membranes for blood sieving, semi-permeable membranes to prepare porosity of any configuration and high cross-linking and for separation of gas mixture.

As a consequence, a large number of studies have been performed on the thin polymeric films, yet these materials need further study to find high quality advanced materials for electrical, electronic, and optical based devices in industrial and scientific applications. Owing to its simplicity, plasma polymerization or plasma-enhanced chemical vapor deposition (PECVD) technique has been selected for the synthesis of the coatings and thin films. For a specific polymeric material one of the three different conduction mechanisms will be dominant. The probable conduction mechanism named as Schottky [8], Poole-Frenkel (PF) [9], and space charge limited conduction (SCLC) [10].

1.2 Brief Reviews of Earlier Research Works on Thin Films

Plasma polymerized organic thin films have molecular structures but different from the conventional polymers. The most significant is that these films have cross linked structure so that they are chemically and physically stable and used for the crucial area in which thermal, mechanical, and electrical strengths are necessary .Now a days, a large number of researchers all over the world have been concentrated to plasma polymerized organic/organometallic thin films for innovating new materials with exciting properties which are suitable for a wide range of modern applications in microelectronic devices, organic diodes etc. A brief review of their research work is given below:

Matin and Bhuiyan [8] investigated on electrical transport mechanism in plasma polymerized 2, 6, diethylaniline (PPDEA) thin films and concluded that the conduction mechanism (Fig. 1.1 (a-b)) in the PPDEA thin films is of Schottky type. They found the surface of the PPDEA thin films is uniform and pinhole free from the scanning electron micrographs and analyzed the electron dispersive X-ray (EDX) spectrum which indicated the presence of carbon, nitrogen and oxygen in the PPDEA thin films.
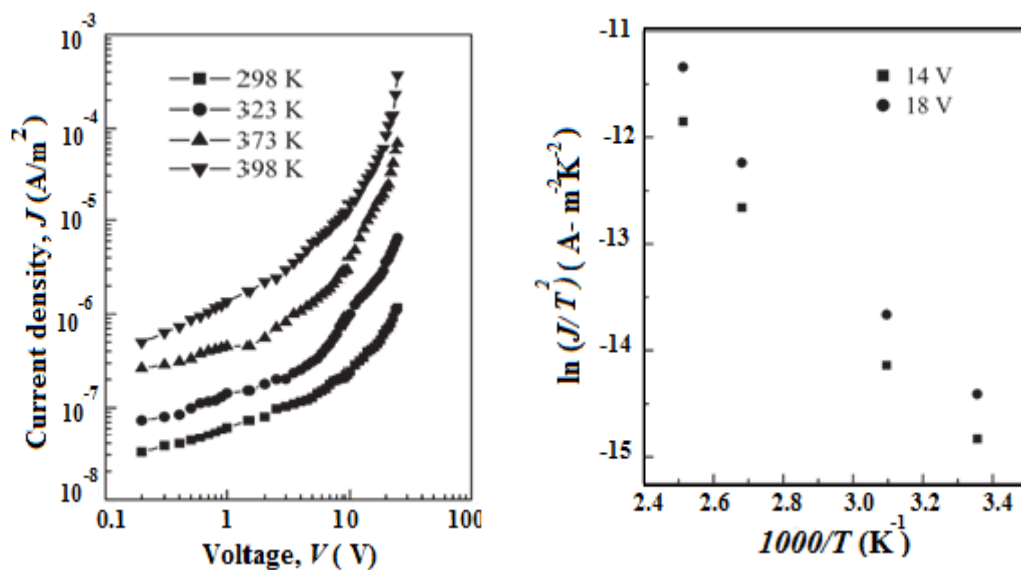
Fig. 1.1 (a) *J–V* plots for PPDEA thin films at different temperatures (d=250 nm), (b) Temperature dependence of the Schottky emission dominated leakage current of PPDEA thin film at different bias voltages (d=400 nm) [8].

Shahjalal *et al.* [9] studied on the conduction mechanism in plasma polymerized m-xylene (PPmX) thin films and concluded that the conduction mechanism in the PPmX thin films is of PF type. They investigated the FTIR spectra at room temperature which indicates that the structure of PPmX thin films deposited by glow discharge polymerization which is different from that of monomer m- xylene because of the possible presence of conjugation and cross-linking structure.
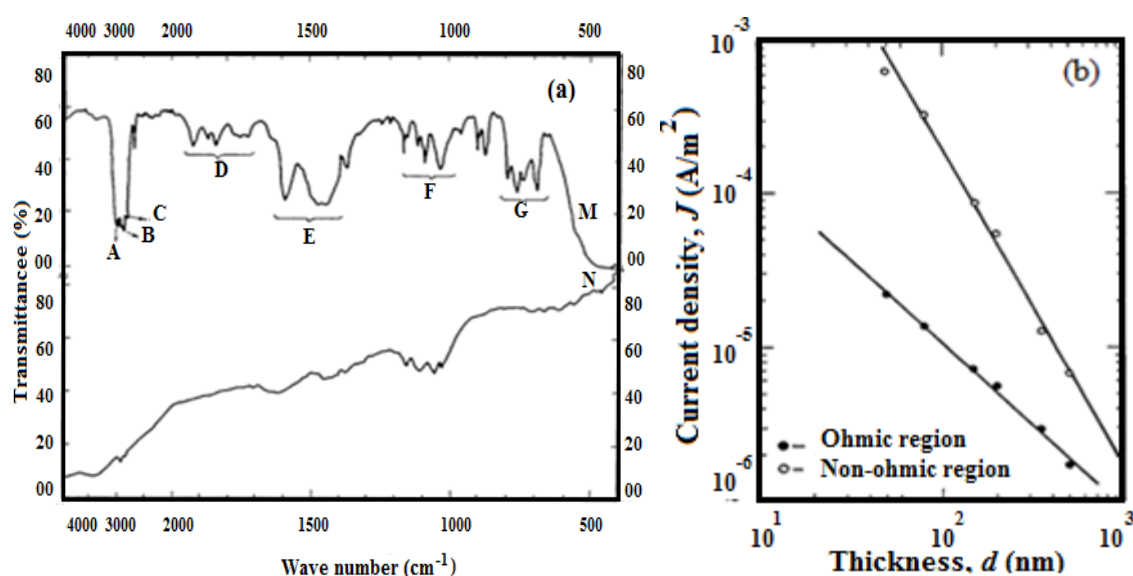
Fig. 1.2 (a) IR spectra of m-xylene monomer (spectrum M) and PPmX (spectrum N), (b) Current density vs thickness graphs [9].

Zaman and Bhuiyan [10] studied on direct current electrical conduction mechanism in plasma polymerized thin films of tetraethylorthosilicate (PPTEOS) and revealed by the elemental analysis that PPTEOS is hydrogen deficient and also concluded that the mechanism of conduction (Fig. 1.3 (a-b)) in PPTEOS thin films is space charge limited conduction. From FTIR spectra (Fig. 1.3 c), they found that the PPTEOS thin film deposited by the plasma polymerization technique contains O–H, C=C and C=O bonds that are not present in TEOS. They declared that this result may help using this material in electronic/microelectronic devices.
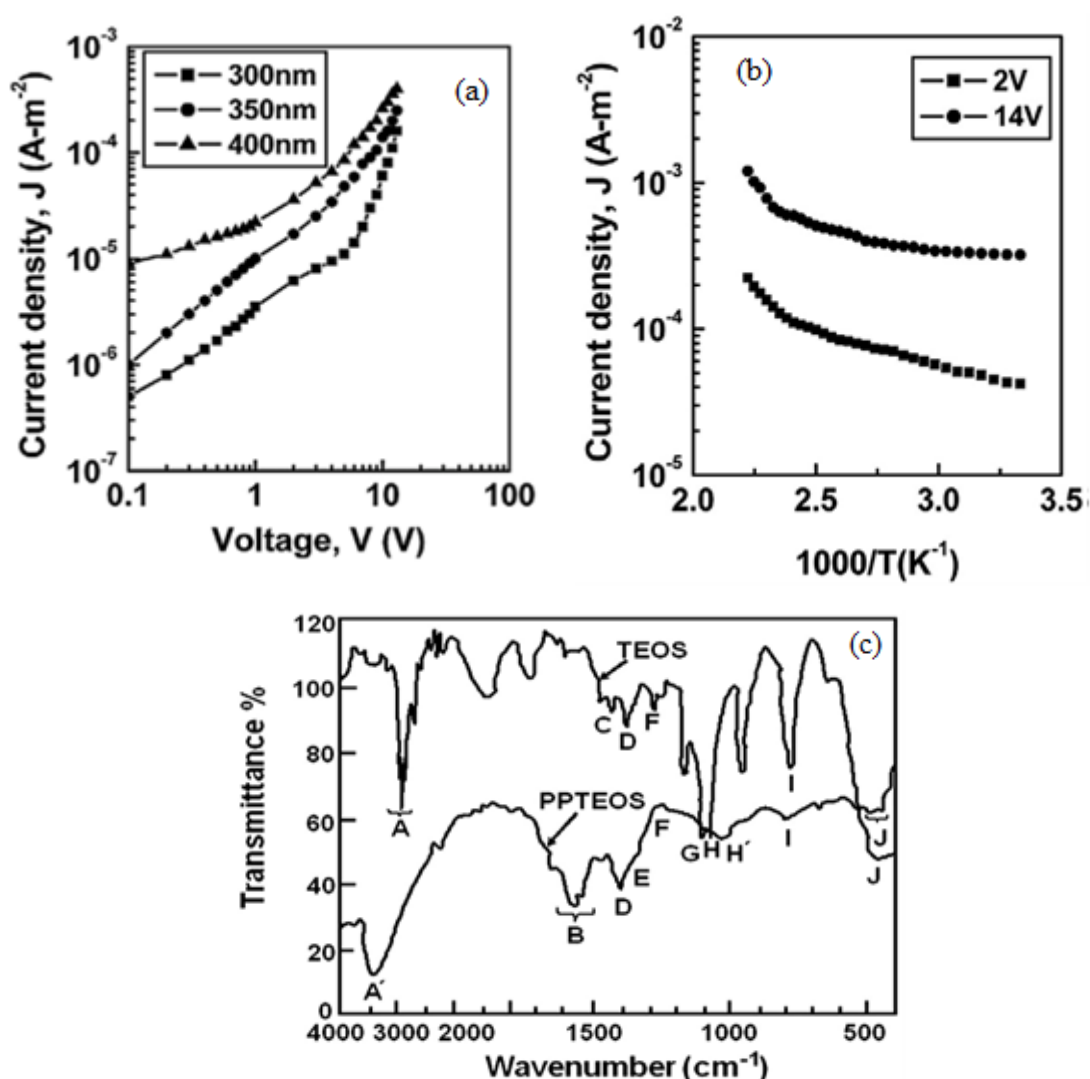
Fig. 1.3 (a) Plots of current density against applied voltage for PPTEOS thin films of different thicknesses recorded at room temperature, (b) Plots of current density against inverse absolute temperature for a PPTEOS sample in Ohmic and non-Ohmic regions (d=350 nm), (c) FTIR spectra of TEOS and PPTEOS [10].

Hu *et al.* [11] studied that preparation, characterization and electronic and optical properties of plasma- polymerized nitriles and revealed by the FTIR that an aromatic ring structure (Fig. 1.5) can be formed in the plasma PPCPD thin films.
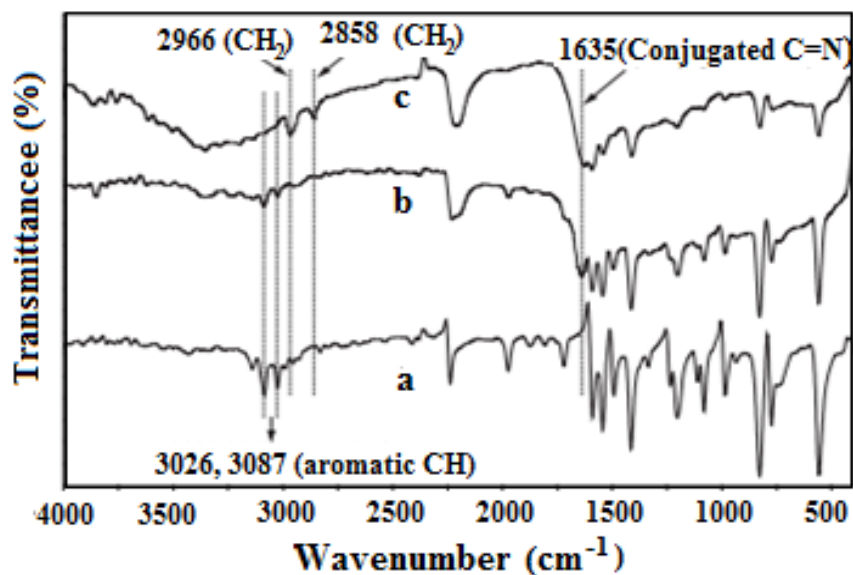
Fig. 1.4 FTIR spectra of the (a) 4-cyanopyridine monomer, (b) PPCPD10, and (c) PPCPD60 [11].

Bae *et al.* [12] studied the comparison of plasma polymerized organic thin films on their electrical and optical properties and from FTIR spectra (Fig. 1.5 a) and UV-visible transmittance spectra (Fig. 1.5 b), they found that the as-grown transparent organic films have high degree cross-linking density with high transmittance. They suggested that their polymer like thin films can be used in both the insulating materials for microelectronics devices.
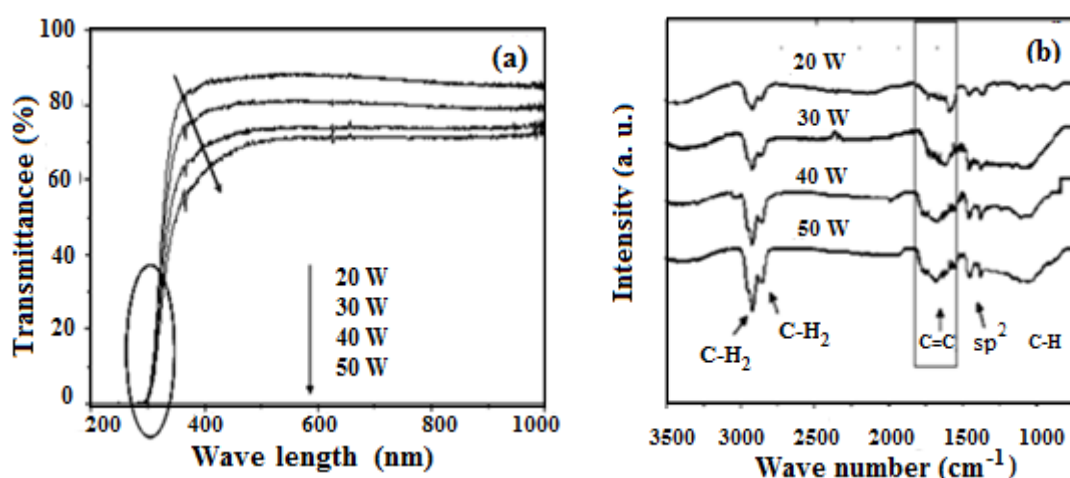
Fig. 1.5 (a) UV-visible transmittance spectra, (b) FTIR Spectra [12].

Bazaka and Jacob [13] studied on the RF plasma polymerization of Terpinen-4-ol monomer with the objective to synthesize a smooth, defect-free and homogenous film from a non-synthetic source. UV–Vis (Fig. 1.6 (a-b)) demonstrated the plasma conditions had effect on morphology and properties of the resultant film. The energy gap estimated to be 2.67 eV confirmed the possibility of using the polymer film in semiconducting applications.
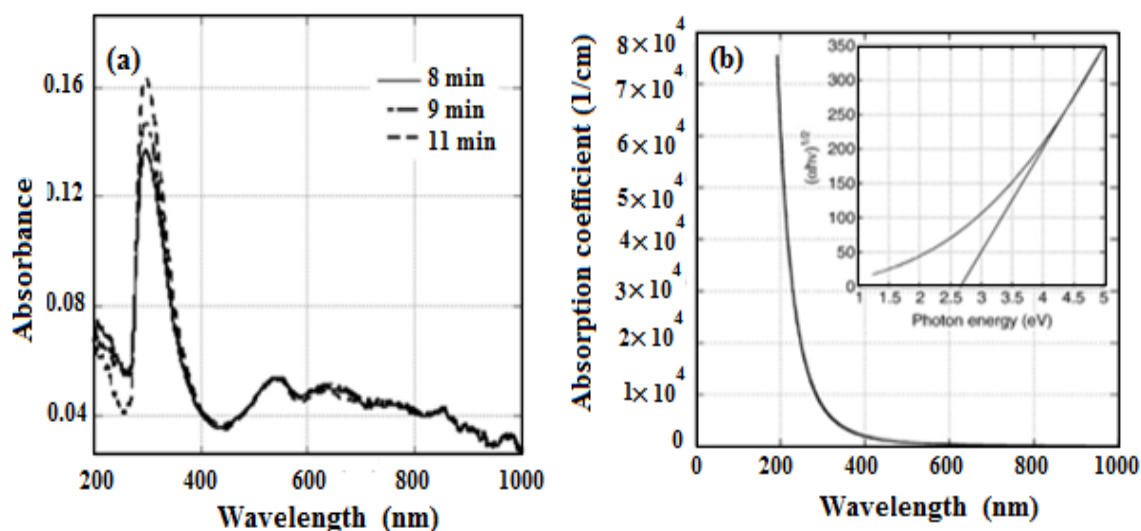
Fig. 1.6 (a) UV–Vis absorption spectrum, (b) Absorption coefficient as a function of wavelength of film deposited at power 25 W [13].

Lim *et al.* [14] studied the plasma polymerized methyl methacrylate (PPMMA), which was formed in a cross-linked 3D network, gate dielectric for organic thin-film transistors (OTFT). Plasma polymerization method has the benefits of polymer gate dielectrics including potentially high capacitive coupling, and shadow mask patterning and in situ dry processing with large area flexible substrates.
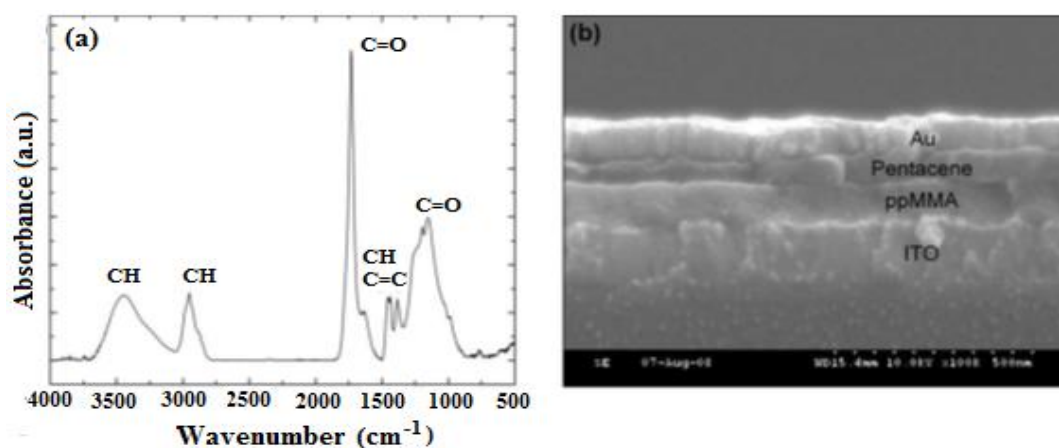
Fig. 1.7 (a) FTIR spectrum of PPMMA, (b) SEM image of the OTFT device [14].

Jumaili *et al.* [15] studied about the retention of antibacterial activity in germanium plasma polymer thin films and found that the topography of all surfaces was uniform and smooth. Independent of input power, films were optically transparent within the visible wavelength range, with the main absorption at ~290 nm and optical band gap of ~3.6 eV. They suggested that geranium extract-derived polymers may potentially be used as antibacterial coatings for contact lenses.
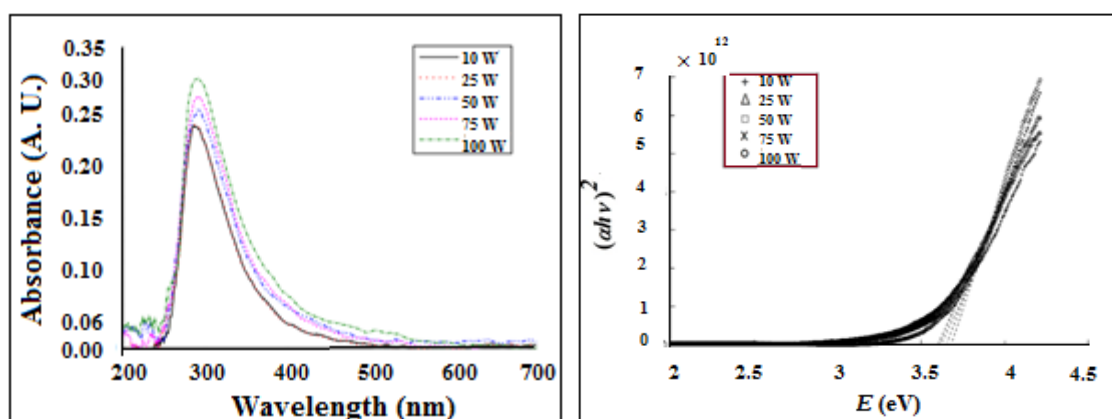
Fig. 1.8 (a) UV-Vis absorption spectrum, (b) The optical energy gap of germanium oil-derived films fabricated at various RF powers [15].

Majumder and Bhuiyan [16] studied on DC conduction mechanism in plasma polymerized vinylene carbonate thin films prepared by glow discharge technique. Due to FTIR spectra, PPVC thin films grown by plasma polymerization technique have slightly different chemical structure from that of the VC. They concluded that the conduction mechanism is Schottky type.
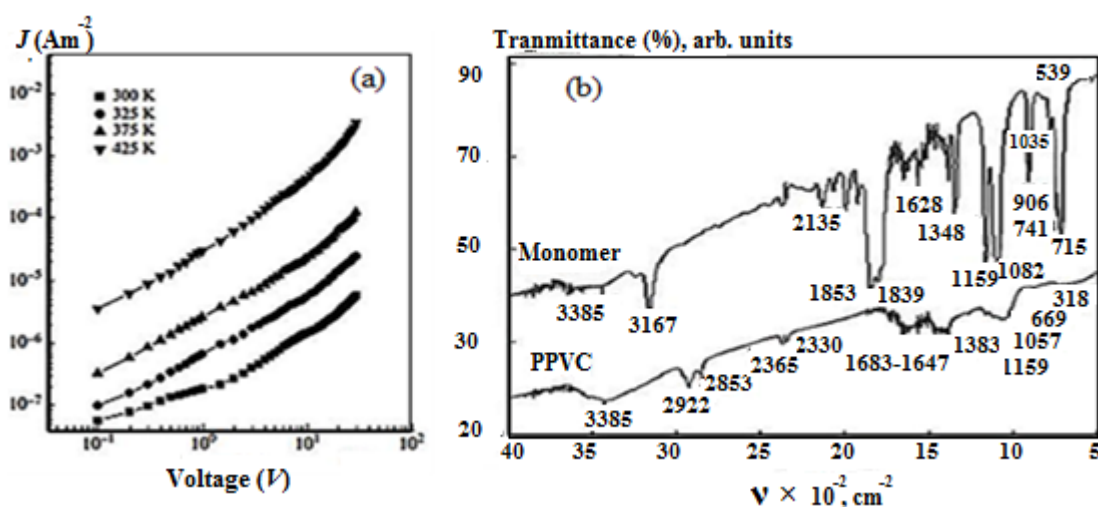
Fig. 1.9 (a) Variation of current density with applied voltage at different temperatures ($d = 130$ nm), (b) The FTIR spectra of monomer VC and PPVC [16].

Afroze and Bhuiyan [17] studied the electrical conduction mechanism in plasma polymerized 2-(diethylamino) ethyl methacrylate thin films and found that the conduction mechanism is SCLC.
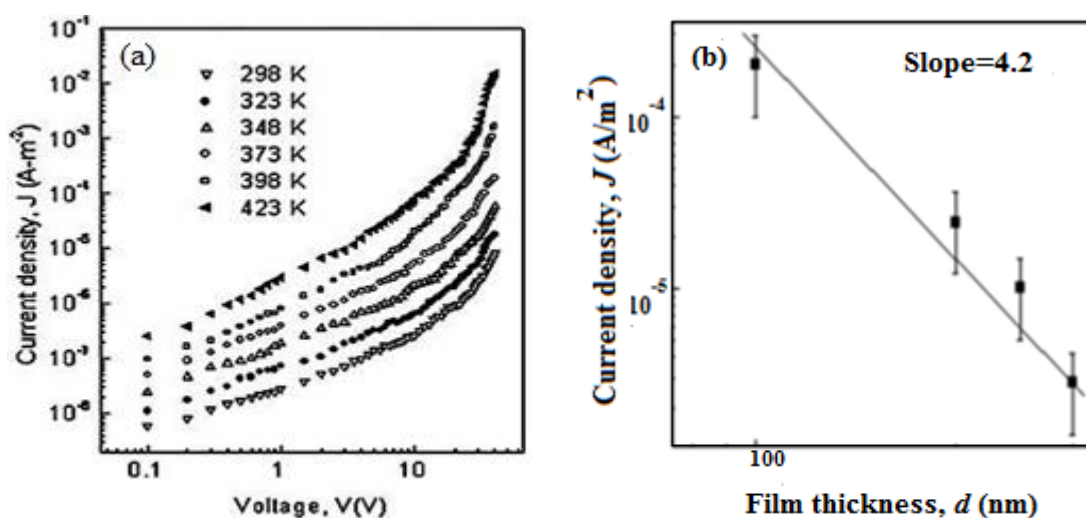
Fig. 1.10 (a) *J-V* curves at different temperatures, (b) *J-d* curves for PPDEAEMA thin films (d=300 nm) [17].

Rahman and Bhuiyan [18] studied the structural and optical properties of plasma polymerized o-methoxyaniline (PPOMA) thin films and found that the films are smooth, flawless and pinhole free morphology with high percentage of oxygen in the polymer due to incorporation of oxygen from the atmosphere and the direct and indirect band gap are around 2.0 eV and around 3.0 eV, respectively. The chemical nature of the films is somewhat different from the monomer OMA after the formation of thin films (solid phase) by plasma polymerization.
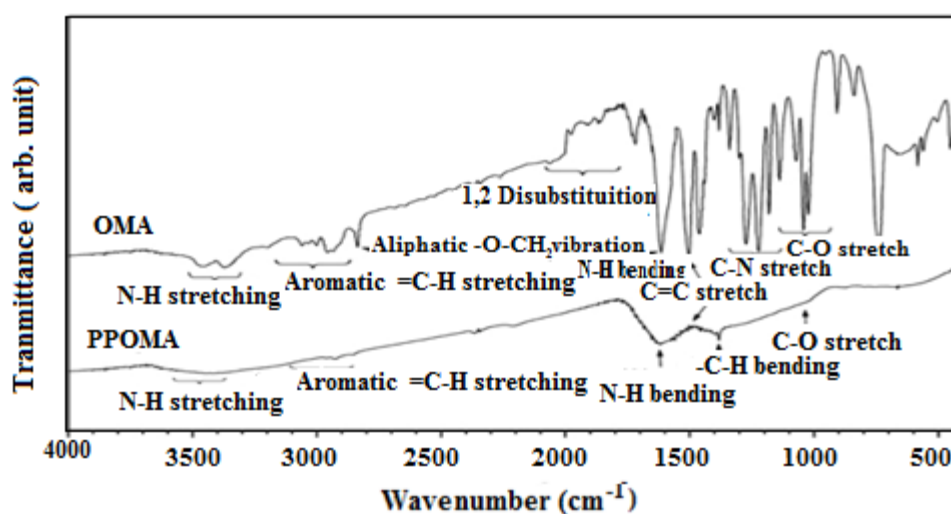
Fig. 1.11 FTIR spectra of PPOMA [18].

Lim *et al.* [19] studied the plasma polymerized thin films of styrene and vinyl acetate that can be applied to functional organic thin film transistor devices as the gate dielectric. FTIR spectra (Fig. 1.12) of polystyrene and polyvinyl acetate show significant amounts of fragmentation and rearrangement during the plasma polymerization process and observed aromatic ring structure.
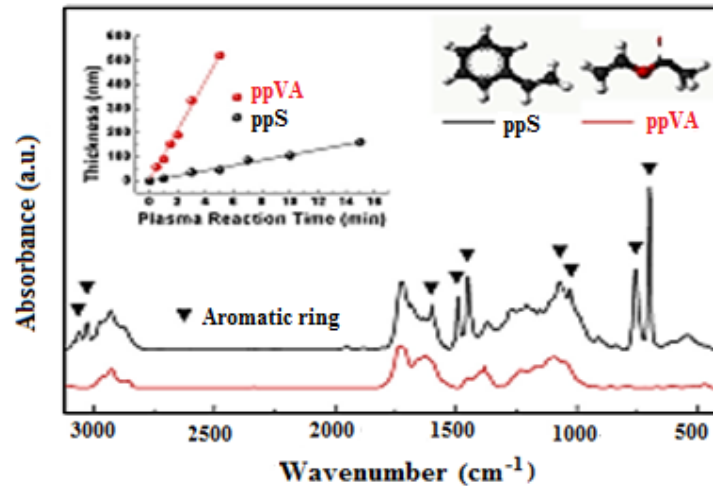
Fig. 1.12 FTIR spectra of the plasma polymer layers [19].

Ahmad *et al.* [20] investigated on the electrical conduction in plasma polymerized γ-terpinene (PPGT) thin films which fabricated by the MIM structure and noticed that the conduction mechanism responsible for the charge transport through the material was recognized as Ohmic in the low voltage region, while Schottky conduction was found to be the dominating mechanism for charge transport through the films at the higher voltage region.
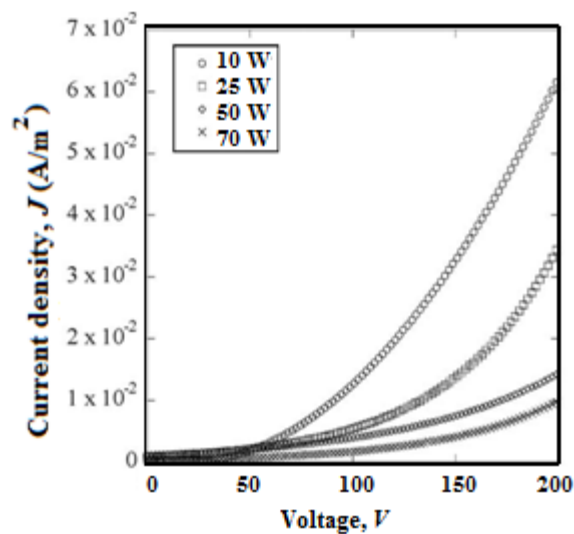
Fig. 1.13 *J-V* relationships for PPGT films [20].

Bazaka *et al.* [21] examined plant-derived cis-β-ocimene as a precursor for biocompatible, transparent, thermally-stable dielectric and encapsulating layers for organic electronics and presented low-temperature, one-step dry synthesis of optically transparent thermally- stable, biocompatible cis-β-ocimene-based thin films for applications as interlayer dielectric and encapsulating layer for flexible electronic devices, e.g. OLEDs. Morphological analysis of thin films showed uniform, very smooth and defect-free moderately hydrophilic surfaces.
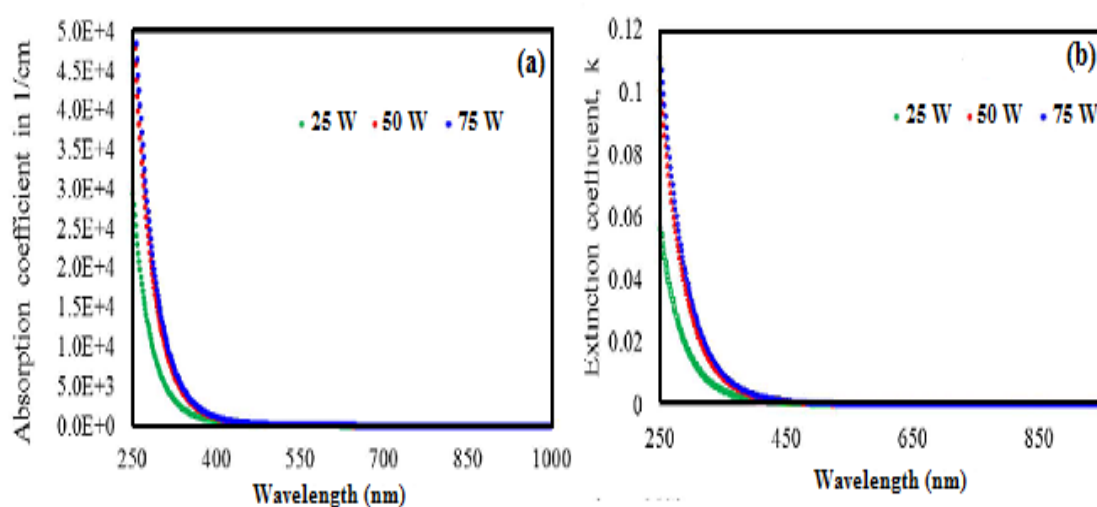
Fig. 1.14 Absorption co-efficient as a function of wavelength with plasma power 25W, 50W, 75W [21].

Li *et. al.*, [22] studied the fabrication and structural characterization of plasma polymerized polypyrole thin film and found the films are smooth and uniform dense.
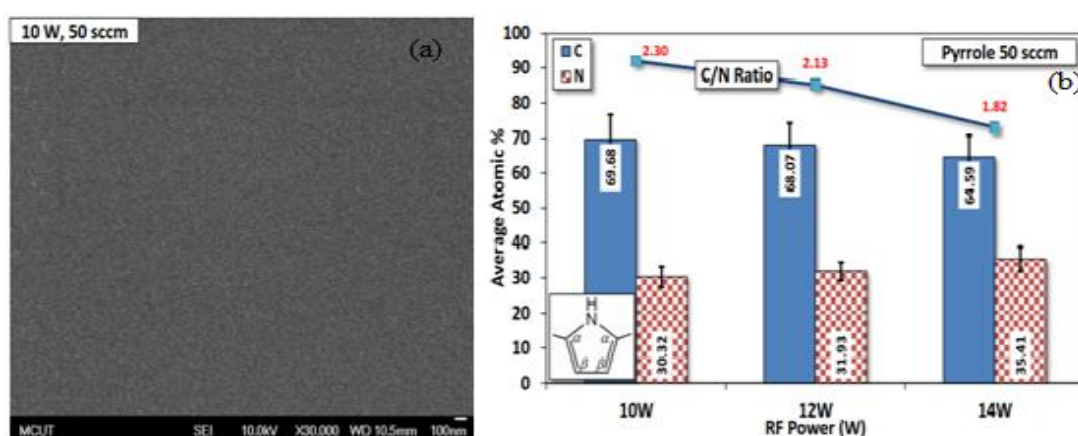
Fig. 1.15 (a) FE-SEM micrograph, (b) EDS analysis of polypyrrole films [22].

Matin and Bhuiyan [23] studied the infrared and ultraviolet spectroscopic analyses of plasma polymerized 2,6 diethylaniline thin films and found that direct and indirect band gap increases with increasing thicknesses and the Urbach energy decreases with increasing thicknesses. The FTIR spectra show that the plasma polymerization technique affects the chemical structure of DEA during the PPDEA thin film formation.
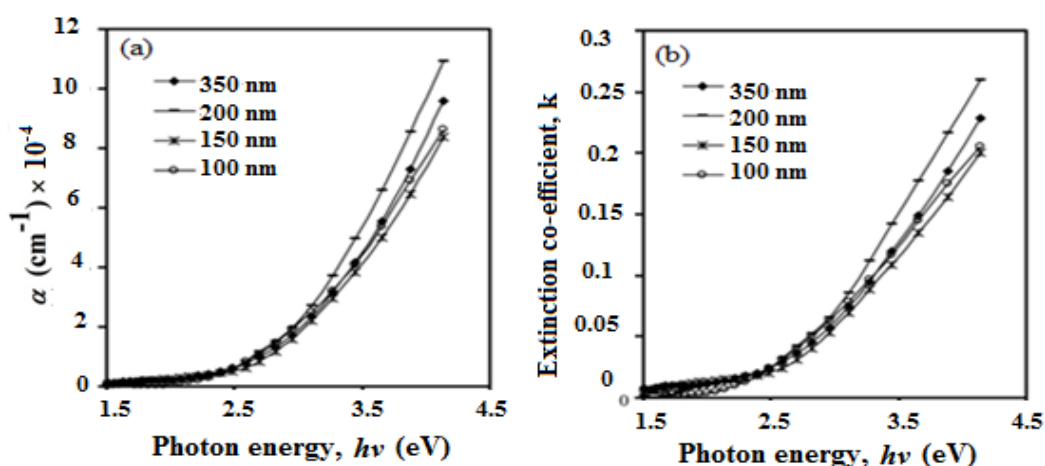
Fig. 1.16 (a) Absorption co-efficient vs photon energy, (b) Extinction co-efficient vs photon energy for the PPDEA thin films [23].

Bazaka *et al.* [24] demonstrated effects of iodine doping on optoelectronic and chemical properties of polyterpenol thin films which were manufactured using RF plasma polymerization and did FTIR studies which revealed that iodine was being incorporated into the backbone of the polymer, and that such incorporation resulted in the notable reduction in the methyl and methylene functional groups and appearance of C=C bond. All films were smooth, defect-free, and uniform.
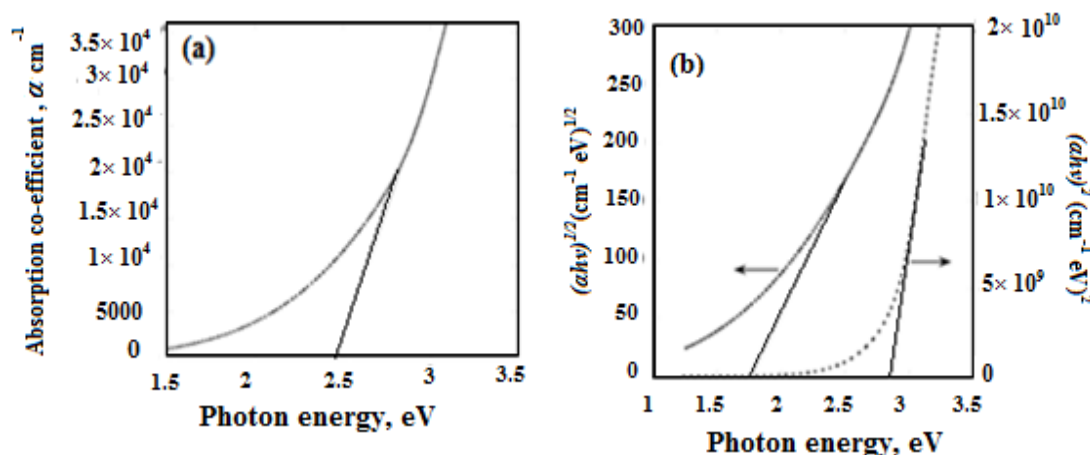
Fig. 1.17 (a) Band gap, (b) direct and indirect allowed transition energies of iodine doped polyterpenol thin films heat treated at 100^0 C for 5 h [24].

Kabir *et al.* [25] investigated the most probable conduction mechanism in the plasma polymerized 2-furaldehyde thin film is of Richardson-Schottky type which was established by the temperature dependence studies of the current density (Fig. 1.18 (a-d)). They also studied SEM that shows the surfaces of the PPFDH films are uniform and pinhole free and EDAX result simply the existence of C, O, Na and Si. However, Na and Si were originated from the glass substrates.
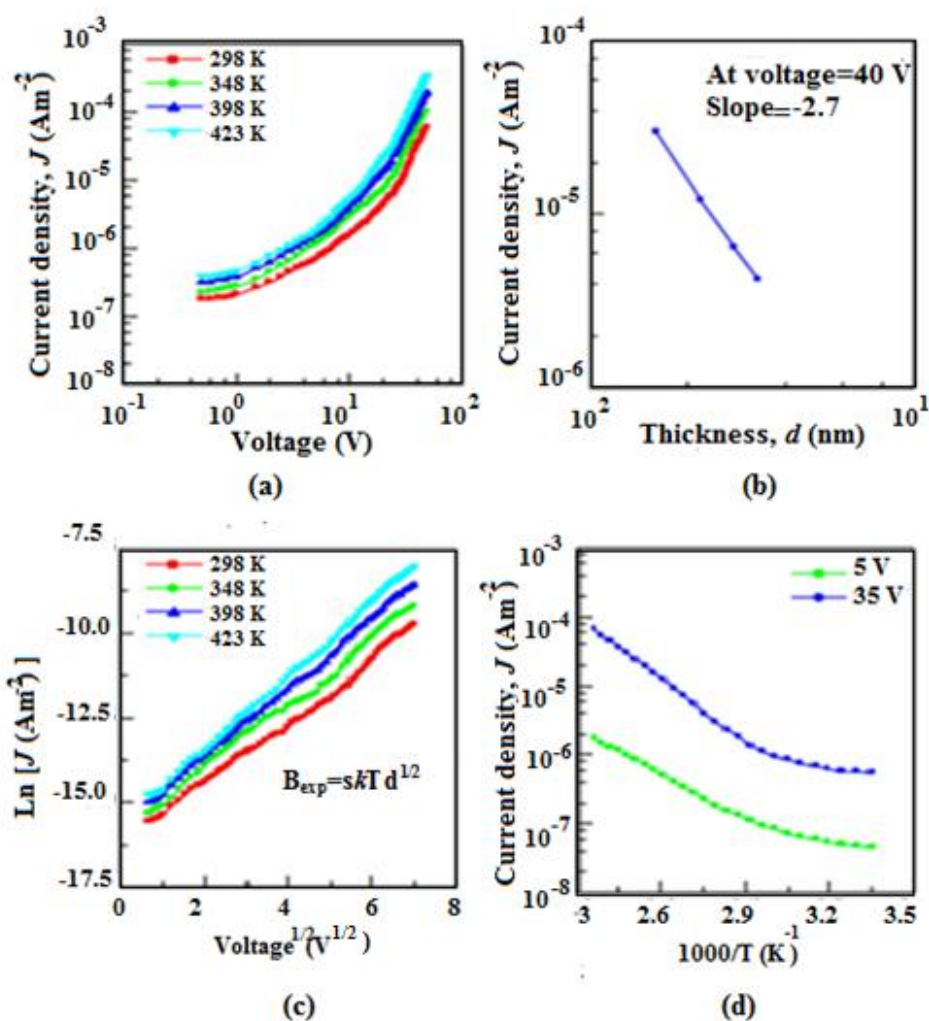
Fig. 1.18 (a) *J-V* curve at different temperatures, (b) Variation of *J* with *d*, (c) ln *J* - $V^{1/2}$ curve, (d) Variation of *J* with *1000/T* for PPFDH thin films [25].

From the review of literature, it is seen that thin films prepared from methyl acrylate derivatives have applications in various electronic and optoelectronic devices. The electrical and optical properties of thin films of methyl acrylate, so far, have not been found in the literature. So in this research work, it is intended to prepare plasma polymerized methyl acrylate thin films and to study the structural, electrical and optical properties.

1.3 The Aim of the Thesis Work

Plasma polymerization is one of the promising modern techniques that can be used to synthesize thin polymer films from a variety of organic compounds. Among the various plasma polymerization processes the glow discharge is the most important and widely used technique. The aim of this thesis work is to prepare thin films of plasma polymerized methyl acrylate (PPMA) by a well-established glow discharge polymerization technique and characterizing those using different physical techniques. The findings of this research would be analyzed with a view to find their suitability in technologically important appliances. In this study, PPMA thin films will be prepared and structural, optical and electrical properties of the PPMA thin films will be investigated. Finally the results will be correlated and possible applications sectors will be suggested. The following studies will be performed:

(a) Structural analyses:

The chemical structure of the methyl acrylate (MA) monomer and PPMA thin films will be investigated by FTIR spectroscopy. A comparative study between the spectra will be done to ascertain the chemical changes occurred in different PPMA thin films.

(b) Thermal analyses:

The TGA, DTA and DTG will be used to characterize the thermal stability and decomposition of the PPMA thin films in air and in N_2.

(c) Morphological and element analyses:

Field emission scanning electron microscopy (FESEM) and Energy Dispersive X-ray Spectroscopy (EDX) analyses will be done to investigate the surface morphology and composition analysis respectively of PPMA thin films.

(d) Optical properties:

The UV- Visible absorption spectroscopic analyses will be done to determine the optical parameters like optical band gaps (direct, indirect transition, Urbach energy and extinction co-efficient) in the PPMA thin films.

(e) Electrical properties:

The DC electrical investigations will facilitate to understand the electrical conduction mechanism such as SCLC, Schottky or PF in the PPMA thin films. In *J-V* measurements, the variation of current density with temperature at different applied voltages will be measured to specify the charge transport mechanism in the PPMA thin films.

CHAPTER II

THEORETICAL BACKGROUND

2.1 Introduction

The details of plasma, polymer and plasma polymerization are illustrated in this chapter. The prime object of this research is to prepare polymer thin films by glow discharge technique which is discussed in this chapter. This chapter also addresses different analytical techniques which are employed at various stages to characterize the samples. For the development of fundamental and applied research and consequently to enrich knowledge in this field it is necessary to do research and analysis. A brief outline of the theory of these experimental techniques is considered a prerequisite for the proper understanding of the methods.

2.2 Plasma

Sir William Crooke was the first who identified "plasma" as a "radiant matter" in a Crooke tube and also used the term "Fourth state of matter" to describe the plasma state in 1879. In 1897, Sir J.J. Thomson, a British physicist, was identified the nature of the Crooke tube. In 1929, Dr. Irving Langmuir, an American physicist and chemist, was first applied the term "Plasma" to ionized gas. Plasma is a partially ionized gas composed of freely moving electrons, ions and neutral species, there being approximately the same density of positive charges as of negative. The term fourth state of matter follows from the idea that as heat is added to solid, it under goes a phase transition usually to a liquid. If heat is added to a liquid the kinetic energy of the molecules become large and it becomes gaseous. The addition of still more energy to the gas, results in the ionization of some of the atoms. Although 99.9% of the apparent universe exists in a plasma state, there is very little in the way of the natural plasma here on earth because the low temperature and high density of the earth. In general, when a molecule is subjected to intense heat, the molecule will ionize. The sun, and other stars in our universe, have temperatures ranging from 5000 to 70,000 K or more, and consist entirely of plasma [26]. Plasma properties are strongly dependent on the bulk parameters. Some of the important plasma parameters are as follows: (i) the degree of ionization, (ii) the plasma temperature, (iii) the density, (iv) the magnetic field in the plasma region. In analysis plasmas are far harder to model than solids, liquids and gases because they act in a self-consistent manner. The separation of electrons and ions produce electric fields and the motion of electron and ions produce both electric and magnetic field. The electric field then tend to accelerate

plasmas to very high energies fields tend to guide the electrons. Plasmas resulting from ionization of neutral gases generally contain equal numbers of positive and negative charge carriers. In this situation, the oppositely charged fluids are strongly coupled and tend to electrically neutralize one another on microscopic length-scales. Such plasmas are termed quasi-neutral ("quasi" because the small deviations from exact neutrality have important dynamical consequences for certain types of plasma mode). Strongly non-neutral plasmas, which may even contain charges of only one sign, occur primarily in laboratory experiments: their equilibrium depends on the existence of intense magnetic fields, about which the charged fluid rotates [27, 28]. In the laboratory, plasma can be created by various techniques such as combustion flames, electrical discharges, controlled nuclear reactions, shocks and other means. The technique of most interest is the glow discharge. Plasmas produced by this technique are called non-equilibrium or cold plasmas in contradistinction to equilibrium plasmas created by arcs or plasma jets. The term non-equilibrium means that there is no thermal equilibrium [29] between electrons and other neutral species and ions. The ambient temperature of plasma in a plasma polymerization reaction however is generally in the vicinity of 380 to 400 K and remains reasonably constant after a steady-state condition is established. Based on the relative temperatures of the electrons ions and neutrals, plasmas are classified as thermal (hot plasma) or non-thermal (cold plasma) [30]. Thermal plasmas have electrons and the heavy particles at the same temperature i.e. they are in thermal equilibrium with each other. Non-thermal plasmas on the other hand have the ions and neutrals at a much lower temperature (ambient temperature) whereas electrons are much 'hotter'. Plasma is sometimes referred to as being hot if it is nearly fully ionized or cold if only a small fraction (for example 1%) of the gas molecules is ionized. Even in 'cold' plasma the electron temperature is still typically several thousand degrees. Plasmas utilized in plasma technology are usually cold in the sense.

2.2.1 Fundamental aspects of plasma

The negative particles in glow discharge plasma are mostly electrons; however negative ions are also formed. When an electric field is applied, the electrons gain energy according to Newton's law,

$$a=qE/m\ldots\ldots\ldots\ldots..(2.1)$$

Where, *a* is the acceleration of the electron, q is its electric charge, m_e is its mass, and E is the electric field.

The different types of collisions can occur between an electron and an atom, depending on the energy K that is transferred to an electron in the atom:

(i) K= 0; the electrons in the atom in the ground state. The collision is elastic, and causes no change in the structure of the atom.

(ii) $0<K<qV_i$; where V_i is the ionization potential of the atom. An electron in the atom is excited to a higher energy level, but returns to the ground state in a short time, releasing the gained energy again. The collision is inelastic.

(iii) $K>qV_i$; the atom is ionized by inelastic collision, and become positive with charge +q.

Between the energy level of the ground state and that of the ionized state, a number of other energy levels can exist. An electron in an atom that receives energy from a primary electron can jump to a higher level, but after a short period of time (of the order of 10^{-8} s) it falls back to lower energy levels or to the ground state. In this process, the electrons excess energy is released e.g. by emission of a photon. When an electron falls back from energy level E_m and E_n, the frequency υ of this photon is given by: $h\upsilon = E_m - E_n$; where h is the Planck's constant. The temperature of colliding species plays an important role on the collision processes occurring in a glow discharge.

2.2.2 Different types of plasma

(i) Ultracold plasma

(ii) Non-neutral plasma

(iii) Dusty plasma and grain plasma

(iv) Artificial plasma

(i) Ultracold plasma:

Laser-cooled atomic vapors can be photoionized to form plasmas at temperature as low as 1 K. This may allow the study of very unusual neutral plasmas with liquid and even crystalline properties. Ultracold plasmas have been created in a number of atomic systems including xenon, rubidium, cesium, strontium, and calcium.

(ii) Non-neutral plasmas:

Non-neutral plasma is plasma for which the total charge is sufficiently different from zero, so that the electric field created by an un-neutralized charge plays an important or even dominant role in the plasma dynamics.

(iii) Dusty plasma

Dusty plasma is a plasma containing milimeter (10^{-3}) to nanometer (10^{-9}) sized particles suspended in it. Dust particles are charged and the plasma and particle behave as plasma. The interaction between a dust grain and the surrounding plasma is an extremely complicated two-way process.

(iv) Artificial plasma

Most artificial plasmasare generated by the application of electric and magnetic fields.
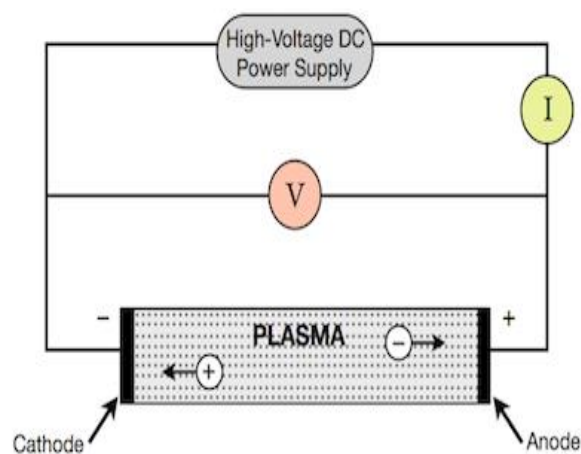
Fig. 2.1 Formation of artificial plasma [31].

Plasma generated in a laboratory setting and for industrial use can be generally categorized by:

(a) The type of power source used to generate the plasma: DC (10 kHz), AC (50 Hz), RF (13.6 MHz) and microwave.

(b) The pressure at which they operate; vacuum pressure (< 10 mTorr), moderate pressure (~10 Torr or 1333.2 Pa), atmospheric pressure (760 Torr or 101.3232 kPa). We usually use 10^{-1} Torr or 10^{-3} Torr in our research laboratory.

(c) The degree of ionization within the plasma; fully ionized, weakly ionized.

(d) The temperature relationships within the plasma: thermal plasma ($T_e = T_{ion} = T_{gas}$), non-thermal or cold plasma ($T_e \gg T_{ion} = T_{gas}$). The electrode configuration used to generate the plasma.

2.2.3 Applications of plasma

The important applications are:

(i) Sterilization.

(ii) Etching of nanometer to micron scale features in materials.

(iii) Activation for adhesion.

(iv) Cleaning i.e., contaminant removal.

(v) Polymerization: Coating of components: protective layers, hydrophobe layers, insulating layers,

(vi) Activation for wetting, i.e., adjustment of the surface energy.

(vii) Deposition of nanometer to micron thick coatings, etc.

2.2.4 Glow discharge

Glow discharges are usually used for the cold plasma [41] generation. A glow discharge is a kind of plasma. It is an ionized gas consisting of equal concentrations of positive and negative charges and a large number of neutral species. In the simplest
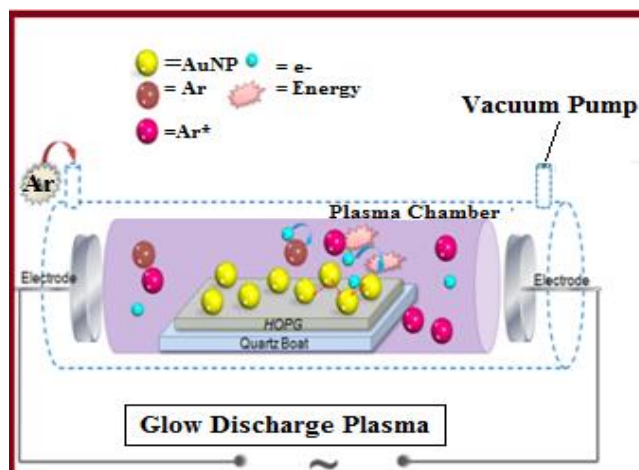
Fig. 2.2 Glow discharge plasma [32].

case, it is formed by applying a potential difference (of a few 100 V to a few kV) between two electrodes that are inserted in a cell or reactor (or that form the reactor walls). The reactor is filled with a gas (an inert gas or a reactive gas) at a pressure ranging from a few mTorr to atmospheric pressure. Due to the potential difference, electrons that are emitted from the cathode by the omnipresent cosmic radiation are accelerated away from the cathode, and give rise to collisions with the gas atoms or molecules (excitation, ionization, dissociation). The **excitation collisions** give rise to excited species, which can decay to lower levels by the emission of light. This process makes that a gas discharge plasma typically emits a
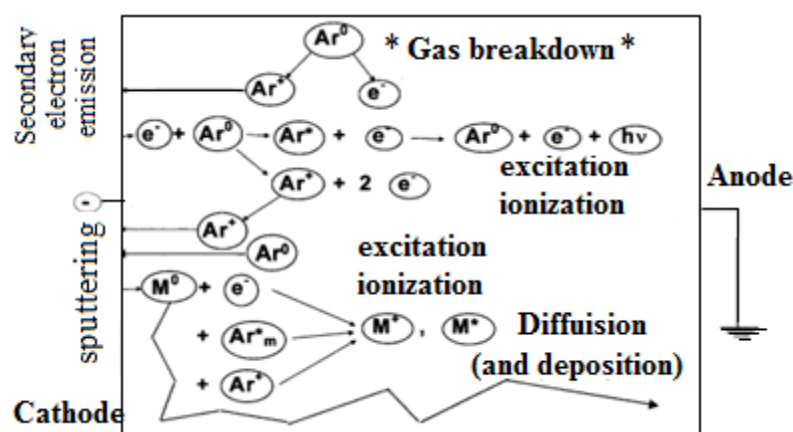
Fig. 2.3 Schematic representation of the basic processes in a glow discharge [33].

characteristic glow (and is therefore also called *"glow" discharge*). The *ionization collisions* create ion-electron pairs. The ions are accelerated toward the cathode, where they release secondary electrons. These electrons are accelerated away from the

cathode and can give rise to more ionization collisions. In its simplest way, the combination of secondary electron emission at the cathode and ionization in the gas, gives rise to self-*sustained plasma [33]*. The character of the gas discharge critically depends on the frequency or modulation of the current.

2.2.5 Overview of glow discharge plasma

(i) Corona discharges

Beside a glow discharge with two electrodes, there also exists another type of pulsed D.C. discharge, with the cathode in the form of a wire. A high negative voltage (in the case of a negative corona discharge) is applied to the wire cathode, and the discharge operates at atmospheric pressure. The name 'corona discharge' arises from the fact that the discharge appears as a lighting crown around the wire. The mechanism of the negative corona discharge [34] is similar to that of a D.C. glow discharge. The positive ions are accelerated towards the wire, and cause secondary electron emission. The electrons are accelerated into the plasma. This is called a streamer, i.e. a moving front of high-energy electrons (with average energy approx. 10 eV), followed by a tail of lower energy electrons (order of 1 eV). The high-energy electrons give rise to inelastic collisions with the heavy particles, e.g. ionization, excitation, dissociation. Hence, radicals can be formed, which can crack larger molecules in collisions. Therefore, there is a clear distinction between the electron kinetics (to create the plasma) and the heavy particle kinetics of interest for the applications (e.g. flue gas cleaning). The separation between both is not accomplished here in space, but in time. It should be mentioned that beside the negative corona discharge, there also exists a positive corona discharge, where the wire has a positive voltage, hence acting as anode. Dust particles are removed from the gas or liquid by the attachment of electrons from the discharge to the dust particles. The latter becomes negatively charged and will be drawn toward the walls.

(ii) Direct current (D.C.) glow discharges

When a sufficiently high potential difference is applied between two electrodes placed in a gas, the latter will break down into positive ions and electrons, giving rise to a gas discharge. The mechanism of the gas breakdown can be explained as follows: a few electrons are emitted from the electrodes due to the omnipresent cosmic radiation. Without applying a potential difference; the electrons emitted from the cathode are not able to sustain the discharge. However, when a potential difference is applied, the

electrons are accelerated by the electric field in front of the cathode and collide with the gas atoms. The most important collisions are the inelastic collisions, leading to excitation and ionization. The excitation collisions, followed by de-excitations with the emission of radiation, are responsible for the characteristic name of the 'glow' discharge. The ionization collisions create new electrons and ions. Ions are accelerated by the electric field toward the cathode, where they release new electrons by ion induced secondary electron emission. The electrons give rise to new ionization collisions, creating new ions and electrons. These processes of electron emission at the cathode and ionization in the plasma make the glow discharge self-sustaining plasma. A D.C. glow discharge can operate over a wide range of discharge conditions. The pressure can vary from below 1 Pa to atmospheric pressure. It should, however, be realized that the product of pressure and distance between the electrodes is a better parameter to characterize the discharge. For instance, at lower pressure, the distance between cathode and anode should be longer to create a discharge with properties comparable to those of high pressure with small distance. The voltage is mostly in the range between 300 and 1500 V, but for certain applications it can increase to several kV. The current is generally in the mA range. The discharge can operate in a rare gas (most often argon or helium) or in a reactive gas (N_2, O_2, H_2, CH_4, SiH_4, SiF_4, etc.), as well as in a mixture of these gases.

(iii) Capacitively coupled radio-frequency discharges

To sustain a D.C. glow discharge, the electrodes have to be conducting. When one or both of the electrodes are non-conductive, e.g. when the glow discharge is used for the spectrochemical analysis of non-conducting materials or for the deposition of dielectric films, where the electrodes become gradually covered with insulating material, the electrodes will be charged up due to the accumulation of positive or negative charges, and the glow discharge will extinguish. This problem is overcome by applying an alternating voltage between the two electrodes, so that each electrode will act alternately as the cathode and anode, and the charge accumulated during one half-cycle will be at least partially neutralized by the opposite charge accumulated during the next half-cycle. The frequencies generally used for these alternating voltages are typically in a most common value of 13.56 MHz. Strictly speaking; capacitively coupled discharges can also be generated by alternating voltages in another frequency range. Therefore, the term 'alternating current' (A.C. discharges, as opposed to D.C. discharges, might be more appropriate. On the other hand, the

frequency should be high enough so that half the period of the alternating voltage is less than the time during which the insulator would charge up. Otherwise, there will be a series of short-lived discharges with the electrodes successively taking opposite polarities, instead of a quasi-continuous discharge.

(iv) Pulsed glow discharges

Besides applying an rf voltage to a glow discharge, the voltage can also be applied in the form of discrete pulses, typically with lengths in the order of milli to microseconds. Because a pulsed discharge can operate at much higher peak voltages and peak currents for the same average power as in a D.C. glow discharge, higher instantaneous sputtering, ionization and excitation can be expected and hence better efficiencies. This is because the basic plasma phenomena, such as excitation and ionization, are highly non-linearly dependent on field strength. Whereas the early analytical investigations dealt primarily with milli second pulsed glow discharges, more recent work has focused mainly on microsecond discharges, where even higher peak voltages and currents, and hence better sensitivities, can be obtained. For the same reason, also in the semiconductor industry, pulsed power operation has emerged as a promising technique for reducing charge-induced damage and etches profile distortion, which is associated with continuous discharges. Another advantage of pulsed D.C. technology glow discharges compared to rf technology is the simpler method of up-scaling due to reduced impedance matching network and electromagnetic interference problems, and the lower price of power supplies for larger reactors.

(v) Alternative current (A.C.) glow discharges

In an A.C. glow discharge, the mechanism depends on the frequency of the excitation. At low frequencies, the system can be looked upon as a D.C. glow discharge with alternating polarity. By increasing the frequency of the applied voltage, positive ions become immobile, because they can no longer follow the periodic changes in field polarity, and only respond to time-averaged fields. At frequencies above 500 kHz, the half-cycle is so short that all electrons and ions stay within the inter electrode volume. This reduces the loss of charged particles from the system significantly, and regeneration of electrons and ions occurs within the body of the plasma through collisions of electrons with gas molecules. In radio frequency plasma (13.56 MHz) therefore, no contact between the electrodes and the plasma is required. The plasma

can be initiated and sustained by external electrodes, at a much lower voltage than is required for maintaining a direct current glow discharge.

2.2.6 Types of reactors

There are few designs for apparatus used in plasma polymerization, one of which is the Bell (static type), in which monomer gas is put into the reaction chamber, but does not flow through the chamber. It comes in and polymerizes without removal. This type of reactor is shown in Fig. 2.4. This reactor has internal electrodes, and polymerization generally takes place on the cathode side. All devices contain the thermostatic bath, which is used to regulate temperature, and a vacuum to regulate pressure. A great number of deposition systems using low pressure plasma were described in the literature. Generally the three types of plasma polymerization deposition systems (reactors) can be distinguished as pointed out [35]: (i) Bell jar reactors (Fig. 2.4 (a)) (ii) Parallel plate electrode reactors (Fig. 2.4 (b)) and (iii) electrodeless microwave or high frequency reactors (Fig. 2.4 (c)). Discharge can be excited either by DC or A.C. and/or RF voltage. DC is used in special cases or in the case where a planer magnetron is used. For plasma polymerization process, more typical is the discharge excitation by A.C. and RF voltages in so called symmetrical arrangement. If the frequency of the excitation voltage is above about 50 kHz (100 kHz) the powered must be delivered through a matching unit and determined by a power meter. In case of the asymmetrical arrangement where the excitation D.C .negative biased in developed on this electrode. In this case the surface (target) of the excitation electrode is sputtered by positive ions (RF sputtering). In some processes this may be the reason for concern as there is a danger of impurities sputtered off from the excitation electrode. In other cases this may be welcome e.g. simultaneous plasma polymerization and co-sputtering of the metallic target for composite metal/plasma polymer film deposition.

Operation: The monomer gas comes into the Bell type reactor [36] as a gaseous species, and then is put into the plasma state by the electrodes, in which the plasma may consist of radicals, anions and cations. These monomers are then polymerized on the cathode surface, or some other surface placed in the apparatus by different mechanisms of which details are discussed below. The deposited polymers then propagate off the surface and form growing chains with seemingly uniform consistency.

Electrodeless microwave reactors [37, 38] are usually composed from a silica tube that passes through the resonant cavity coupled to a microwave power supply (typically 2.45 GHz). Plasma is generated in the tube within the cavity and substrates are positioned
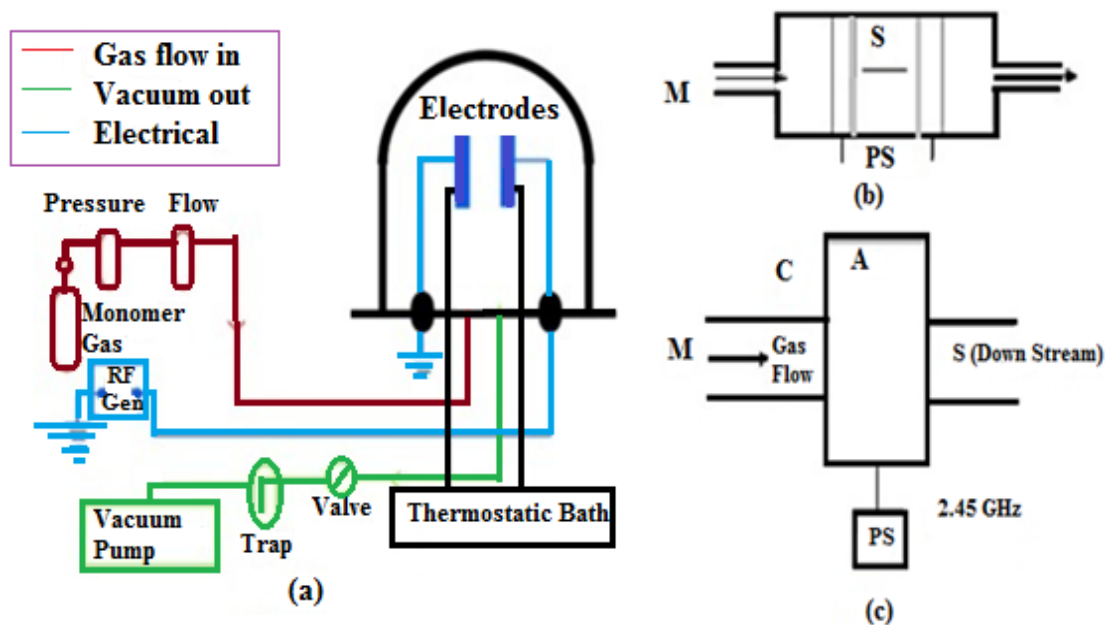
Fig. 2.4 Glow discharge reactor: (a) bell jar type [36], (b) parallel plate electrode reactor [5], and (c) electrode less microwave reactor [37, 38].

downstream of the plasma. The cavity actually acts instead of the RF excitation coil or ring electrodes. Another popular reactor type is the flow through reactor (continuous flow reactor), which also has internal electrodes, but this reactor allows monomer gas to flow through the reaction chamber as its name implies, which should give a more even coating for polymer film deposition. It has the advantages that more monomer keeps flowing into the reactor in order to deposit more polymers. Atmospheric-pressure plasma system is also growing in popularity, which is useful for depositing thin polymer films. This system by passes the requirements for special hardware involving vacuums, which then makes it favorable for integrated industrial uses. It has been shown that polymers formed at atmospheric pressure can have similar properties for coating as those found in the low-pressure systems.

2.3 Polymers

The word polymer is derived from the classical words "poly" meaning "many" and "mers" meaning "parts". Simply stated, a polymer is a material whose molecules contain a very large number of smaller structural units called monomers linked by

covalent bonds in any conceivable pattern, which makes polymers macromolecules. In certain cases, it is more accurate to call the structural or repeat unit a monomer residue because monomers are eliminated from the simple monomeric unit during some polymerization process [39]. Certain polymers available in nature are proteins cellulose; silk etc., where many others including polystyrene, polyethylene and nylon are produced only by synthetic routes.

2.3.1 Classification based upon different factors related to polymers

A. On the basis of origin polymers are divided into three classes:

Polymers

(a) Natural   (b) Semi-synthetic   (c) Synthetic
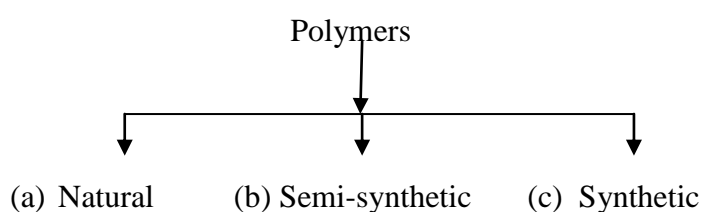
B. According to backbone chain polymers can be divided into two classes:

Polymers

(a) Organic   (b) Inorganic
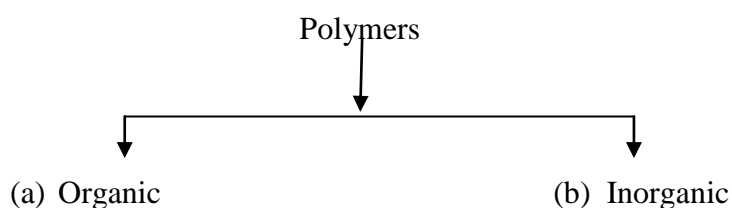
C. The most common way of classifying polymers (on the basis of thermal response) is to separate them into three groups as follows;

Polymers

(a) Thermoplastics   (b) Thermosets   (c) Elastomers

(i) Crystalline (ii) Amorphous
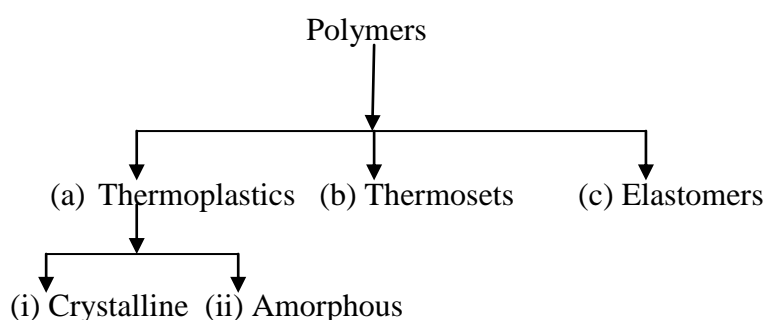
(a) Thermoplastics:

Molecules in a thermoplastic are held together weak intermolecular forces so that the materials soften when exposed to heat and then return to its original condition when cooled. Thermoplastics polymers can be heat-softened in order to process into a

desired form and then can be solidified by cooling. Most linear and slightly branched polymers are thermoplastics as shown in Fig. 2.5 (a). All the major thermoplastics are produced by chain polymerization.

(i) Crystalline polymer:

An important feature of crystalline polymer is that they consist not only of crystalline but amorphous regions as well. As a matter of fact, the crystalline and amorphous regions are separated by portions with an intermediate degree of ordering. As a rule there is no sharp borderline between the crystalline and amorphous regions. This is associated not to a small degree with the fact that one macromolecule may run through several crystalline and amorphous regions. This existence of such two phase chains is a characteristics feature of crystalline polymers. It is sometimes believed that a crystalline polymer may be regarded as an amorphous matrix in which small crystallite are randomly distributed. Obviously such a model is unsuitable for highly crystalline polymers in which the cystallinity 70-90%. It will be more natural to treat a crystalline polymer as a certain lattice in which the voids are filled with amorphous matter.

(ii) Amorphous polymer:

It has long been thought that amorphous polymers are aggregates of randomly entangled molecules. The concept of molecular felt is developed, which was assumed to correspond to the structure of an amorphous polymer. On the basis of X-ray studies it may be concluded that in amorphous polymers there are regions of short range order in which a single type of spatial type of orderliness is retained at a distance of 10-15 A^0 from any point.

(b) Thermosets:

A thermosetting plastics or thermoset solidifies or sets irreversibly when heated. Thermosets cannot be reshaped by heating. Thermosets usually 3-D network polymers (Fig. 2.5 (b)) as linked by covalent bonds during polymerization or by subsequent chemical or thermal treatment during fabrication. These polymers possess a high degree of cross-linking between polymer chain, which restrict the motion of the chain and lead to a rigid material.

(a) Thermoplastics   (b) Thermosets   (c) Elastomers
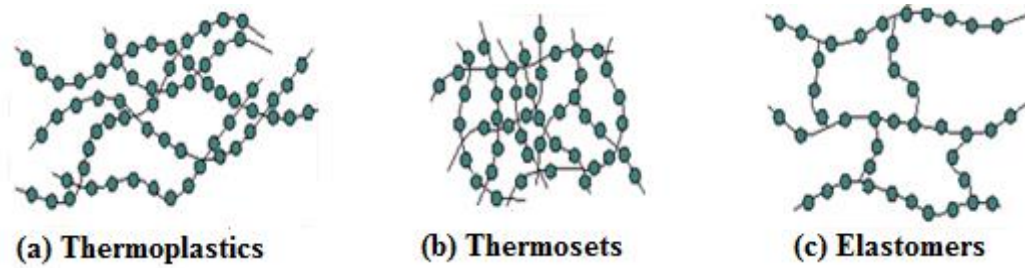
Fig. 2.5 (a) Thermoplastics, (b) Thermosets, and (c) Elastomeric polymers.

(c) Elastomers:

Elastomers are rubbery polymers that can be stretched easily to several times their unstretched length and which rapidly return to their original dimensions when the applied stress is released. Elastomers are cross-linked but have a low cross-linked density as shown in Fig. 2.5 (c). The polymer chain still have some freedom to move, but are prevented from permanently moving relative to each other by the cross-links. To stretch, the polymer chain must not be part of a rigid solid either a glass or a crystal. An elastomer must be above its glass transition temperature, T_g and have allow degree of crystallinity.

2.3.2 Polymerization

Polymerization is a chemical process that combines several monomers to form a polymer or polymeric compound. The monomer molecules may be all alike, or they may represent two, three, or more different compounds. Usually at least 100 monomer molecules must be combined to make a product that has certain unique physical properties-such as elasticity, high tensile strength, or the ability to form fibres-that differentiate polymers from substances composed of smaller and simpler molecules; often, many thousands of monomer units are incorporated in a single molecule of a polymer. The formation of stable covalent chemical bonds between the monomers sets polymerization [39, 40] apart from other processes, such as crystallization, in which large numbers of molecules aggregate under the influence of weak intermolecular forces.
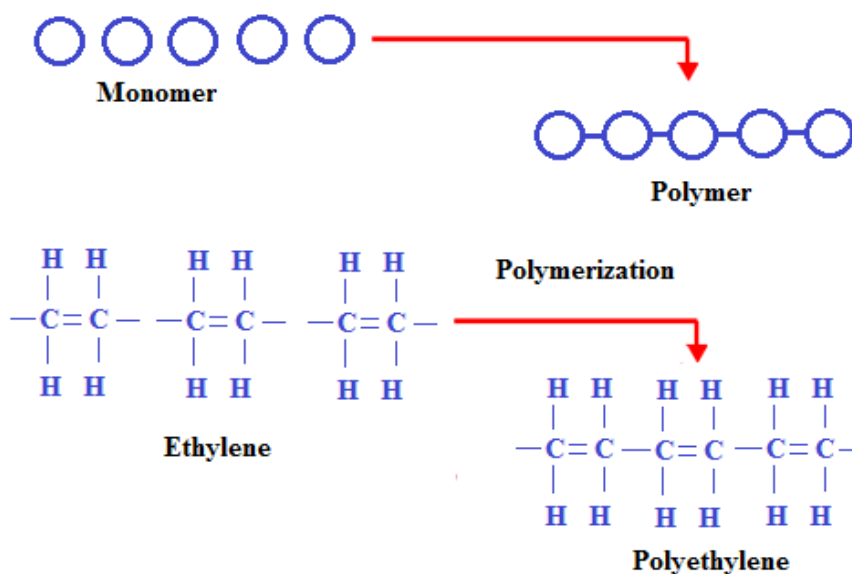
Fig. 2.6 Polymerization process.

2.3.3 Different polymerization processes

(i) Step-growth polymerization

Step-growth polymerization refers to a type of polymerization mechanism in which bi-functional or multifunctional monomers react to form first dimers, then trimers, longer oligomers and eventually long chain polymers. Many naturally occurring and some synthetic polymers are produced by step-growth polymerization, e.g. polyesters,
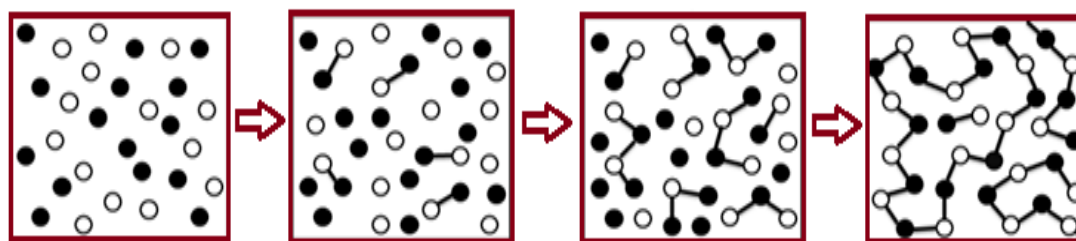
Fig. 2.7 A generic representation of a step-growth polymerization.

polyamides, polyurethanes, etc. Due to the nature of the polymerization mechanism, a high extent of reaction is required to achieve high molecular weight. The easiest way to visualize the mechanism of a step-growth polymerization is a group of people reaching out to hold their hands to form a human chain-each person has two hands (=

reactive sites). There also is the possibility to have more than two reactive sites on a monomer: In this case branched polymers are produced.

(ii) Chain-growth polymerization

Chain-growth polymerization is a polymerization technique where unsaturated monomer molecules add onto the active site of a growing polymer chain one at a time. Growth of the polymer occurs only at one (or possibly more) ends. Addition of each monomer unit regenerates the active site. Polyethylene, polypropylene, and polyvinyl chloride (PVC) are common types of plastics made by chain-growth polymerization. They are the primary component of four of the plastics specifically labeled with recycling codes and are used extensively in packaging.
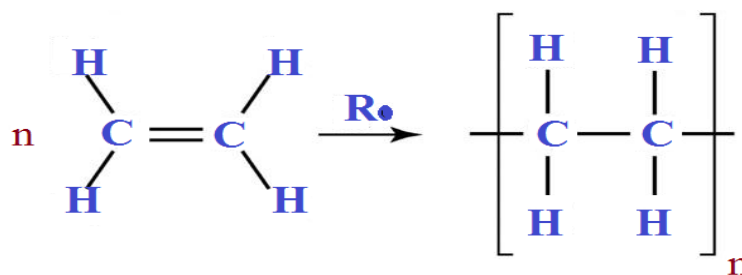
Fig. 2.8 Chain-growth polymerization.

(iii) Free radical polymerization

Free-radical polymerization is a chain polymerization in which the kinetic-chain carriers are free radicals which can be formed by a number of different mechanisms, usually involving separate initiator molecules. It is one of the most common and useful reaction for making polymers. It is a key synthesis route for obtaining a wide variety of different polymers and material composites. It is used to make polymers from vinyl monomers, that is, from small molecules containing carbon-carbon double bonds. Polymers made by free radical polymerization include polystyrene, poly (methyl methacrylate), poly (vinyl acetate) and branched polyethylene. The relatively non-specific nature of free-radical chemical interactions makes this one of the most versatile forms of polymerization available and allows facile reactions of polymeric free-radical chain ends and other chemicals or substrates.

Monomer

$$\begin{array}{cc} H & H \\ | & | \\ -C-C- \\ | & | \\ H & H \end{array}$$

Initiation

$$R\cdot + \begin{array}{cc} H & H \\ | & | \\ -C-C- \\ | & | \\ H & H \end{array} \longrightarrow R - \begin{array}{cc} H & H \\ | & | \\ C-C\cdot \\ | & | \\ H & H \end{array}$$

Propagation

$$R - \begin{array}{cc} H & H \\ | & | \\ C-C\cdot \\ | & | \\ H & H \end{array} + \begin{array}{cc} H & H \\ | & | \\ -C-C- \\ | & | \\ H & H \end{array} \longrightarrow R - \begin{array}{cccc} H & H & H & H \\ | & | & | & | \\ C-C-C-C\cdot \\ | & | & | & | \\ H & H & H & H \end{array}$$
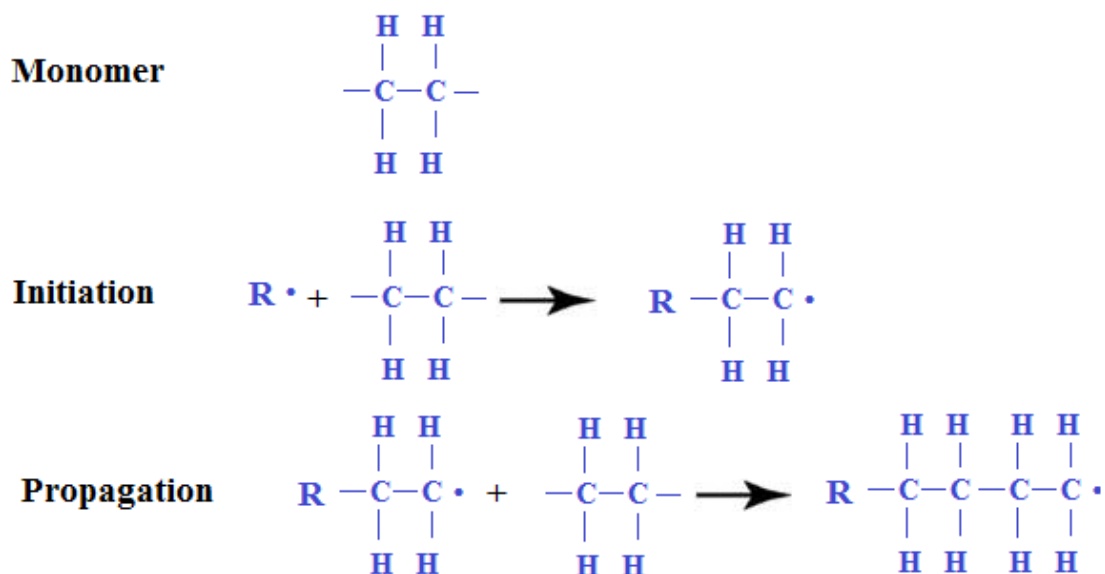
Fig. 2.9 Free radical polymerization.

2.4 Plasma Polymerization

The formation of polymeric materials under the influence of plasma is called plasma polymerization. It is a technique for the deposition of films with functional properties suitable for a wide range of modern applications. It is also well known to be a useful method to fabricate highly branched and cross-linked polymer films, which are ultra-thin, pinhole-free, homogeneous and highly adherent to a variety of substrates including conventional polymer, glass and metal surfaces. Plasma polymerization is a procedure, in which gaseous monomers, simulated through plasma, condense on freely selectable substrates, as high cross-linked layers.

Conditions for the plasma polymerization process (Fig. 2.10) are the presence of chain producing atoms, such as carbon, silicium or sulfer in the networking gas. In this process monomer gas is pumped into a vacuum chamber where it is polymerized by plasma to form a thin, clear coating. The monomer starts out as a liquid. It is converted to a gas in an evaporator and is pumped into a vacuum chamber. Plasma polymerization uses plasma sources to generate a gas discharge that provides energy to active or fragment gaseous or liquid monomer, often containing a vinyl group, in order to initiate polymerization. Polymers formed from this technique are generally highly branched and highly cross-linked, and adhere to solid surfaces well. The

biggest advantage to this process is that polymers can be directly attached to a desired surface while the chains are growing, which reduces
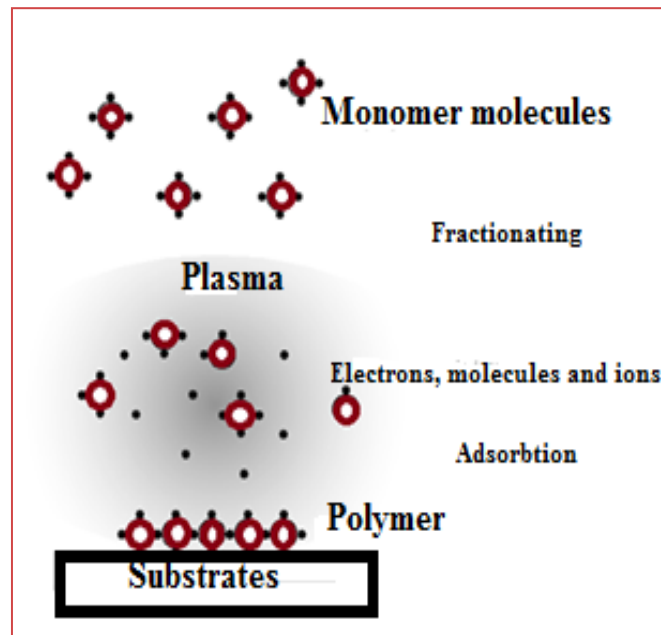
Fig. 2.10 A schematic plasma polymerization configuration.

steps necessary for other coating processes such as grafting. Historically, proposed mechanisms of plasma polymerization [42, 43] have been based on conventional chain growth polymerization such as free radical or ionic polymerization. Plasma polymerization should be considered as a method of forming new types of materials rather than a method of preparing conventional polymer.

2.4.1 Characteristics differences of plasma polymers from the conventional polymers

(i) Plasma polymers have a higher elastic modulus than the conventional polymers.

(ii) Low water vapor or gas permeability than the conventional polymers.

(iii) The properties of plasma polymer are much more dependent on the processing factors and morphology than the conventional polymers. For example, properties of plasma polymers are directly or indirectly related to the number of free radicals.

(iv) Internal stress in a plasma polymer is a characteristics property which is not found in most polymers.

(v) Solvent resistance of plasma polymers is generally higher than the conventional polymers.

(vi) The surface energies of plasma polymers of hydrocarbons are generally higher than those of conventional hydrocarbon polymers due to the presence of O containing groups.

2.4.2 Overall reactions and growth mechanism in plasma polymerization

In plasma, monomer molecules gain high energy from electrons, ions and radicals and are fragmented into activated small fragments, in some cases into atoms. These activated fragments are recombined sometimes accompanying rearrangement, and the molecules grow to large molecular weight ones in a gas phase or at the surface of the substrates. The repetition of activation, fragmentation, and recombination leads to a polymer formation. The chemical structure of polymers formed by plasma polymerization, if the same monomer (which is used in conventional polymerization) was used, is never predicted from the structure of the monomer, because the fragmentation and rearrangement of the monomers occur in the plasma.

Plasma polymerization consists of several reaction steps:

At first, generation of free radicals and atoms are occurred by collisions of electrons and ions with monomer molecules, or by dissociation of monomers absorbed on the surface of the sample. Secondly, propagation of the formation of polymeric chain which can take place both in the gas phase (by adding radicals atoms to other radicals or molecules) and on the deposited polymer film (by the interaction of the surface free radicals with either gas phase or absorbed monomers). Finally termination can also take place in the gas phase or at the polymer surface, by similar process as in the propagation step, but ending either with the final product or with a closed polymer chain. The individual steps and reaction that occur in plasma polymerization generally depends on the system. This type of polymerization can be presented by the following statements.

Initiation or Reinitiation

$$M_i \longrightarrow M_i^*$$

$$M_k \longrightarrow M_k^*$$

Propagation and Termination

$$M_i^* + M_k^* \longrightarrow M_i - M_k$$

$$M_i^* + M_k \longrightarrow M_i - M_k$$
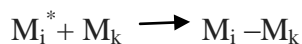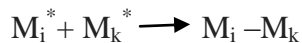
In which i and k are the number of repeating units (i.e. i=k=1 for the starting material), and M^* represents a reactive species, which can be ion of either charge, an excited molecule, or a free radical produced by M but not necessarily retaining the molecular structure of the starting material. In plasma state polymerization, the polymer is formed by the repeated stepwise reaction. Yasuda suggested that the growth mechanism of plasma polymerization would vary likely be the rapid step growth reaction,

$$[M_m^* + M_n^* \longrightarrow M_{m+n}] \times N ;$$

Where M^* is the mono functional reactive species such as a free radical $R^.$, N is the number of repititions of similar reactions and m and n reperesnts different reactive species. In case of monofunctional reactive species, a single elementary step is indeed a termination process and does not contribute without additional elementary step. For a difunctional reactive species, such as a diradical, the polymerization can be represented by

$$N^* M^* \longrightarrow {}^*(M_n)^*.$$
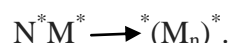
It shows that as polymerized polymers contain a measurable quantity of free radicals. The overall polymerization mechanism based on the rapid step growth principle is shown in Fig. 2.11, where M_X refers to a neutral species, M^* is the monofunctional activated species and ${}^*M^*$ is the difunctional. The subscripts i, j, k indicates the difference in the size of species involved.

Cycle-1 is via the repeated activation of the reaction products from monofunctional activated species, and Cycle- 2 is that of difunctional. The species participating in the rapid step growth polymerization can be mono-or multifunctional (radical, cation, cation-radical, diradical, etc.).
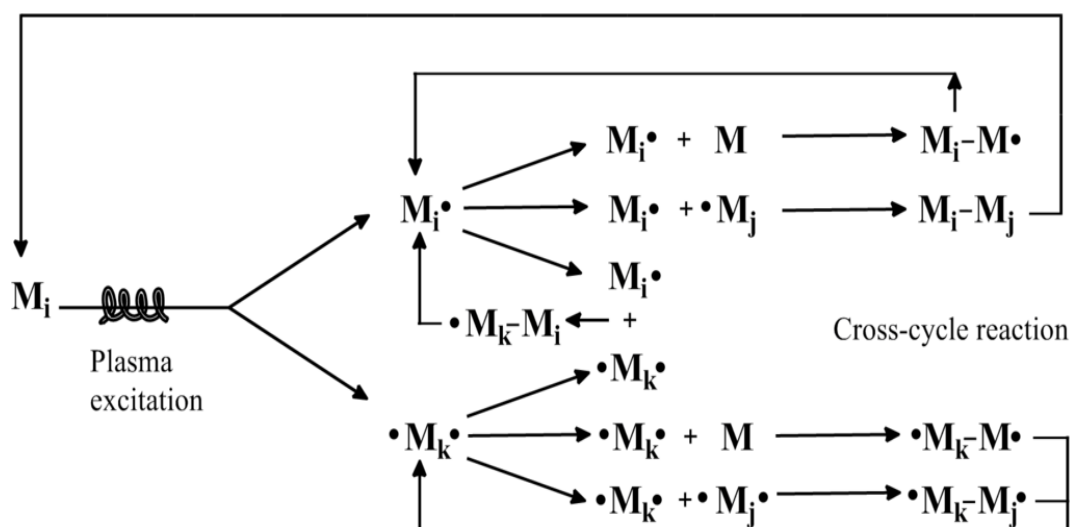
Fig. 2.11 Schematic representation of bicycle step growth mechanism of plasma polymerization [5].

2.4.3 Advantages and disadvantages of plasma polymerization

The deposition of thin films on solid substrates by the plasma polymerization process has been practiced for over two decades. The plasma polymerization of the simple organic monomers (i.e. hudrocarbons or silanes) produces films that are highly cross-linked, pinholefree, thermally and chemically stable, and very adherent. Furthermore, plasma polymerized films can be prepared from monomers that cannot be polymerized by conventional chemical techniques(i.e. methane, ethane, saturated hydrocarbons, organo-metallics).The characteristics of the plasma formed films (adhesion, mechanical properties, extent of crosslinking etc.) are dictated by the choice of kinetic formation parameters such as RF power input, plasma pressure, and reaction time.

The significant advantages of depositing thin films via plasma polymerization include:

(i)   The starting material does not have to contain the type of functional groups normally associated with conventional polymerization.

(ii) Plasma polymerized films are often highly adherent to a variety of substrates.

(iii) Deposition is achieved without the use of solvent.

(iv) The thickness of plasma polymerized films can be easily varied from 2 nm to 1000 nm.

(v) Through careful control of the plasma polymerization parameters, plasma polymerized films can be tailored to contain specific functional groups.

(vi) Plasma polymerized films can be deposited directly onto an activated substrate without breaking vacuum.

(vii) In the surface modification, plasma polymerization is limited to the top of the surface layer and does not affect the bulk properties of the polymer.

(viii) The modification of the plasma processes is largely independent on the structural or chemical reactivity of the substrates.

(ix) A broad range of functional groups can be introduced by the surface, by variation of the gas that is used. In general, the modification is fairly uniform over the whole substrate.

(x) The plasma treatment or plasma polymerization is a simple one-step procedure, and is an all-dry process.

Some of the disadvantages inherent to plasma processes are summarized in the following list:

(i) A vacuum system is required for plasma treatments. This demand increases the cost of the operation.

(ii) Due to complexity of plasma processes, it is not easy to achieve a good control over the chemical composition of the surface after modification. The influence of process parameters such as reactor geometry, input power, and gas flow on the chemical composition of the modified material should be investigated separately to find the optimal treatment conditions for each gas.

The main drawback in this case is related to the presence of the energetic species in the plasma which dissociate the precursors and so the obtained materials contains only in a small extent the original bonding environment. Therefore, the challenge in using plasma polymerization for obtaining conductive polymers is to find proper configurations and deposition conditions to preserve the conjugated double bonds [44].

2.5 Plasma polymerized thin films

2.5.1 Process of plasma polymerized thin films
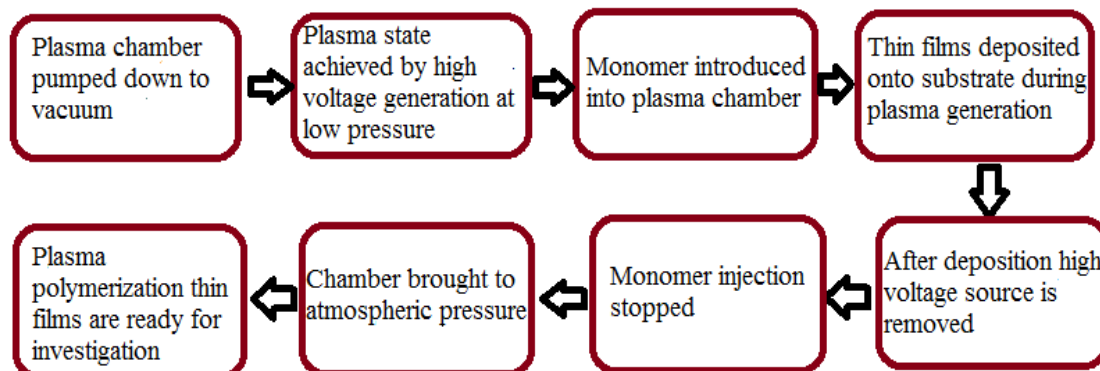
2.5.2 General properties of plasma polymerized thin films

(i) Plasma polymerized thin films [45] are thin (100 A^0 to several microns) and pinhole free.

(ii) Plasma polymerized thin films are insoluble in conventional organic solvents, indicating the highly cross-linked nature of the polymer.

(iii) The differential scanning calorimetry and differential thermal gravimetric analyses have been used by several authors to show that plasma derived polymers have no phase transitions until decomposition occurs. They have remarkable thermal stability for example 80 wt% of a film prepared from methyl chloride remains at 800^0C and 40 wt% of a styrene derived films remains at 700^0C.

(iv) Plasma derived films have a mesh structure, with only short chain segments between branched and cross-linked points. Its structure generally contains numerous unsaturated groups, aromatic groups and side branches.

(v) Plasma polymerized thin organic films are, in general, dielectric materials with insulating properties and extremely low conductivities.

2.6 Characterization Techniques of the Plasma Polymerized Thin Films

Researchers have been given extensive attention to be innovation and characterization of thin films of polymeric materials. Plasma polymerized thin organic films conjugated polymer thin films have received great attention in recent years for their optical response by delocalized electrons which yielded impressive properties for

various potential technological applications like thermal collectors, photo-voltaic thermal solar panels, solar selective absorbers, and photovoltaics etc [46, 47]. A brief discussion on the characterizing techniques which are useful to ascertain the general properties of plasma polymers are started below.

2.6.1 Thermogravimetric analysis

Thermogravimetric analysis (TGA) is a thermal analysis technique involving the determination of the change in weight of a sample as a function of temperature and/or time of heating. Weight loss information is useful in the characterization of materials, such as polymers, soils, or adhesives, and in problem solving. The instrument has an integral mass flow control, gas switching capability (nitrogen or air), and superb software which provides quality results for each analysis. The TGA can be used to determine polymer composition, thermal stability, degree of hydration, and level of residual solvent or moisture [48]. TGA is performed either in an inert nitrogen environment or in an oxidative environment (air). In certain sample types, different mechanisms of degradation may be present in oxidative and inert environments. Thus, the number of degradation steps and the temperatures at which the steps occur can be studied in different environments. Sample weight changes are measured as described in Fig. 2.12.
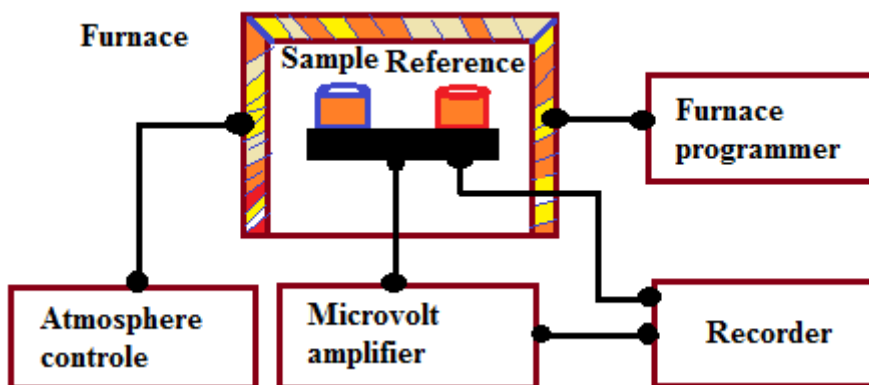
Fig. 2.12 A pictorial set-up for TGA measurements.

Fig. 2.12 shows the sample balance beam and reference balance beam are independently supported by a driving coil/pivot. When a weight change occurs at the beam end, the movement is conveyed to the opposite end of the beam via the driving coil/pivot, when optical position sensors detect changes in the position of a slit. The signal from the optical position sensor is sent to the balance circuit. The balance

circuit supplies sufficient feedback current to the driving coil so that the slit returns to the balance position. The current running to the driving coils to the sample side and the current running to the driving coil on the reference side is detected and converted into weight signals.

2.6.2 Differential thermal analysis

Differential thermal analysis (DTA) is a thermo-analytic technique in recording the temperature and heat flow associated with thermal transitions in a material. This enables to determine the phase transitions characteristics (e.g., melting point, glass transition temperature, crystallization etc.) (Fig. 2.13) . In DTA the material under study and an inert reference are made to undergo identical thermal cycles, while recording any temperature difference between sample and reference. This differential temperature is then plotted against time, or against temperature (DTA curve or thermogram). Changes in the sample, either exothermic or endothermic, can be detected relative to the inert reference. Thus, a DTA curve provides data on the transformations that have occurred, such as glass transitions, crystallization, melting and sublimation. The area under a DTA peak is the enthalpy change and is not affected by the heat capacity of the sample.
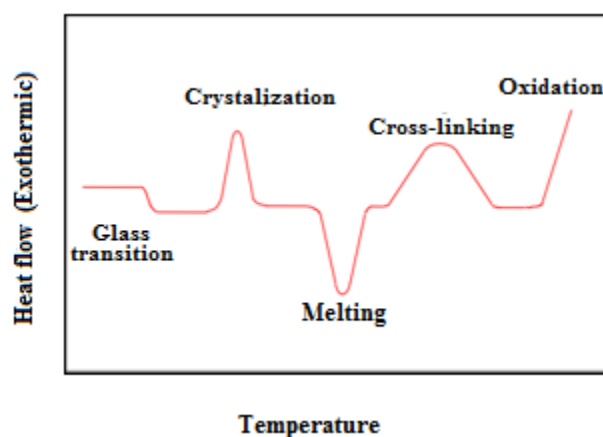
Fig. 2.13 Phase transitions.

DTA was constructed soon after the development of the thermocouple (1887, Le Chatelier) [49]. It was made for the examination of different materials. Most of the research efforts were made on clay and carbonate materials. The limitation in the DTA apparatuses is its sensitivity.
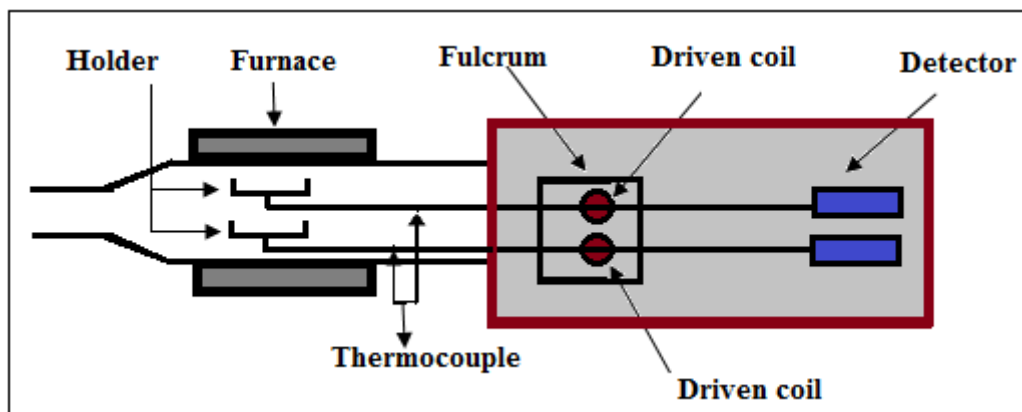
Fig. 2.14 Block diagram of a horizontal DTA instrument.

Fig. 2.14 shows a block diagram of a DTA cell. It contains two holders attached with thermocouples. Sample is inserted in one holder and a reference sample is placed in the other. The difference in temperature is measured from the difference in electromotive force (emf) between the thermocouples. These differences of temperatures appear because of the phase transitions or chemical reactions in the sample involving the evolution of heat and are known as exothermic reaction or absorption of heat known as endothermic reaction. The exothermic and endothermic reactions are generally shown in the DTA traces as positive and negative deviations respectively from a base line. So DTA offers a continuous thermal record of reactions in a sample.

2.6.3 Field emission scanning electron microscopy

Nanotechnology has strongly driven the development of recent electron microscopy, with demands not only for increasing resolution but also for more information from the sample. Electron microscopes use a beam of highly energetic electrons to probe objects on a very fine scale. It is the mostly used technique to obtain surface morphological information of plasma polymerized thin films.
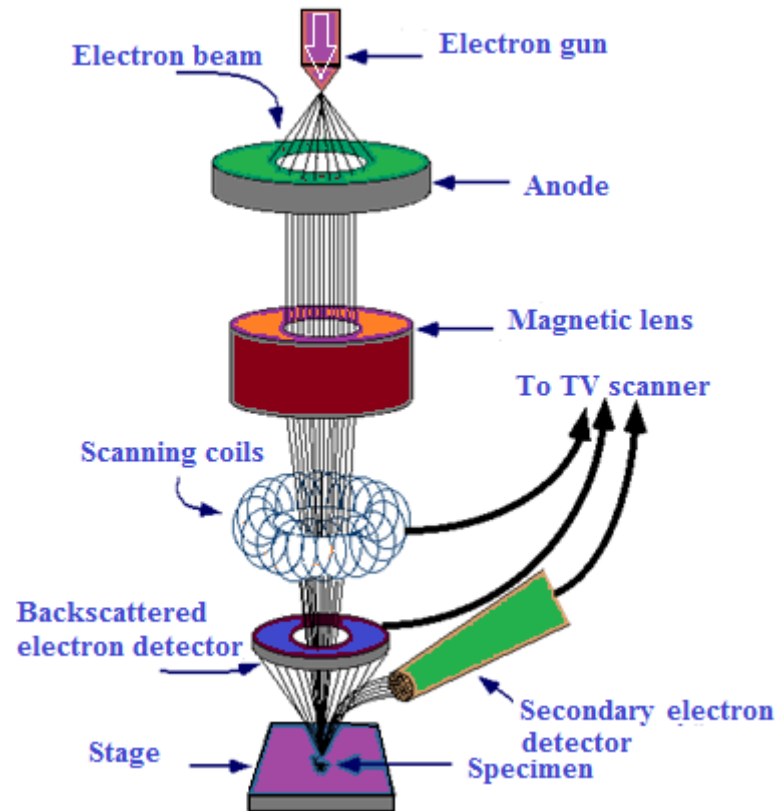
Fig. 2.15 A Schematic diagram of a field emission scanning electron microscope.

The combination of higher magnification, larger depth of focus, greater resolution and ease of sample observation makes FESEM one of the most widely used instruments in research areas today. **It** use a thermal emission source (i.e., tungsten filament) to generate the electron beam are generally adequate for most samples and provide satisfactory resolution at magnifications up to about $1,00,000 \times$. However, for high resolution and high magnification imaging a cold field emission (FE) gun provides the best resolution available for SEM. The cold FE gun extracts electrons from the FE cathode by applying a strong electrical field close to a very sharp tip. This method of electron extraction results in a higher electron yield and a smaller beam size, which thus provides a brighter signal with better resolution. The useful magnification for FESEM imaging ranges up to $500000 \times$. A second advantage of FESEM is that high resolution imaging can be performed with very low accelerating voltages. At low voltage, very fine features are more readily observed and many non-conductive materials can be examined without applying a conductive coating. Low voltage FESEM examination is ideal for imaging nano-materials, polymers, and thin films. For secondary electron imaging, samples must be electrically conductive. Nonconductive materials can be evaporatively coated with a thin film of carbon, gold

or other conductive material to obtain conductivity without significantly affecting observed surface morphology Samples must be compatible with at least a moderate vacuum. For high-resolution secondary electron imaging, the sample environment is at a pressure of 1×10^{-5} Torr or less. The pressure can be adjusted up to about 2 Torr for vacuum sensitive samples.

2.6.4 Energy dispersive X-ray spectroscopy

Energy dispersive X-ray spectroscopy (EDS or EDX) is a chemical microanalysis technique used in conjunction with scanning electron microscopy (SEM). The EDS technique detects x-rays emitted from the sample during bombardment by an electron beam to characterize the elemental composition of the analyzed volume. Features or phases as small as 1 μm or less can be analyzed. When the sample is bombarded by the SEM's electron beam, electrons are ejected from the atoms comprising the sample's surface. The resulting electron vacancies are filled by electrons from a higher state, and an x-ray is emitted to balance the energy difference between the two electrons' states. The x-ray energy is characteristic of the element from which it was emitted. The EDS x-ray detector measures the relative abundance of emitted x-rays versus their energy. The detector is typically lithium-drifted silicon, solid-state device. When an incident x-ray strikes the detector, it creates a charge pulse that is proportional to the energy of the x-ray. The charge pulse is converted to a voltage pulse (which remains proportional to the x-ray energy) by a charge-sensitive preamplifier. The signal is then sent to a multichannel analyzer where the pulses are sorted by voltage. The energy, as determined from the voltage measurement, for each incident x-ray is sent to a computer for display and further data evaluation. The spectrum of x-ray energy versus counts is evaluated to determine the elemental composition of the sampled volume.

2.6.5 Theory of infrared spectroscopy

IR Spectroscopy is an extremely effective method for determining the presence or absence of a wide variety of functional groups in a molecule. Infrared (IR) spectroscopy [50, 51] measures different IR frequencies by a sample positioned in the path of an IR beam and it reveals information about the vibrational states of a molecule. The main goal of IR spectroscopic analysis is to determine the chemical functional groups in the sample. Different functional groups absorb characteristic

frequencies of IR radiation and this absorption results due to the changes in vibrational and rotational status of the molecules. Actually, a molecule, when exposed to radiation produced by the thermal emission of a hot source (a source of IR energy), absorbs only at frequencies corresponding to its molecular modes of vibration in the region of the electromagnetic spectrum between visible (red) and short waves (microwaves). These changes in vibrational motion give rise to bands in the vibrational spectrum; each spectral band is characterized by its frequency and amplitude. The absorption frequency depends on the vibrational frequency of the molecules, whereas the absorption intensity depends on how effectively the infrared photon energy can be transferred to the molecule, and this depends on the change in the dipole moment that occurs as a result of molecular vibration. As a consequence, a molecule will absorb infrared light only if the absorption causes a change in the dipole moment. Thus, all compounds except for elemental diatomic gases such as N_2, H_2 and O_2, have infrared spectra and most components present in a flue gas can be analyzed by their characteristic infrared absorption. Furthermore, using various sampling accessories, IR spectrometers can accept a wide range of sample types such as gases, liquids, and solids. Thus, IR spectroscopy is an important and popular tool for structural elucidation and compound identification.

(i) Infrared frequency range and spectrum presentation

Infrared radiation spans a section of the electromagnetic spectrum having wave-numbers from roughly 3000 to 10 cm^{-1}, or wavelengths from 0.78 to 1000 μm. IR absorption positions are generally presented as either wave-numbers ($\bar{v}$) or wavelengths (λ). Thus, wave-numbers are directly proportional to frequency, as well as the energy of the IR absorption. In the contrast, wavelengths are inversely proportional to frequencies and their associated energy. Wavenumbers and wavelengths can be inter-converted using the following equation:

$$\bar{v}(cm^{-1}) = \frac{1}{\lambda(\mu m)} \times 10^4 \quad \text{....………………...……………………} (2.1)$$

$$A = \log_{10}(1/T) = \log_{10}(I_0/I) \quad \text{………………………………………}(2.2)$$

Table 2.1 Three smaller areas in IR region.

	Near IR	Mid IR	Far IR
Wavenumber	$13000 - 4000$ cm^{-1}	$4000 - 200$ cm^{-1}	$200 - 10$ cm^{-1}
Wavelength	$0.78 - 2.5$ µm	$2.5 - 50$ µm	$50 - 1000$ µm

The IR region is commonly divided into three smaller areas: near IR, mid IR, and far IR. The region of most interest for chemical analysis is the mid-infrared region (4,000 cm^{-1} to 400 cm^{-1}) which corresponds to changes in vibrational energies within molecules. The far infrared region (400 cm^{-1} to 10 cm^{-1}) is useful for molecules containing heavy atoms such as inorganic compounds but requires rather specialized experimental techniques. The far- and near IR are not frequently employed because only skeletal and secondary vibrations (overtones) occur in these regions producing spectra that are difficult to interpret.

(ii) Infrared absorption

At temperatures above absolute zero, all the atoms in molecules are in continuous vibration with respect to each other. When the frequency of a specific vibration is equal to the frequency of the IR radiation directed on the molecule, the molecule absorbs the radiation.

For a molecule to absorb IR, the vibrations or rotations within a molecule must cause a net change in the dipole moment of the molecule. The alternating electrical field of the electromagnetic radiation interacts with fluctuations in the dipole moment of the molecule. If the frequency of the radiation matches the vibrational frequency of the molecule then radiation will be absorbed, causing a change in the amplitude of molecular vibration. The energy of a molecule consists of translational, rotational, vibrational and electronic energy

$$E = E_{electronic} + E_{vibrational} + E_{rotational} + E_{translational}$$

Translation energy of a molecule is associated with the movement of the molecule as a whole, for example in a gas. Rotational energy is related to the rotation of the molecule, whereas vibrational energy is associated with the vibration of atoms within the molecule. Finally, electronic energy is related to the energy of the molecule's electrons. Like radiant energy, the energy of a molecule is quantized too and a

molecule can exist only in certain discrete energy levels. Within an electronic energy level a molecule has many possible vibrational energy levels. The vibrational energy of a molecule is not determined by the orbit of an electron but by the shape of the molecule, the masses of the atoms and, eventually by the associated vibronic coupling. For example, simple diatomic molecules have only one bond allowing only stretching vibrations. More complex molecules may have many bonds, and vibrations can be conjugated. The atoms in a CH_2 group [52], commonly found in organic compounds, can vibrate in six different ways: symmetrical and antisymmetrical stretching, scissoring, rocking, wagging and twisting. The major types of molecular vibrations are stretching and bending. The various types of vibrations are illustrated in Fig. 2.16 and Fig. 2.17. Infrared radiation is absorbed and the associated energy is converted into these types of motions. The absorption involves discrete, quantized energy levels. However, the individual vibrational motion is usually accompanied by other rotational motions. These combinations lead to the absorption bands, not the discrete lines, commonly observed in the mid IR region.

Stretching: Change in inter-atomic distance along bond axis. There are two types of Stretching vibrations:

  (a) Symmetrical stretching: The atoms of a molecular either move away or towards the central atoms, but in the same direction.
  (b) Asymmetric stretching: One atom approach towards the central atom while other departs from it.
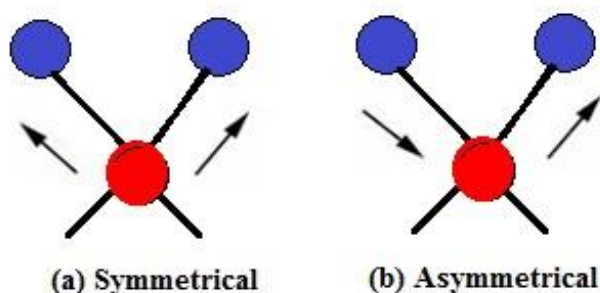
Fig. 2.16 Stretching vibrations.

Bending: Change in angle between two bonds. There are four types of bending:

(i) Rocking, (ii) Scissoring (iii) Wagging, (iv) Twisting.

(i) In plane scissoring (ii) In plane rocking (iii) Out of plane twisting (iv) Out of plane wagging
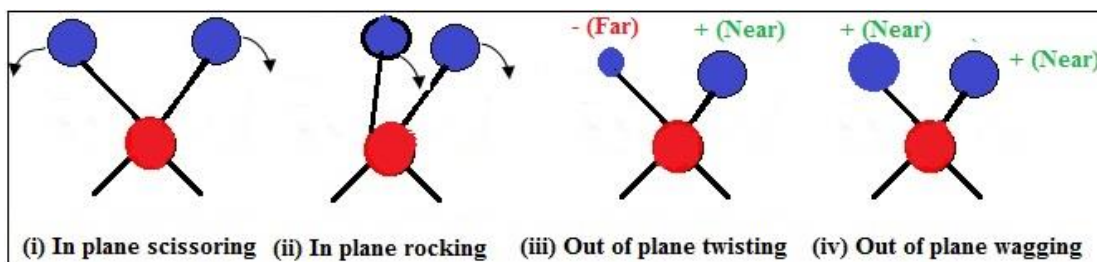
Fig. 2.17 Bending vibrations.

In general, a polyatomic molecule with n atoms has $3n - 6$ distinct vibrations. Each of these vibrations has an associated set of quantum states and in IR spectroscopy the IR radiation induces a jump from the ground (lowest) to the first excited quantum state. Although approximate, each vibration in a molecule can be associated with motion in a particular group [53].

2.6.6 Theory of ultraviolet-visible spectroscopy

The wavelength of light that a compound will absorb is the characteristic of its chemical structure. Specific regions of the electromagnetic spectrum (Fig. 2.18) are absorbed by exciting specific types of molecular and atomic motion to higher energy levels. Absorption of visible and ultraviolet (UV) radiation is associated with excitation of electrons, in both atoms and molecules, to higher energy states. Most molecules required very high energy radiation. Light in the UV-Visible (UV-Vis) region is adequate for molecules containing conjugated electron systems and as the degree of conjugation increases, the spectrum shifts to lower energy.
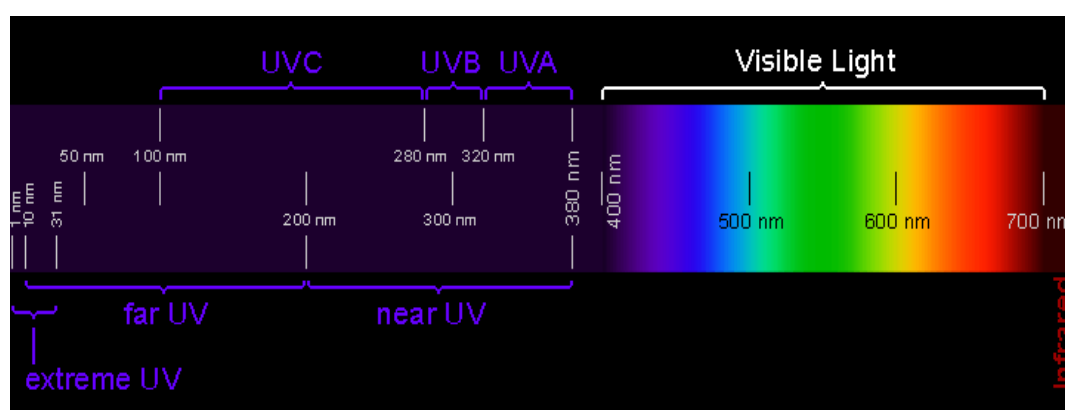
2.18 Light Spectrum.
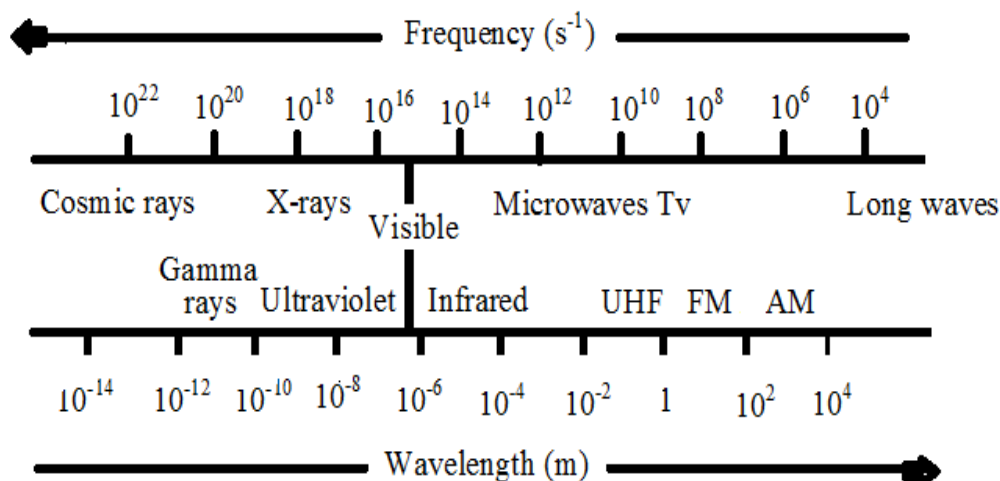
When a molecule absorbs UV-Vis radiation, the absorbed energy excites an electron into an empty, higher energy orbital. This Absorption of UV-Vis radiation in organic molecules is restricted to certain functional groups (chromophores) that contain valence electrons of low excitation energy. The spectra of a molecule containing these chromophores are complex. This is because the superposition of rotational and vibrational transitions on the electronic transitions gives a combination of overlapping lines. This appears as a continuous absorption band.

Possible electronic transitions of π, σ, and **n** electrons (Fig. 2.19) are:

$\boldsymbol{\sigma \to \sigma^*}$ ***transitions*** : An electron in a bonding σ orbital is excited to the corresponding antibonding orbital. The energy required is large. For example, methane (which has only C-H bonds, and can only undergo $\boldsymbol{\sigma \to \sigma^*}$ transitions) shows an absorbance maximum at 125 nm. Absorption maxima due to $\boldsymbol{\sigma \to \sigma^*}$ transitions are not seen in typical UV-Vis. spectra (200 - 700 nm).

$\boldsymbol{n \to \sigma^*}$ ***transitions***: Saturated compounds containing atoms with lone pairs (non-bonding electrons) are capable of $\boldsymbol{n \to \sigma^*}$ transitions. These transitions usually need less energy than $\boldsymbol{\sigma \to \sigma^*}$ transitions. They can be initiated by light whose wavelength is in the range 150 - 250 nm. The number of organic functional groups with $\boldsymbol{n \to \sigma^*}$ peaks in the UV region is small.

$\boldsymbol{n \to \pi^*}$ ***and*** $\boldsymbol{\pi \to \pi^*}$ ***transitions*** : Most absorption spectroscopy of organic compounds is based on transitions of $\boldsymbol{n}$ or $\boldsymbol{\pi}$ electrons to the $\boldsymbol{\pi^*}$ excited state. This is because the absorption peaks for these transitions fall in an experimentally convenient region of the spectrum (200 - 700 nm). These transitions need an unsaturated group in the molecule to provide the $\boldsymbol{\pi}$ electrons.
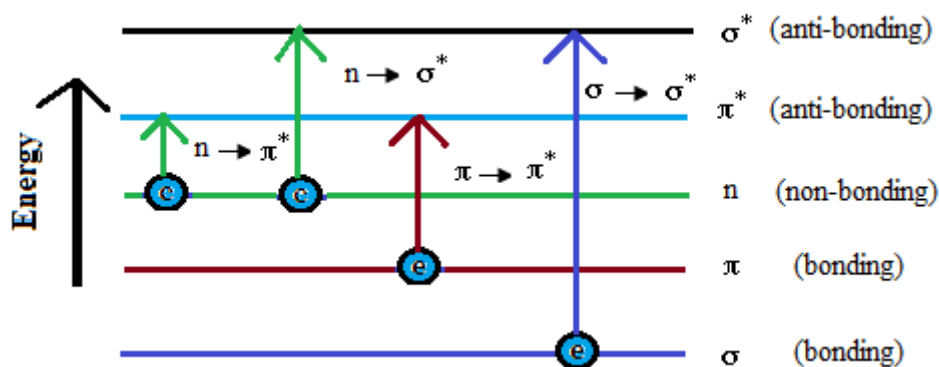
Fig. 2.19 Summary of electronic energy levels.

The solvent in which the absorbing species is dissolved also has an effect on the spectrum of the species. Peaks resulting from $n \rightarrow \pi^*$ transitions are shifted to shorter wavelengths (*blue shift*) with increasing solvent polarity. Often (but *not* always), the reverse (i.e. *red shift*) is seen for $\pi \rightarrow \pi^*$ transitions. This is caused by attractive polarization forces between the solvent and the absorber, which lower the energy levels of both the excited and unexcited states.

2.6.6.1 The Beer-Lambert law

The absorption spectrum can be analyzed by Beer-Lambert law, which governs the absorption of light by the molecules. It states that, "When a beam of monochromatic radiation passes through a homogeneous absorbing medium the rate of decrease in intensity of electromagnetic radiation in UV-Vis region with thickness of the absorbing medium is proportional to the intensity coincident radiation". The general Beer- Lambert law is usually written as:

$$A = \varepsilon\, bc \ldots\ldots\ldots\ldots\ldots\ldots\ldots\ldots\ldots\ldots\ldots\ldots\ldots\ldots\ldots\ldots\ldots\ldots(2.3)$$

If I_o is the intensity of the incident radiation, I is the intensity of the transmitted radiation: $\quad\quad\quad I = I_0 e^{-\alpha d} \ldots\ldots\ldots\ldots\ldots\ldots\ldots\ldots\ldots\ldots\ldots\ldots\ldots\ldots(2.4)$

Where d is the path length of the absorbing species and α is the absorption co-efficient.

(i) Derivation of the Beer-Lambert law

The Beer-Lambert law can be derived from an approximation for the absorption co-efficient for a molecule by approximating the molecule by an opaque disk whose cross-sectional area, σ', represents the effective area seen by a photon of frequency ν.

If the frequency of light is far from resonance, the area is approximately 0, and if v is close to resonance the area is a maximum. Taking an infinitesimal slab, dz, of sample which is shown in Fig. 2.20. I_o is the intensity entering the sample at z=0, I_z is the intensity entering the infinitesimal slab at z, dI is the intensity absorbed in the slab, and *I* is the intensity of light leaving the sample.
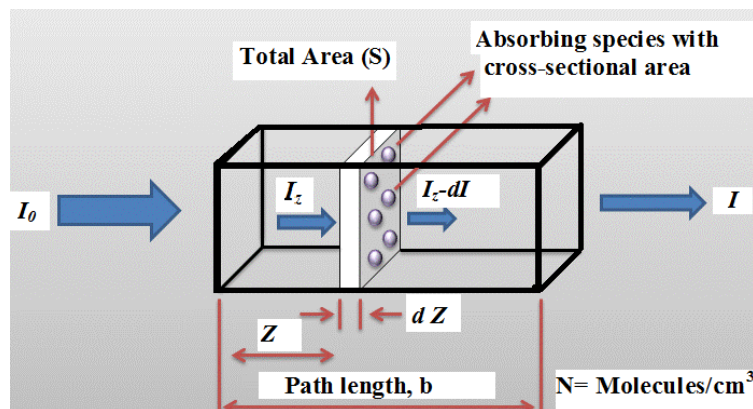
Fig. 2.20 Absorption of light by a sample.

Then the total opaque area on the slab due to the absorbers is, $\sigma' N\, Adz$. Then the fraction of photons absorbed will be $\sigma' N\, Adz/A$ so,

$$\frac{dI}{I_z} = -\sigma' N\, dz \dots\dots\dots\dots\dots\dots\dots\dots\dots\dots\dots\dots\dots\dots\dots\dots\dots\dots\dots\dots\dots(2.5)$$

Integrating this equation from z = 0 to z = b gives:

$$ln(I)\text{-}ln(I_o) = -\sigma' Nb$$

$$or,\ \text{-}ln(I/I_0)= -\sigma' Nb\dots\dots\dots\dots\dots\dots\dots\dots\dots\dots\dots\dots\dots\dots.........(2.6)$$

Since N (molecules / cm^3) (1 mole/6.023×10^{23} molecules) 1000 cm^3 / litre = c (moles/ litre) and $2.303 \times log_{10}(x) = ln(x)$ then

$$\text{-}log_{10}\ (I/I_0) = \sigma'(6.023 \times 10^{23}/2.303)\ cb$$

$$Or,\ \text{-}\ log_{10}\ (I/I_0) = A = \varepsilon\ bc\dots\dots\dots\dots\dots\dots\dots..\dots\dots\dots\dots..\dots\dots.\dots......(2.7)$$

where, $\varepsilon = \sigma'\left(6.023 \times \frac{10^{23}}{2.303}\right) = \sigma'(2.61 \times 10^{20})$ and ε is called the molar absorptivity.

Thus the intensity of the transmitted light can be expressed as $I = I_0 e^{-\alpha d}$ where, d is the path length of the absorbing species and α is the absorption coefficient.

Thus the absorption co-efficient, α [54] can be calculated from the absorption data as; $\alpha = \dfrac{2.303\ A}{d}$; where $A = \log_{10}\left(\dfrac{I_0}{I}\right)$ is the Absorbance. ……………..….............…(2.8)

The relation of extinction co-efficient k with α is

$\alpha = \dfrac{4\pi k}{\lambda}$; where λ is the wavelength.……………………………………….......(2.9)

To estimate the nature of absorption a random phase model is used where the momentum selection rule is completely relaxed. The integrated density of states $N(E)$ has been used and defined by

$$N(E) = \int_{-\infty}^{+\infty} g(E)dE$$ ………………………………………….……….....(2.10)

The density of states per unit energy interval may be represented

$$g(E) = \dfrac{1}{V}\Sigma\, \delta\,(E - E_n)$$ ………………………………………….....….…(2.11)

where, V is the volume, E is energy at which $g(E)$ is to be evaluated and E_n is the energy of the n th state.

If $g_v \propto E^p$ and $g_c(E) \propto (E-E_{opt})^q$, where energies are measured from the valance band mobility edge in the conduction band, and substituting these values into an expression for the random phase approximation, the relationship obtained $v^2 I_2\ (v) \propto (hv\text{-}E_o)^{p+q+1}$, where $I_2(v)$ is the imaginary part of the complex permittivity. If the density of states of both band edges is parabolic, then the photon energy dependence of the absorption becomes $\alpha v \propto v^2\, I_2(v) \propto (hv\text{-}E_{opt})^2$. So for higher photon energies the simplified general equation is

$$\alpha hv = B(hv - E_{opt})^n$$ ………………………………………….……...…(2.12)

where, E_{opt} is the optical band gap energy, hv is the energy of absorbed light, n is the parameter connected with distribution of the density of stales and B is the proportionality factor. The index n equals *1/2* and *2* for allowed direct transition and indirect transition energy gaps respectively [55].

Thus, from the straight-line plots of $(\alpha h v)^2$ versus $h v$ and $(\alpha h v)^{1/2}$ versus $h v$ the direct and indirect energy gaps of insulators and/or dielectrics can be determined.

2.6.6.2 Direct and indirect optical transitions

Materials are capable of emitting visible luminescence when subjected to some form of excitation such as UV light.

(a) Direct - gap materials.   (b) Indirect - gap materials.
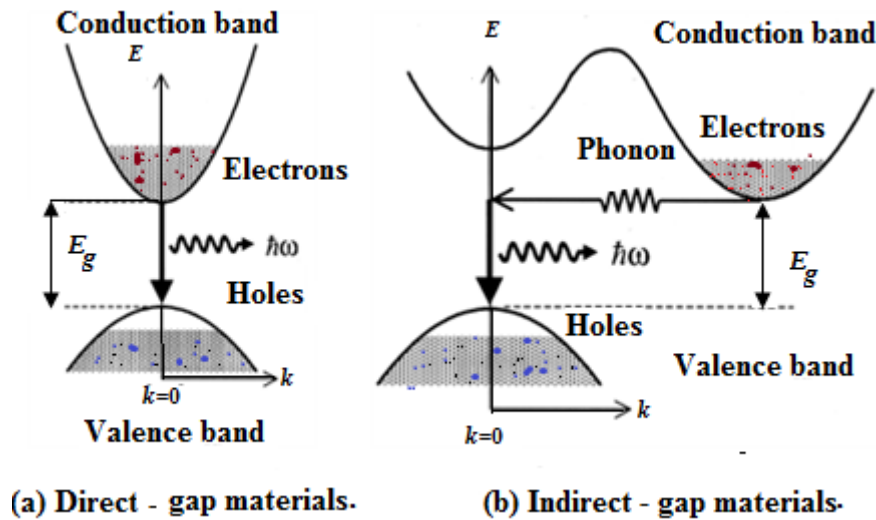
Fig. 2.21 Schematic band diagrams for the photoluminescence processes in (*a*) a direct gap materials, (*b*) an indirect gap materials.

The *E-k* diagrams for a direct band gap material and an indirect gap material is schematically illustrated in Fig. 2.21, where *E* and *k* are respectively the kinetic energy and wave vector of the electron or hole ($E = k^2 \hbar^2 / 2m$, where $\hbar = h / 2\pi$ and *m* is the electron or hole effective mass) [56].

The shaded states at the bottom of the conduction band and the empty states at the top of the valence band respectively represent the electrons and holes created by the absorption of an UV or visible photon with an energy $\hbar \omega_{exc}$ exceeding the band gap E_g of the material, an electron-hole pair is created and the electron (hole) is excited to states high up in the conduction (valence) band.

In a direct gap material (Fig. 2.21 *a*), the conduction band minimum and the valence band maximum occur at the same *k* values which implies that the electron wave vector should not change significantly during a photon absorption process i.e., $\hbar \vec{k}_i + \hbar \vec{k}_{phot} \approx \hbar \vec{k}_i = \hbar \vec{k}_f$, since the wave vector of the absorbed photon $\vec{k}_{phot}$ is

negligible compared to the electron wave vector. This is represented by photon absorption and emission processes by vertical arrows on *E-k* diagrams.

In contrast, for an indirect band gap material (Fig. 2.21 b), of which the conduction band minimum and the valence band maximum have different *k* values, conservation of momentum implies that the photon absorption process must be assisted by either absorbing (indicated by a "+" sign) or emitting (indicated by a "-" sign) a phonon (a quantum of lattice vibration), because the electron wave vector must change significantly in jumping from the valence band in state (E_i, $\vec{k}_i$) to a state (E_f, $\vec{k}_f$) in the conduction band, and the absorption of a photon alone cannot provide the required momentum change since $\left|\vec{k}_{phot}\right| << \left|\vec{k}_i - \vec{k}_f\right|$.

2.6.6.3 UV-Vis spectrophotometer

In this work a dual-beam UV-Vis spectrophotometer is used and a schematic diagram of the dual-beam UV-Vis spectrophotometer is given in Fig. 2.22. The functioning of this instrument is relatively straightforward. A beam of light from a visible and/or UV light source is separated into its component wavelengths by a prism or diffraction grating. Each monochromatic (single wavelength) beam in turn is split into two equal intensity beams by a half-mirrored device. One beam, the sample beam (colored magenta), passes through a small transparent container (cuvette) containing a solution of the compound being studied in a transparent solvent. The other beam, the reference (colored blue), passes through an identical cuvette containing only the solvent. The intensities of these light beams are then measured by electronic detectors and compared. The intensity of the reference beam, which should have suffered little or no light absorption, is defined as I_0. The intensity of the sample beam is defined as I. Over a short period of time, the spectrometer automatically scans all the component wavelengths in the manner described. The ultraviolet (UV) region scanned is normally from 200 to 400 nm, and the visible portion is from 400 to 800 nm.
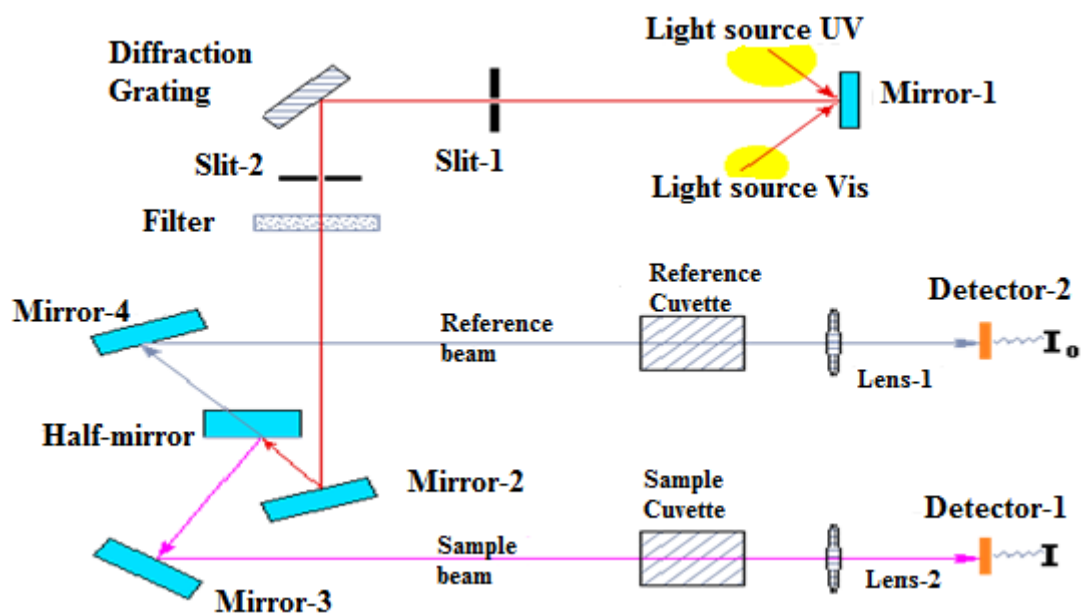
Fig. 2.22 Schematic diagram of a dual-beam UV-Vis spectrophotometer.

If the sample compound does not absorb light of a given wavelength, $I = I_0$. However, if the sample compound absorbs light then Iis less than I_0, and this difference may be plotted on graph absorption versus wavelength. Absorption may be presented as transmittance ($T = I/I_0$) or absorbance ($A = log\ I_0/I$). If no absorption has occurred, $T = 1.0$ and $A = 0$. Most spectrometers display absorbance on the vertical axis, and the commonly observed range is from 0 (100% transmittance) to 2 (1% transmittance). The wavelength of maximum absorbance is a characteristic value, designated as λ_{max}.

2.6.6.4 Urbach tail analysis

In 1953, Urbach [57] proposed an empirical rule for the optical absorption co-efficient (α) associated with the electronic transition from the valence to conduction band tail in disordered solids. This rule states that $\alpha = \alpha_0\ exp\ (hv/E_u)$ where α_0 is a constant and E_u is the Urbach energy. The models for the explanation of the Urbach tail are the density of states of the electron band at the absorption edge [58]. The disorder giving rise to the exponential band tails is produced by lattice vibration, impurities and other deviations from the perfect periodicity of the lattice. The thermal and structural disorder are additive and suggests that the disorder is a fundamental factor in the optical band gap. In the case of crystalline semiconductors the width of the exponential tail is a direct measurement of the temperature independent component of Urbach edge.

2.7 DC Electrical Conduction Mechanism

Electrical properties of insulating polymers are there responses when an electric field is applied to them. The subject of electrical properties of polymers covers an extremely diverse range of molecular phenomena. In contrast to metals, in which the electrical field response is one of electronic conduction, polymers may respond in a more varied manner, and a whole set of delicate electrical effects may be observed. No known polymer is completely free of conduction processes, however small the quantity of charge carriers it may possess. Low level conduction in insulating polymers can take a variety of forms. Conduction may very often be contributed by impurities that provide a small concentration of charge carriers in the form of electrons or ions. At high fields, the electrodes may inject new carriers (holes and electrons) into polymers. At very high fields, these and other processes will lead to complete breakdown of polymers as insulating materials. The imposition of an electrical field upon a polymer will cause a redistribution of any charges in the polymer, provided they are mobile enough to respond in the time scale in the applied field. If some of the mobile charges are able to diffuse throughout the specimen and charge migration through the electrode sample interface is possible, then the charges will support a dc conductance. It should be mentioned that the vacuum-deposited thin film insulators can contain a large density of both impurity and trapping centers. A well-judged study of electrical conduction in vacuum deposited thin films cannot be accomplished without consideration of these possibilities. A power law [25] can express the variation of current density with voltage in a material generally:

$$J \propto V^n \ldots\ldots\ldots\ldots\ldots\ldots\ldots\ldots\ldots\ldots\ldots\ldots(2.13)$$

where, n is a power factor. When n is unity, the conduction is ohmic. If the value of n is less or more than unity, then the conduction process is other than ohmic.

Many scientists have investigated three worth-mentioning electrical conduction mechanisms which are operative in the thin films of various organic compounds:

➢ The injection of carriers from the electrode by means of thermal or field assisted emission usually referred to as Schottky emission.

➢ The other process in which carriers are produced by the dissociation of donor-acceptor centers in the bulk of the material, is called Poole-Frenkel generation.

➢ If the generation process is slower than transport by the carriers through the material, the conduction is controlled by generation, specifically by either the Schottky, or Poole-Frenkel (PF) mechanism. Conversely, when the transport is slower than generation, it constitutes the rate-determining step, and the conduction is described by the theory of space-charge-limited current (SCLC). The phenomenon is, if a charge is injected at the electrode polymer interface, a large excess carrier density at the injecting electrode will exist and a space-charge-limited current will flow. A brief explanation of these conduction mechanisms is stated below.

2.7.1 Schottky mechanism

Charge injected from a metal to an insulator or semiconductor at medium fields may take place by field-assisted thermionic emission, a process known as Richardson-Schottky effect or simply Schottky emission. This is a procedure of image force induced lowering potential energy for charge carrier emission when an electric field is applied. The potential step changes smoothly at the metal insulator interface as a result of the image force. This happens when the metal surface become polarized (positively charged) by an escaping electron, which in turn exerts an attractive force

$$F_{im} = -\frac{e^2}{16\pi\varepsilon_0\varepsilon' x^2}$$ on the electron.

The potential energy of the electron due to the image force is thus

$$\emptyset_{im} = -\frac{e^2}{16\pi\varepsilon_0\varepsilon' x} \dots\dots\dots\dots\dots\dots\dots\dots\dots\dots\dots\dots\dots\dots\dots\dots(2.14)$$

where, x is the distance of electron from the electrode surface.

The potential step at a neutral barrier with attendant image potential as a function of the distance x from the interface is given by,

$$\emptyset(x) = \emptyset_0 + \emptyset_{im} = \emptyset_0 - \frac{e^2}{16\pi\varepsilon_0\varepsilon' x} \dots\dots\dots\dots\dots\dots\dots\dots\dots\dots\dots\dots(2.15)$$

where, ϕ_0 = Coulombic barrier height of the electrode-polymer interface in Schottky conduction. The barrier potential $\phi(x)$ in the presence of image forces is illustrated by the line AB in Fig. 2.23. Schottky assumed that the image force holds only for x greater than some critical distance x_0. For $x < x_0$, he assumes a constant image force,

i.e. the potential energy is a linear function of x, and such that it matches the bottom of the electrode conduction band at the surface.

When an electric field exists at a metal-insulator interface, it interacts with the image force and lowers the potential barrier. The line CD represents the potential due to a uniform applied field. The dotted line represents the potential $\Delta\phi_s$, when the potential due to a uniform electric field is added to the barrier potential $\phi\ (x)$ and thus it is lower than that of without the electric field. Under the influence of the field the potential energy of the barrier with respect to Fermi level of the electrode can be given by

$$\emptyset(x = \emptyset_0 - \frac{e^2}{16\pi\varepsilon_0\varepsilon'x} - eFx \dots\dots\dots\dots\dots\dots\dots\dots\dots\dots\dots\dots\dots(2.16)$$
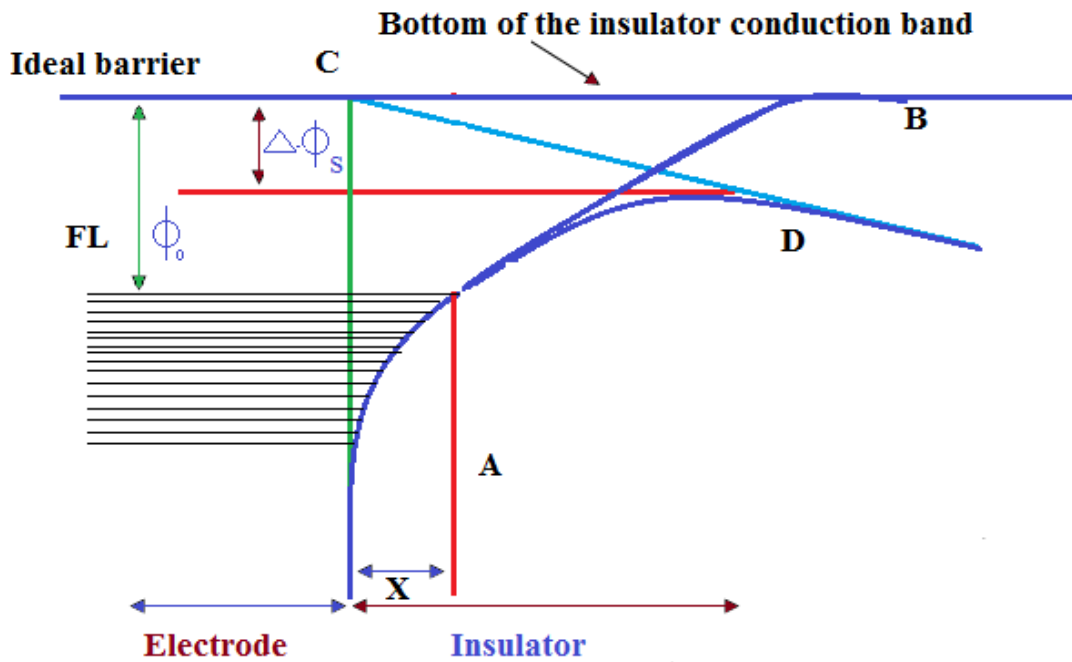
Fig. 2.23 Schottky effect at a neutral contact.

This equation has a maximum at $x_m = \left(\frac{e}{16\pi\varepsilon'\varepsilon_0\ F}\right)^{1/2}$. Therefore, the change $\Delta\emptyset_s = \emptyset_0 - \emptyset(x_m)$ in the barrier height due to the interaction of the applied field with the image potential can be given by

$$\Delta\emptyset_s = \left(\frac{e^3}{4\pi\varepsilon_0\varepsilon'}\right)^{1/2} F^{1/2} \equiv \beta_s F^{1/2} \dots\dots\dots\dots\dots\dots\dots\dots\dots\dots\dots(2.17)$$

Because of image force lowering of the barrier, the electrode limited current does not saturate according to the Richardson law, $J = AT^2 exp(-\frac{\emptyset_0}{kT})$ ………..…..(2.18) but rather obeys the Richardson-Schottky law,

$$J = AT^2 exp(-\frac{\emptyset_0 - \Delta\emptyset}{kT})$$ ……………………………....……………….(2.19)

$$J = AT^2 exp(\frac{\beta_s F^{1/2} - \emptyset_0}{kT})$$ ……………………..…..………………..…….(2.20)

where, $A = 4\pi em(kT)^2/h^2$ is the Richardson constant, F = static electric field and is equal to V/d, V = applied voltage, d = film thickness, T = Temperature in Kelvin, k = Boltzmann constant and β_s is the Schottky coefficient which is given by,

$$\beta_S = \left(\frac{e^3}{4\pi\varepsilon_0\varepsilon'}\right)^{1/2}$$ ……………………….…………………………….…….(2.21)

where, e = elementary charge of the electron and ε' is the high frequency dielectric constant of the material. The electrode limited Richardson-Schottky effect in insulators appears to have been first observed by Emptage and Tantraporn, who reported a *log I* vs. $F^{1/2}$ relationship in their samples. It was suggested that the plot should have to be linear in nature for Schottky type conduction mechanism [59, 60].

2.7.2 Poole-Frenkel mechanism

The Poole- Frenkel (PF) conduction mechanism is a field assisted thermal ionization process and is the bulk analogue of the Schottky effect at an interfacial barrier. This effect is lowering of a Coulombic potential barrier when it interacts with an electric field, as shown in Fig. 2.24. The PF lowering of a Coulombic barrier $\Delta\phi_{PF}$ in a uniform electric field is twice that due to the Schottky effect at a neutral barrier, because the potential energy of an electron in a Coulombic field $-\frac{e^2}{4\pi\varepsilon_0\varepsilon x}$ is four times that due to image force effects in Schottky mechanism; i.e.

$$\Delta\emptyset_{PF} = 2\Delta\emptyset_s = 2\left(\frac{e^3}{4\pi\varepsilon_0\varepsilon'}\right)^{1/2} F^{1/2} \equiv \beta_{PF} F^{1/2}$$…………………………..(2.22)

where, β_{PF} is PF coefficient.
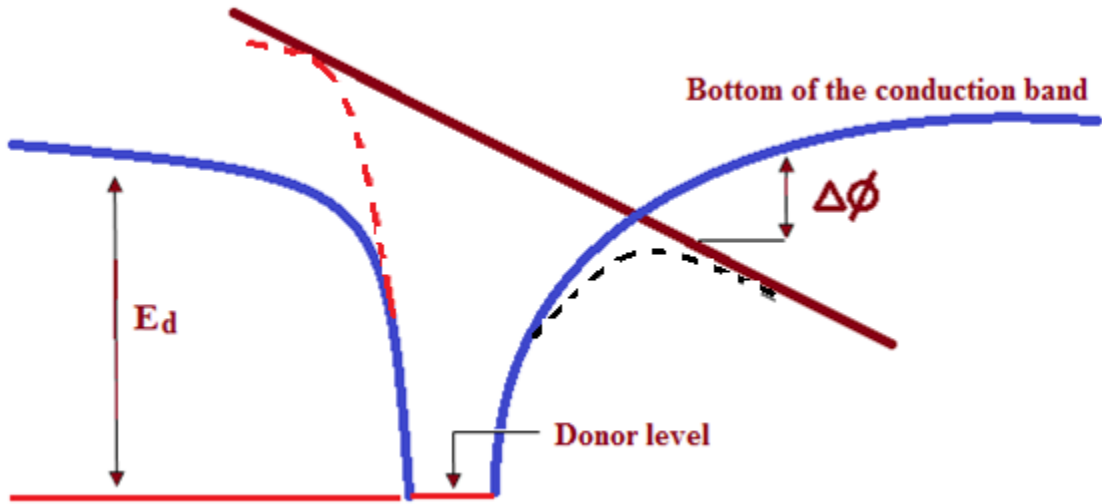
Fig. 2.24 Poole-Frenkel effect at a donor center.

From this we can conclude that $\beta_{PF} = 2\left(\dfrac{e^3}{4\pi\varepsilon_0\varepsilon'}\right)^{1/2} = 2\beta_S$ ....(2.23)

i.e. $2\beta_S = \beta_{PF}$..(2.24)

In the bulk limited PF mechanism, the thermal emission of trapped carriers from the bulk material gives rise to conductivity $J = \sigma_0 F\, exp(\dfrac{\beta_{PF}F^{1/2}-\phi_c}{kT})$ ....(2.25)

where, ϕ_c is the ionization potential of the PF centers. Consequently, a general expression of the form: $J = J_0\, exp(\dfrac{\beta F^{1/2}-\phi}{kT})$ ....(2.26)

holds equally well for both Schottky and PF mechanisms. Where, J is the current density at a biased voltage. By taking natural logarithms of equation (2.26) we can write, $\beta_{exp} = skTd^{1/2}$...(2.27)

where, β_{exp} denotes the value of β obtained experimentally and $s = \dfrac{\Delta lnJ}{\Delta V^{\frac{1}{2}}}$ is the slope of graph plotted between ln J and $V^{1/2}$.

2.7.3 Space charge limited conduction mechanism

When an Ohmic contact is made to the insulator, the space charge injected into the conduction band of the insulator is capable of carrying current and when the transport is slower than generation, it constitutes the rate-determining step, and the conduction is described by the theory of space-charge-limited current (SCLC) [9].
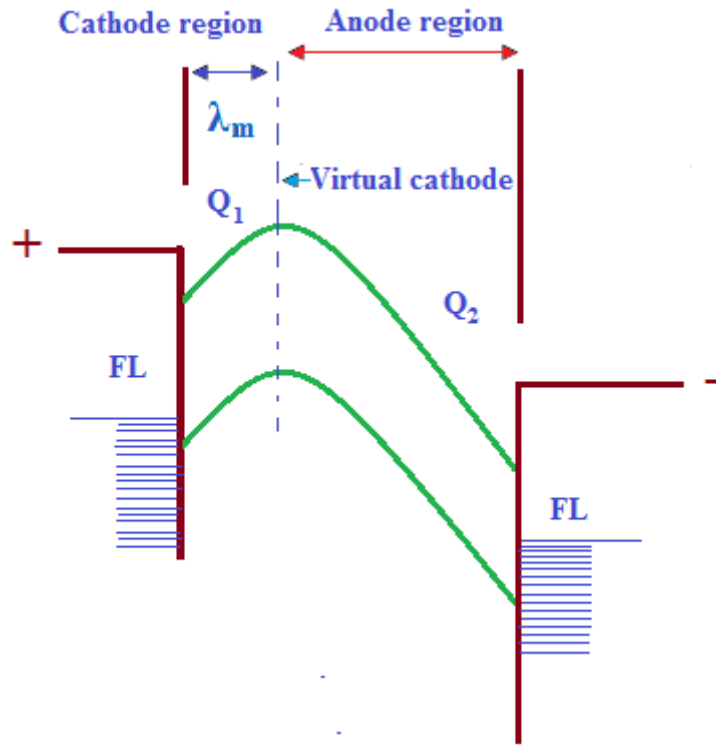
Fig. 2.25 Energy diagram for different regions under space charge limited conduction mechanism.

When a voltage bias is applied to the metal electrodes, this results an addition of positive charge to the anode and negative charge to the cathode. If now the voltage bias increases, the net positive charge on the anode increases and that on the cathode decreases. Assuming that the anode region extends throughout the insulator and neglecting the diffusion effect the current can be interpreted by the Mott and Gurney

[65] relation: $J = \dfrac{9\mu\varepsilon'\varepsilon_0 V^2}{8d^3}$……………….…………………….……….….(2.28)

Where, μ is the mobility of charge carriers, ε is dielectric constant, ε_0 is the permittivity of free space, V is the applied voltage and d is the thickness.

If the insulator contains N_t shallow traps positioned an energy E_t below the conduction band then the free component of the space charge

$\rho_f = eN_c \, exp(-\dfrac{E_F}{kT})$……………………….…….………………….......(2.29)

and trapped component of space charge

$\rho_t = eN_t \, exp(-\dfrac{E_t}{kT})$……………………………………...…….….(2.30)

thus trapping factor, θ is defined as $\theta \equiv \dfrac{\rho_f}{\rho_t} = \dfrac{N_c}{N_t}\, exp(-\dfrac{E_t}{kT})$ ………..……......(2.31)

where, N_c is the effective density of states in the conduction band, and N_t the density of trapping levels situated at an energy, E_s below the conduction band edge.

The SCLC current density with traps is defined by

$$J = \frac{9\mu\varepsilon'\varepsilon_0 V^2}{8d^3}\,\theta$$ …………………..………………….………...……….………......(2.32)

For a shallow trap SCLC and trap-free SCLC, $\theta = 1$. According to equation (2.32), J varies as d^1 in the Ohmic region and as d^3 in the SCLC region for the trap-filled SCLC part.

For a fixed V, the dependence of ln J on ln d should be linear with slope $l \geq$ -3.

Lampert calculated the voltage at which the transition from the Ohmic to shallow trap SCLC region (V_{tr}) occurs is given by $V_{tr} = \dfrac{8}{9}n_0\,\dfrac{ed^2}{\varepsilon}$ …………………….…………..(2.33)

where, volume generated free carrier density, n_0 is independent of both μ and J [61].

According to Fig. 2.26 it was found that the second linear region would extend up to a certain voltage, called as the crossover voltage, and beyond which the current would vary with the voltage as a power law: $I \propto V^2$ ………………………….(2.34)

which would continue until the current is close to the saturation current, i.e. the maximum current that the electrode could supply. However in real samples which contain several trap sites to capture the electrons that had been injected inside the sample. There are two types of traps; the ones above the Fermi level are the shallow traps, and the others below the Fermi level being the deep traps. During trapping both shallow and deep traps would get filled.

The voltage at which all the traps would get completely filled is called the trap filled limit (TFL). Beyond V_{TFL} all the excess charges would be injected into the conduction band and the current would approach the trap free square law as described in equation (2.34) [59, 60].
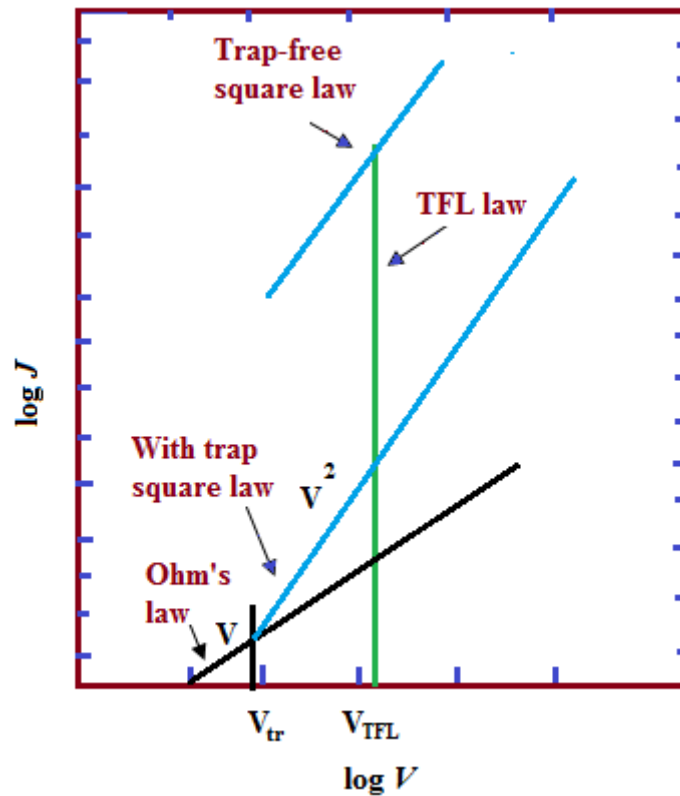
Fig. 2.26 Space charge limited conduction characteristic for an insulator containing shallow traps.

2.7.4 Thermally Activated Conduction Processes

Electronic conduction in organic, molecular compounds differs in several important ways from the more familiar kind in metals and semiconductors. An important feature of the band system is that electrons are delocalized and spread over the lattice. Some delocalization are naturally expected when an atomic orbital of any atom overlaps appreciably with those of more than one of its neighbors, but delocalization reaches an extreme form in the case of a regular 3 dimensional lattice. The band theory assumes that the electrons are delocalized and can extend over the lattice. When electronic conduction is considered in polymers, band theory is not totally suitable because the atoms are covalently bonded to one another, forming polymeric chains that experience weak intermolecular interactions. But macroscopic conduction will require electron movement, not only along the chain but also from one chain to another. If two solids are put in contact, the Fermi levels equalize at the interface, the other energy levels moving to accommodate this. In pure insulator the Fermi level bisects the forbidden band. Impurities may introduce allowed levels into the forbidden band, and this moves the Fermi level up and down.

As the temperature is increased the charge carrier concentration increases strongly with temperature. This dominates the temperature dependence of the conductivity, giving it an Arrhenius-like character. It is difficult to generalize about the temperature dependence of DC conduction whether it is ionic or electronic since so many processes are possible. Ohmic (low field) conduction whether ionic or electronic, the dependence of current density, *J* on temperature is given by

$$J = J_0 \, exp(-\frac{\Delta E}{kT}) \quad \text{...(2.35)}$$

where, J_0 is the current density at thermal equilibrium and *ΔE* is the activation energy for carrier conduction. Now,

$$J = Ne\mu \quad \text{...(2.36)}$$

where, *N* is the number of charge carriers, *e* is their charge, and *μ* is their mobility. With extrinsic electronic conduction, the electrons may move by hopping. However, if the electronic conduction is by excitation into the conduction band, the production of free electrons, n not their mobility, μ is activated. Whatever the Ohmic mechanism, a log *J* vs. *1/T* plot (Arrhenius plot) will usually exhibit increasing linear slopes (activation energies) as *T* is raised [60]. For variable range hopping the electrical conductivity is given by

$$\sigma = \sigma_0 exp\{-\left(\frac{T_0}{T}\right)^{\frac{1}{d+1}}\} \quad \text{...(2.37)}$$

where, "*d*" is the dimensionality of transport, σ is the conductivity, σ_o is the initial value of conductivity, *T* is the absolute temperature and T_o is the activation energy in terms of temperature.

In bulk material ionic conduction occurs due to the drift of defect under the influence of an applied electric field. The degrees of ionic impurities that may be totally ignored in the context of other properties may have a significant effect on conductivity.
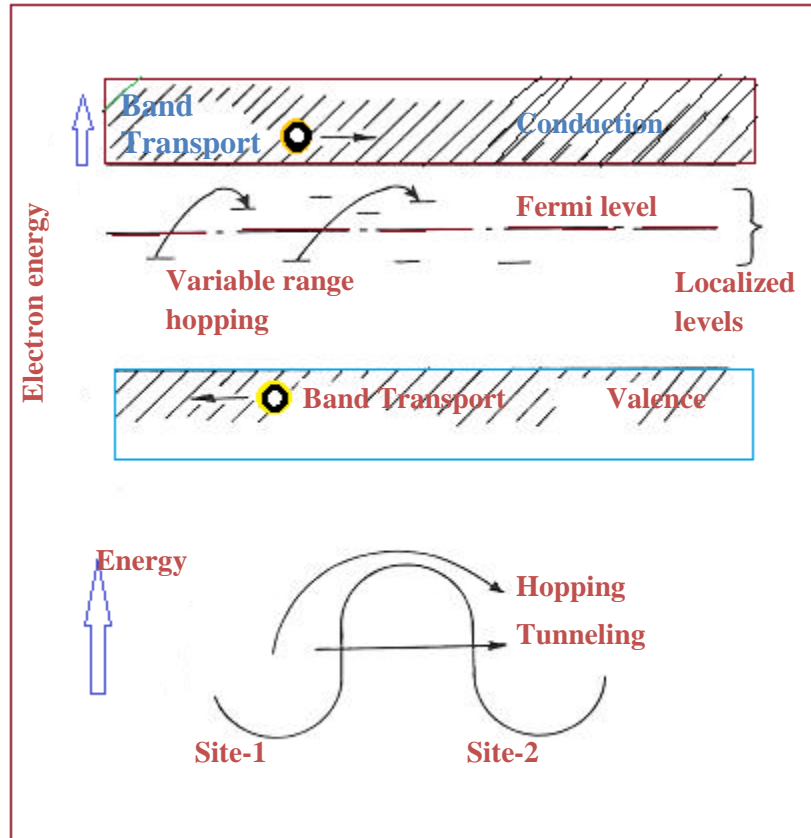
Fig. 2.27 Diagram of electron-transfer mechanisms between adjacent sites separated by a potential-energy barrier.

A theoretical expression maybe derived for the current density,

$$J = sin\ h\ (\ eaE/2kT) \quad \dots\dots\dots\dots\dots\dots\dots\dots\dots\dots\dots\dots\dots..(2.38)$$

where, E is the electric field, a is the distance between neighboring potential wells, e is the electronic charge.

CHAPTER III

EXPERIMENTAL DETAILS

3.1 Introduction

This chapter deals with the plasma polymerization scheme of methyl acrylate (MA) which includes the details of monomer, substrate, capacitively coupled glow discharge plasma polymerization set up for polymer formation. The techniques applied for characterization of thin films, such as FESEM, DTA, FTIR, for structural, UV-visible spectroscopy for optical, DC measurements for electrical characterization are discussed in details.

3.2 Sample Preparation

The Monomer and formation of polymer

The liquid monomer methyl acrylate which is colorless liquid used as organic precursor in this investigation was purchased from the VWR International Ltd, Poole, BH15 1TD, England. Chemical structure of monomer (methyl acrylate) is shown in Fig. 3.1. In the plasma polymerization process, the monomer methyl acrylate was pumped into the vacuum chamber where it is polymerized by plasma to from a thin and clear coating. The starting monomers were converted into gases phase in evaporation and pumped into the vacuum chamber where the polymerization process was launched by glow discharge. The excited electrons generated onto the glow discharge helped to ionize the monomer molecules which are fragmented to create free electrons, ions, excited molecules and radicals and were absorbed, condensed and polymerized onto the glass substrates. Finally, with the deposited molecules, the electrons and ions were cross-linked to form chemical bonds and dense-hard polymer films.
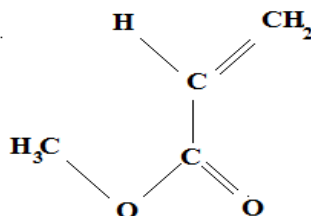
Fig. 3.1 The chemical structure of methyl acrylate ($C_4H_6O_2$).

Some properties of methyl acrylate

(i) Methyl acrylate is an organic compound with the formula: $CH_2CHCO_2CH_3$.

(ii) It is the methyl ester of acrylic acid.

(iii) It is a colorless liquid with a characteristics acrid odor. It is mainly produced to make acrylate fiber.

(iv) Molecular Formula: $C_4H_6O_2$.

(v) Density: 950 kg/m³.

(vi) Molar mass: 86.09 g/mol.

(vii) Boiling point: 176 °F (80 °C).

(viii) IUPAC ID: Methyl prop-2-enoate.

(ix) Melting point: -101 °F (−74 °C).

3.3 Substrate Materials and its Cleaning Process

The substrates used prewashed glass slides (25.4 mm ×76.2 mm ×1.2 mm) of Sail Brand, China, purchased from local market. The samples were prepared by depositing the PPMA thin films and electrodes onto them. To get a homogeneous, smooth and flawless thin polymer film, which is a common property of plasma polymers, it is essential to make the substrate as clean as possible using acetone and distilled water in an ultrasonic bath. The clean glass plates were next rinsed with de-ionized water and then dried by a drier.

3.4 Capacitively Coupled Plasma Polymerization Setup

A glow discharge is a kind of plasma and the plasma polymerization setup has been used enormously in recent years to form various kinds of plasma polymers. Different configuration of polymerization set up varies the properties of plasma polymers i.e. the geometry of the reaction chamber, position of the electrodes, nature of input power etc. The glow discharge plasma polymerization setup which was used to deposit the PPMA thin films consists of the components.

(i) Plasma reaction chamber

(ii) Electrode system

(iii) Pumping unit

(iv) Vacuum pressure gauge

(v) Input power for plasma generation

(vi) Monomer injection system

(vii) Flow meter

3.5 Generation of Glow Discharge Plasma in the Laboratory

Glow discharges are produced by an applied static or oscillating electric field where energy is transferred to free electrons in vacuum.

1. High voltage power supply
2. Pirani gauge
3. High tension leads
4. Gas inlet valve
5. Gauge head
6. Monomer injection valve
7. Flow meter
8. Monomer container
9. Pyrex glass dome
10. Electrodes stands
11. Gasket
12. Lower flange
13. bottom flange
14. Brass tube
15. Valve
16. Rotary pump
17. Switch
18. Variac
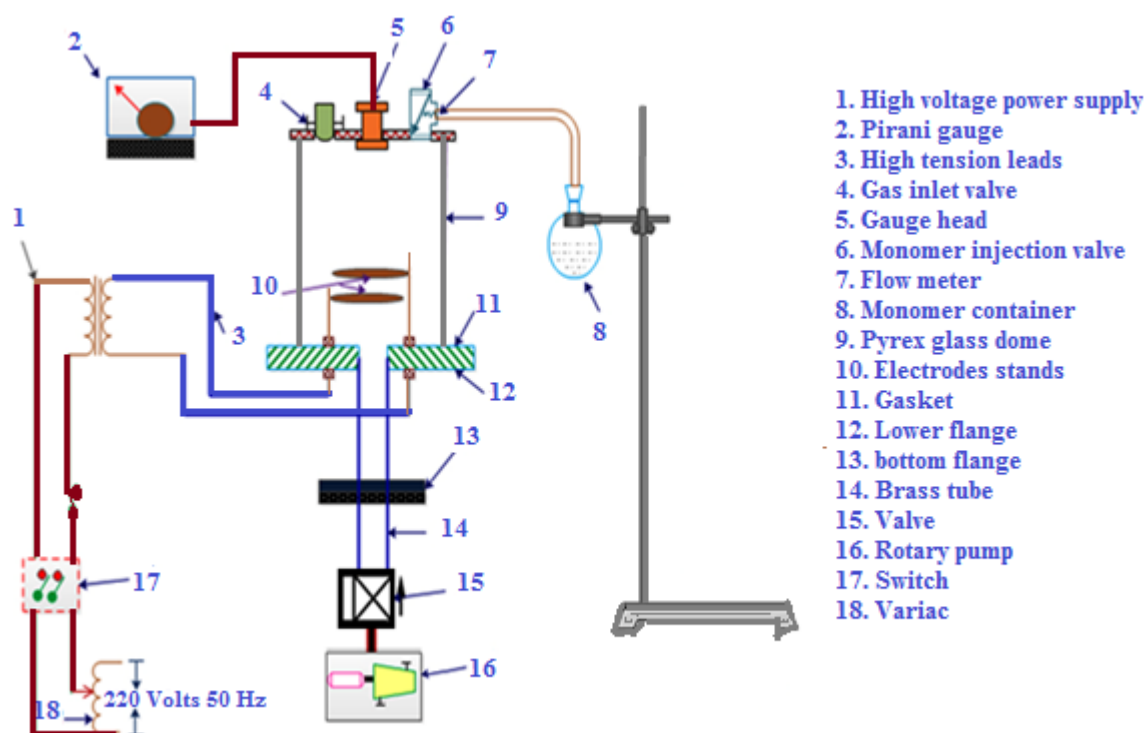
Fig. 3.2 Schematic diagram of the plasma polymerization set up.

In elastic collisions of the energetic free electrons with the gas molecules generated free radicals, ion, and species in electronically excited states. This process also generates more free electrons, which is necessary for a self-sustaining glow The

excited species produced are very active and can react with the surfaces of the reactors as well as themselves in the gas phase. The chamber of the glow discharge reactor is evacuated to about 1 Pa. A high-tension transformer along with a variac is connected to the feed-through attached to the lower flange. While increasing the applied voltage, the plasma is produced across the electrodes at around 13 Pa chamber pressure.

3.6 Deposition of Plasma Polymerized Thin Films

The important feature of glow discharge plasma is the non-equilibrium state of the overall system. In the plasmas considered for the purpose of plasma polymerization, most of the negative charges are electrons and most of the positive charges are ions. Due to large mass difference between electrons and ions, the electrons are very mobile as compared to the nearly stationary positives ions and carry most of the current. Energetic electrons as well as ions, free radicals, vacuum ultraviolet light can possess energies well in excess of the energy sufficient to break the bonds of typical organic monomer molecules which range from approximately 3 to 10 eV. Some typical energy of plasma species available in glow discharge as well as bond energies encounter at pressure of approximately 1 Pa [5]. After finding the desired plasma glow in the reactor the monomer vapor is injected downstream to the primary air glow plasma for some time.

Fig. 3.3 The plasma polymerization chamber.

Incorporation of monomer vapor changed the usual color of plasma into a light bluish color. Figure 3.3 is the photograph of light bluish color monomer plasma in the plasma reactor. The deposition time was varied from 45-90 minutes to get the PPMA

thin films of 70 to 260 nm thick. The optimization condition of thin film formation for the present study is:

Separation between two electrodes	3.9 cm
Position of the substrate	Lower electrode
Deposition power	35 W
Base Pressure in the reactor chamber	About 1.33 Pa
Pressure in the reactor during deposition	About 13.3 Pa
Deposition time	45-90 minutes
Line frequency	50 Hz

3.7 Optimization of PPMA Thin Films Deposition Condition

In order to determine the appropriate experimental parameters that would result in desired deposition of PPMA thin films, the thickness of the thin films deposited at different powers are considered. It is seen from Fig. 3.4 that at 22 W the plasma is low to gain the film thickness properly and at 28 W plasma is high enough causing slower deposition of the thin films with increasing time. In view of above observations, PPMA thin films were prepared at 35 W plasma powers for investigation. After attaining the optimized condition for glow discharge the monomer vapor from a monomer container flowed through a fine needle valve attached to the upper flange and connected to a flow meter (Glass Precision Engineering Ltd, Meterate, England) at the flow rate of about 20 cm^3/ min [10]. The deposition time was varied from about 45 to 90 minutes to get the film thickness ranging from 120 nm to 290 nm.
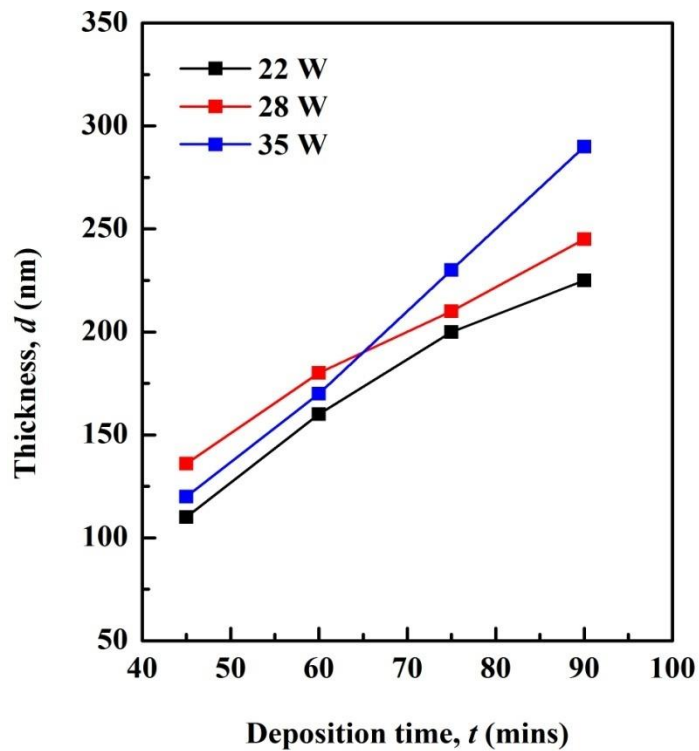
Fig. 3.4 Thickness of the films as a function of deposition time at different optical power for the PPMA thin films.

3.8 Measurement of thickness of the thin films

Thickness is the single most significant film parameter. Any physical quantity related to film thickness can in principle be used to measure the film thickness. It may be measured either by several methods with varying degree of accuracy. The methods are chosen on the basis of their convenience, simplicity and reliability. Since the film thickness are generally of the order of a wavelength of light, various types of optical interference phenomena have been found to be most useful for measurement of film thickness. Several of the common methods are:

(i)   Multiple-beam interferometry, (Tolansky Fezeau fringes method, Fringes of equal   chromatic order, Donaldson method etc.).

(ii)   Michelson interferometer.

(iii)   Using a hysteresis graph and other order methods used in film-thickness determination with particular reference to their relative merits and accuracies.

3.8.1 Multiple-Beam interferometry

This method utilizes the resulting interference effects when two silvered surfaces are brought close together and are subjected to optical radiation. This interference technique, which is of great value in studying surface topology in general, may be applied simply and directly to film-thickness determination. When a wedge of small angle is formed between unsilvered glasses plates, which are illuminated by monochromatic light, broad fringes are seen arising from interference between the light beams reflected from the glass on the two sides of the air wedge. At points along the wedge where the path difference is an integral and odd number of wavelengths, bright and dark fringes occur respectively. If the glass surface plates are coated with highly reflecting layers, one of which is partially transparent, then the reflected fringe system consists of very fine dark lines against a bright background. A schematic diagram of the multiple-beam interferometer along with a typical pattern of Fizeau fringes from a film step is shown in Fig. 3.5. As shown in the figure, the film whose thickness is to be measured is over coated with a silver layer to give a good reflecting surface and a half-silvered microscope slide is laid on top of the film whose thickness is to be determined. A wedge is formed by the two microscopic slides, a light multiple reflected between the two silvered surfaces forms an interference pattern with a discontinuity at the film edge as shown in Fig. 3.5. A travelling microscope measure the step height and width of the Fizeau fringes that are formed due to interference of light reflected from the air/film surface and film/substrate interfaces, where the optical path difference between successive beams is an integral number of wavelengths.

The thickness of the film "d" [62] can be determined by the relation

$$d = \frac{\lambda}{2} \frac{b}{a}$$ …….…………………………………...(3.1)

where, λ is the wavelength of the monochromatic sodium light source, $\frac{b}{a}$ is the fractional discontinuity identified in the figure.
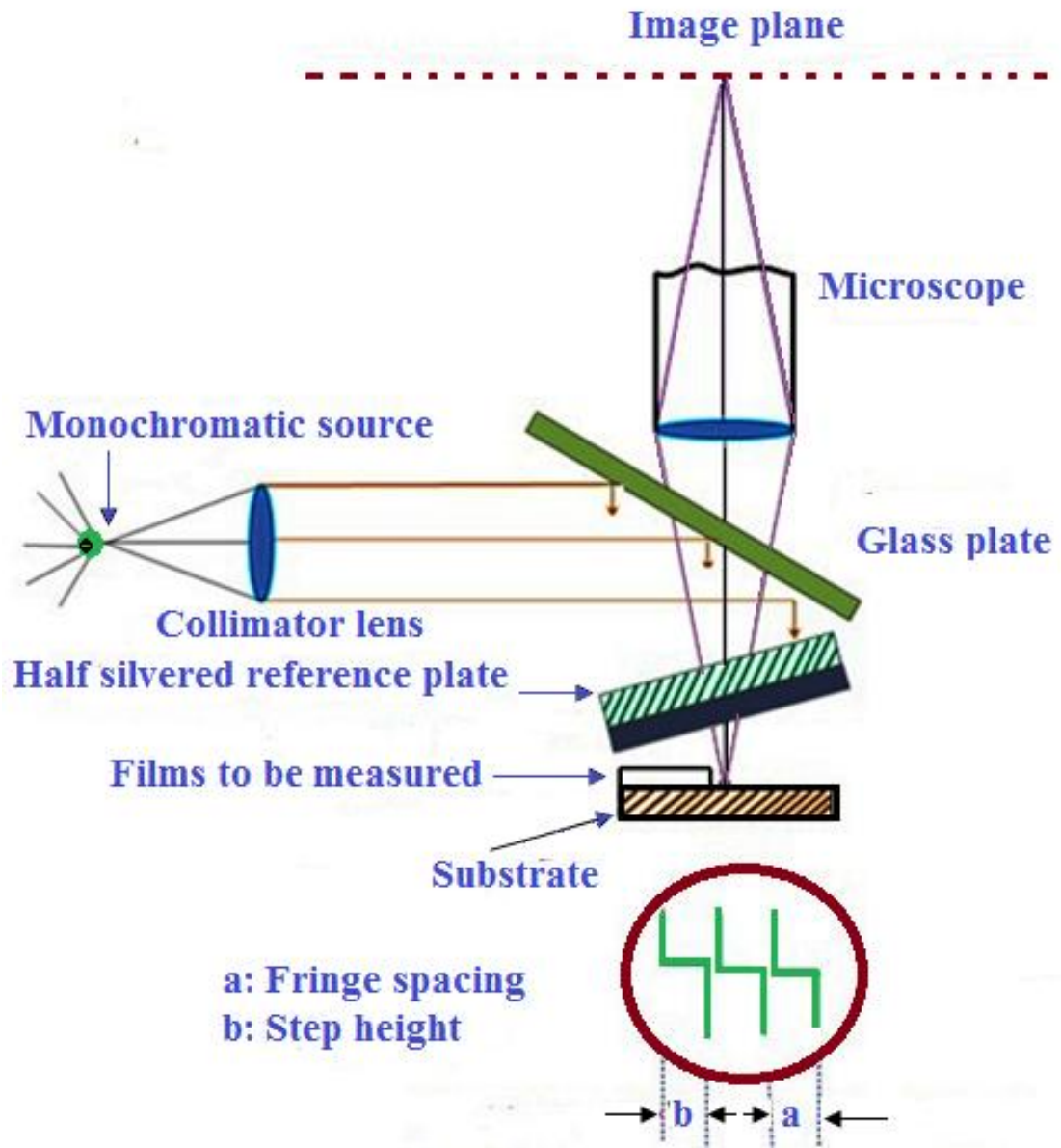
Fig. 3.5 Interferometer arrangements for producing reflection Fizeau fringes of equal thickness.

In conclusion it might be mentioned that the Tolansky method of film-thickness measurement is the most widely used and in many respects also the most accurate and satisfactory one.

3.8.2 Measurement of Thickness of the PPMA Thin Films

Mutiple-Beam Interferometry technique was employed for the measurement of thickness of the PPMA thin films. A travelling microscope (Fig. 3.6) is used for this purpose. For film thickness measurement a separate glass slide is used in addition to

the sample substrates. Two irons disks attached with screws were used for the formation of the wedge small angle between two glass samples. To generate the step of the PPMA thin film onto the glass substrate, Teflon tape was used to cover 50% area of the cleaned glass, which was not exposed to plasma environment during plasma polymerization. After deposition, the Teflon tape was carefully removed from the glass slide and placed under the microscope. The Fizeau pattern is generated from the surface of the glass slide was used to measure the film thickness. A monochromatic sodium light source of wavelength, $\lambda = 589.3$ nm was used for the measurement of thickness. The thickness of the film "d" is determined according to the relation in equation 3.1.

Fig. 3.6 Multiple Beam Interferometric set-up in the laboratory.

3.9 Contact electrode for electrical measurements

3.9.1 Electrode material

Aluminium (Al) (purity of 4 N British Chemical Standard) was used for electrode deposition. Al has been reported to have good adhesion with glass slides. Al film has advantage of easy self-healing burn out of flaws in sandwich structure.

3.9.2 Electrode deposition

Electrodes were deposited using a vacuum coating unit (Hind High Vacuum Company, Bangalore, India) Model 12A4D which is a versatile laboratory model coating unit for thin film applications with facilities for evaporation, glow discharge cleaning etc. The system was evacuated by an oil diffusion pump backed by an oil rotary pump. The chamber could be evacuated to a pressure less than 10^{-5} Torr. The glass substrates with mask were supported by a metal rod 0.1 m above the tungsten filament. For the electrode deposition Al was kept on the tungsten filament. The filament was heated by low-tension power supply of the coating unit. The low-tension power supply was able to produce 100 A current at a potential drop of 10 V. During evacuation of the chamber by diffusion pump, the diffusion unit was cooled by the flow of water. When the penning gauge reads about 10^{-5} Torr, the Al on tungsten filament was heated by low-tension power supply until it was melted. The Al was evaporated, thus lower electrode onto the glass slide was deposited. Al coated glass substrates were taken out from the vacuum coating unit and were placed on the middle of the lower electrode of the plasma deposition chamber for methyl acrylate thin film deposition under optimum condition. The top Al electrode was also prepared on the PPMA film as described in Fig. 3.7 to Fig. 3.8.

Fig. 3.7 Hind High Vacuum coating unit.
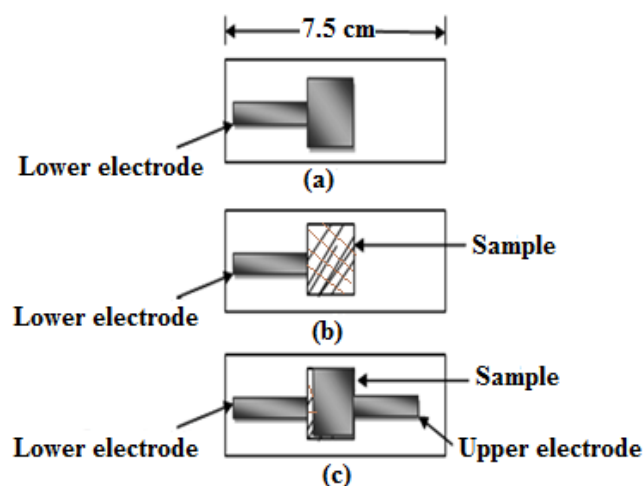
Fig. 3.8 (a) Lower electrode, (b) Lower electrode and the sample, (c) Sample in between the lower and upper electrodes.

3.10 Characterizing Instruments and Measurements

3.10.1 Differential thermal analysis and thermogravimetric analysis

Thermogravimetric analysis or thermal gravimetric analysis (TGA) is a method of thermal analysis in which changes in physical and chemical properties of materials are measured as a function of increasing temperature. TGA is commonly used to determine selected characteristics of materials that exhibit either mass loss or gain due to decomposition, oxidation, or loss of volatiles (such as moisture) . TGA and DTA were taken in air and nitrogen environment using a computer controlled TGA/DTA 6300 system connected to an EXSTAR 6000 station, Seiko Instruments Inc., Japan which is shown in Fig. 3.9. The TGA/DTA model uses a horizontal system balance mechanism. The heating rate was 10 K/min in air. The PPMA powder was controlled from the substrate surface. During tracing Alumina was used as the reference material.

Fig. 3.9 TGA/DTA Instruments (Model: EXSTAR 6000 station, Seiko Instruments Inc., Japan).

3.10.2 Field emission scanning electron microscopy

For FESEM and EDX analyses, PPMA thin films were deposited onto a small piece of chemically cleaned glass substrates. The PPMA thin films were coated with a thin layer of platinum by ion sputtering method (Model: JFC 1600, Auto Fine Coater).

Then sample holder was mounted on a holder and inserted in FESEM. The FESEM and EDX analyses were performed by a field emission scanning electron microscope, FESEM (JEOL JSM 7600F) which is shown in Fig. 3.10. Micrographs were taken at various spots of the samples and at different magnifications for microstructural study.

3.10.3 Energy dispersive X-ray analyses

Energy Dispersive X-ray Spectroscopy (EDS or EDX) is an emerging chemical microanalysis technique used in conjunction with field emission scanning electron microscopy (FESEM). The EDX technique detects x-rays emitted from the sample during bombardment by an electron beam to characterize the elemental composition of the analyzed volume. Features or phases as small as 1μm or less can be analyzed.

Fig. 3.10 FESEM instruments (Model: JEOL JSM 7600F) with an Auto Fine Coater (Model: JFC 1600).

When the sample is bombarded by the FESEM's electron beam, electrons ejected from the atoms comprising the sample's surface. The resulting electron vacancies are filled by electrons from a higher state, and X-ray is emitted to balance the energy difference between the two electron's states. The x-ray energy is characteristics of the element from which it was emitted. EDX systems include a sensitive x-ray detector, a liquid nitrogen dewar for cooling, and software to collect and analyze energy spectra. The compositional analysis was performed for the same samples by EDX.

3.10.4 Attenuated total reflectance - fourier transform infrared spectroscopy

The ATR-FTIR analysis of PPMA thin films was carried out by a double beam (Bruker Alpha ATR-FTIR) spectrophotometer which is shown in Fig. 3.11. All the spectra were recorded in transmittance mode in the wave number range from 4000 to 600 cm^{-1}. ATR generally allows qualitative analysis of samples with little sample preparation. For ATR-FTIR spectroscopic analysis, powder of PPMA was collected from the substrate surface by scrapping method. The sample for ATR-FTIR measurements was prepared by potassium bromide (KBr) disk technique. Between 1 and 3 mg of ground material needs to be mixed thoroughly with about 350 mg of ground KBr. The mixture is now shifted to a die that has a barrel diameter of 13 mm.

Fig. 3.11 ATR-FTIR instruments   Fig. 3.12 UV-Vis spectrophotometer
 (Model: Bruker Alpha ATR-FTIR).   (Model: Shimadzu UV-1601, Japan).

Then placing the thick sample on the ATR crystal (Diamond Miracle) and applying pressure generates a nearly perfect result. The total analysis time for the thick polymer and chemical by ATR was less than 1 minute. The FTIR spectra of the MA and PPMA were recorded in transmittance (%) mode. The FTIR spectrum of methyl acrylate (MA) liquid monomer was also recorded by putting the liquid monomer in a KBr measuring cell.

3.10.5 Ultraviolet visible spectroscopy

The optical properties of the PPMA thin films deposited onto uncoated glass substrates having a dimension of 18mm × 18mm × 2 mm were studied by UV-Visible spectroscopic measurement. The optical absorption measurement of PPMA thin films

was made in the wavelength range from 250 to 500 nm, at room temperature. The absorption spectra were recorded for PPAM thin films of thickness 70, 150, 210 and 260 nm. A blank glass slide was used as the reference during the optical absorption measurements. UV-Vis analysis was performed by a dual beam (Shimadzu UV-1601, Japan) UV-Vis spectrophotometer which is shown in Fig. 3.12.

3.10.6 Current density-voltage (*J-V*) Measurement

The current density- voltages (J-V) characteristics of the PPMA thin films of different thickness were studied in Al/PPMA/Al configuration with an effective Al electrode area of 10^{-4} m^2 at room temperature. Al (Purity 4 N, British chemical standard) was used as the metal electrode. The Al electrode was deposited on to the substrate through a mask by evaporating it from a tungsten filament to form the base electrode in a conventional metal coating unit (Edward 306, England, UK) at a pressure of about 1.33×10^{-3} Pa.
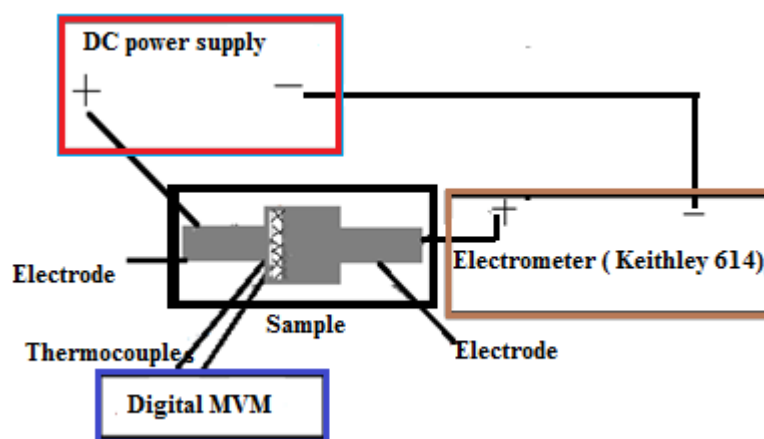
Fig. 3.13 Schematic diagram of DC electrical measurement.

Then PPMA thin film was deposited on the lower Al electrode through a square shaped mask $(1.5 \times 1.5) \times 10^{-4}$ m^2 to form the PPMA thin film. The substrate was taken out of the reactor to deposit the upper Al electrode. The current across the thin films was measured by a high impedance electrometer (Model: 614, Keithley Instruments Inc., USA) and DC voltage was supplied step by step by a stabilizer DC power supply (Model: 6545A, Agilent, Japan). The capacitance of the samples was measured by a low frequency analyzer (Model: 4192A, Agilent Technologies Japan Ltd., Tokyo, Japan). The DC measurement set up is shown in Fig. 3.13. The thermally activated current or the temperature dependence of current across the PPMA thin films was measured at the
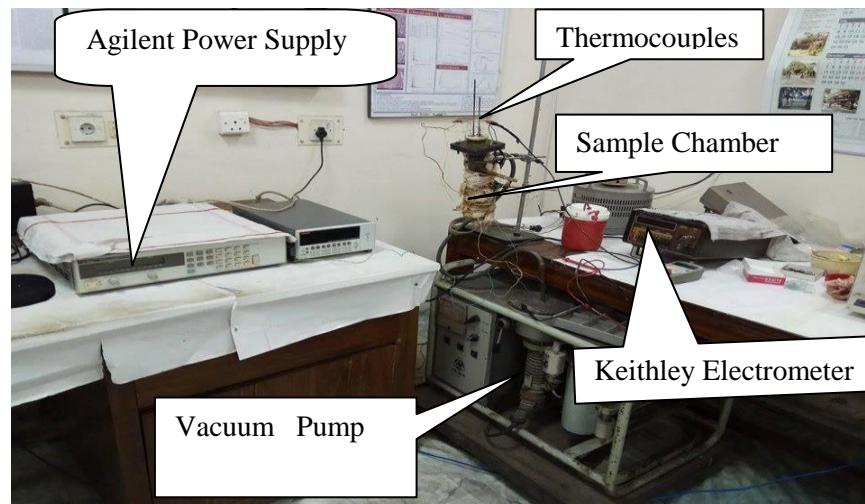
Fig. 3.14 Arrangement for DC electrical measurement.

applied voltages of 8 and 60 using the above mentioned electrometer. The measurements were performed 298 to 398 K. For these measurements the samples were heated by a heating coil which was wrapped around the specific chamber. The temperature was measured by a Chromel-Alumel (Cr-Al) thermocouple placed very close to the sample which was connected to a 197A digital microvolt (DMV) meter. The block diagram for DC measurements is shown in Fig. 3.14.

CHAPTER IV

RESULTS AND DISCUSSION

4.1 Introduction

This chapter includes the studies of thermal properties, surface structure, chemical structure and optical absorption of PPMA thin films by means of DTA, TGA, DTG; FESEM, EDX; FTIR and UV-Vis spectroscopic analyses, respectively. The DC electrical properties of PPMA thin films are also studied by DC electrical measurements.

4.2 Differential Thermal, Thermogravimetric and Differential Thermogravimetric Analyses

The DTA, TGA, and DTG were used to characterize the decomposition and the thermal stability of the PPMA. The DTA, TGA and DTG curves taken for PPMA in the temperature range of 309–850 K at a scan rate of 10 K/min in air and in N_2 environment which can be divided into three regions namely A, B, and C for different stages of thermal changes as shown in Fig. 4.1 and 4.2.

4.2.1 PPMA in air environment

Fig. 4.1 represents the DTA, TGA and DTG curves of PPMA powder samples in air environment. The TGA curve shows that the weight losses, which actually occur due to heating, in A, B and C regions are 2.73 %, 8.75 %, and 77.26 %, respectively and remaining weight is 11.26 % which are recorded in Table 4.1. In region A, the 2.73 % weight loss up to 343 K may be due to removal of small amount of absorbed water or moisture in PPMA. The corresponding DTA trace shows a small peak in this region. In region B, up to temperature 534 K in TGA curve with a weight loss of about 8.75 % which may be occurred due to the removal of some unreacted monomers or oligomers. In region C, the thermal decomposition/breakdown reaction of PPMA is observed as a large weight loss of about 77.26 % from 534 K to about 767 K in TGA trace and corresponding DTG trace has indicated the same phenomenon by a medium size peak. DTA trace shows that in region C, two-stage degradation reaction might have taken place which is represented by two exothermic peaks at the temperatures 564 K and 650 K. DTG trace also shows that in region C two stage degradation reactions represented by two exothermic peaks at the temperature 559 K and 650 K. This two-stage decomposition reaction might have occurred due to the evolution of low molecular weight hydrocarbon compounds.

Thus, it can be seen that the thermal stability of PPMA in air environment is up to 534 K.
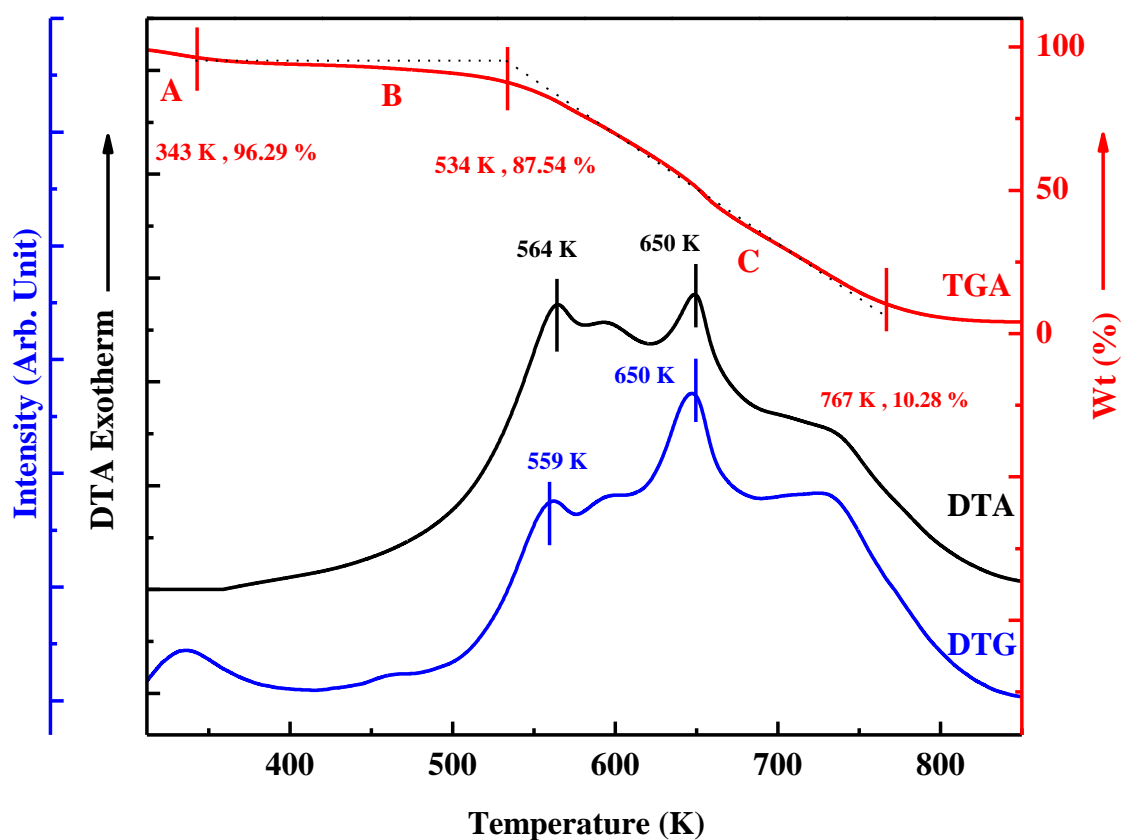

Fig. 4.1 DTA, TGA and DTG thermograms of PPMA in air environment.

4.2.1 PPMA in N_2 environment

Fig. 4.2 represents the DTA, TGA and DTG curves of PPMA powder samples in N_2 environment. The TGA curve shows that the weight losses, which actually occurs due to heating, in A, B and C regions are 1.1 %, 3.68 %, and 30.8%, respectively and remaining weight is 64.43 % which are recorded in Table 4.1. In region A, the 1.08 % weight loss up to 337 K may be due to removal of some amount of water or moisture in PPMA. The corresponding DTA and TGA traces show a small peak in this region. In region B, up to temperature 543 K in TGA curve with a weight loss of about 3.68 % which may be occurred due to the removal of some unreacted monomers or oligomers. In region C, the thermal decomposition of PPMA is observed as a large weight loss of about 30.81% from 543 K to about 820 K. In TGA trace and corresponding DTG trace has indicated the same phenomenon by a broad peak.
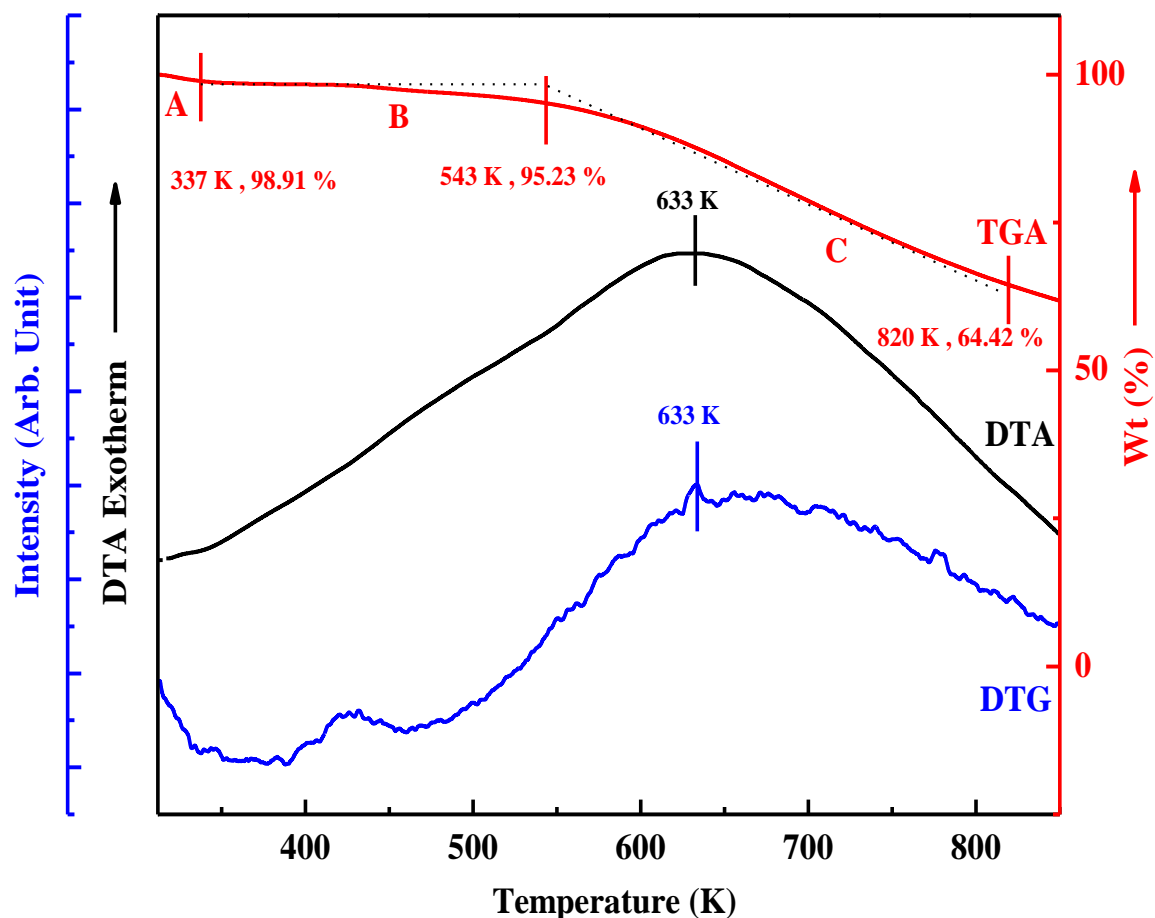
Fig. 4.2 DTA, TGA and DTG thermograms of PPMA in N_2 environment.

In DTA curve, a broad exothermic peak is seen during long time which might have occurred due to evolution of low molecular weight hydrocarbon compounds. Thus it can be seen that the thermal stability of PPMA thin films in nitrogen environment is up to 543 K.

Table 4.1 TGA and DTA analysis for PPMA thin films at different temperature.

Region	Traces	Air	N_2
A	TG Wt loss (%)	2.73 %	1.1 %
	DTA at Temp. (K)	343	337
B	TG Wt loss (%)	8.75 %	3.68 %
	DTA at Temp. (K)	534	543
C	TG Wt loss (%)	77.26 %	30.8 %
	DTA at Temp. (K)	650	633
Stability Temperature (K)		534	543

Fig. 4.3 Comparison of weight loss of PPMA in air and N_2 environments.

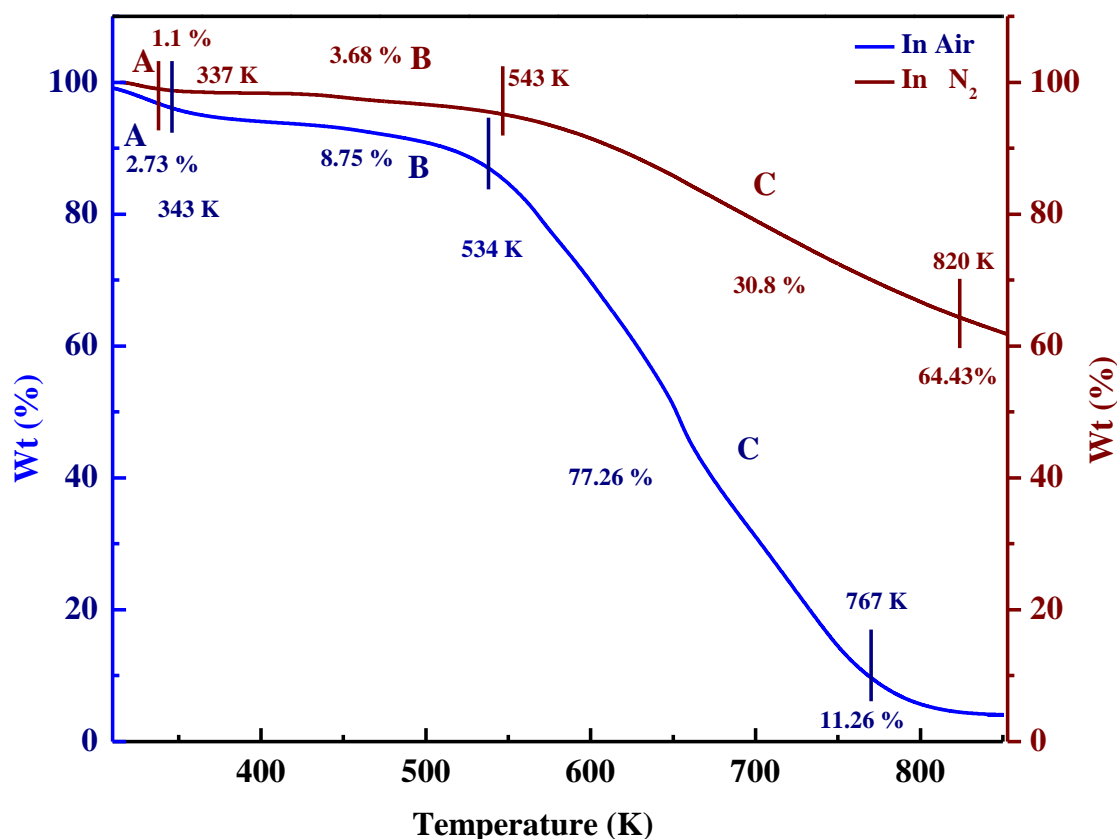Fig. 4.3 demonstrates the curves of TGA curves of PPMA powder samples in air and N_2 environments. For air, the weight losses, which actually occur due to heating, in A, B and C regions are 2.73 %, 8.75 %, and 77.26 %, respectively and remaining weight is 11.26 % whereas for N_2 environment, the weight losses in A, B and C regions are 1.1 %, 3.68 %, and 30.8 %, respectively and remaining weight is 64.43 %. So the weight loss in air is greater than N_2 environment. For air and N_2 environment, the maximum weight losses are occurred in 650 K and 633 K, respectively.

4.3 Field Emission Scanning Electron Microscopy

The FESEM micrographs of PPMA thin films of thicknesses 170, 220, and 290 nm were recorded at various points with magnifications ×50 k, ×100 k and ×150 k at accelerating voltage of 10 kV and are shown in Fig. 4.4, Fig. 4.5 and Fig. 4.6, respectively. It is observed that the surface features of the PPMA thin films become clear with the magnification ×150 k. It is seen that the film with the lower thickness has clear clusters/agglomeration like structure separated by boundaries whereas this feature diffuses with the increase of thickness.

Fig. 4.4 FESEM micrographs of PPMA thin films of thickness (a) 170 nm with ×50 k.
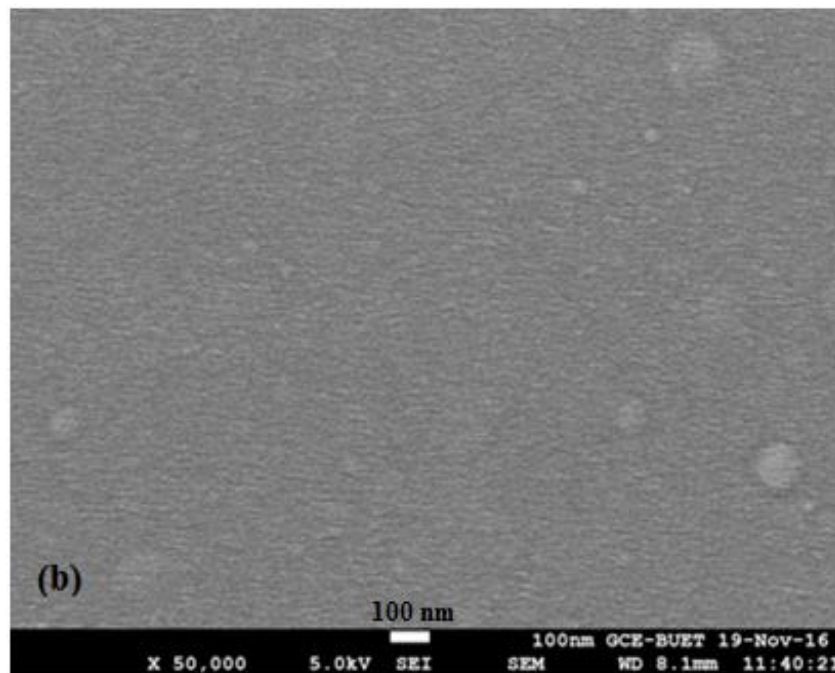
Fig. 4.4 FESEM micrograph of PPMA thin films of thickness (b) 220 nm with ×50 k.
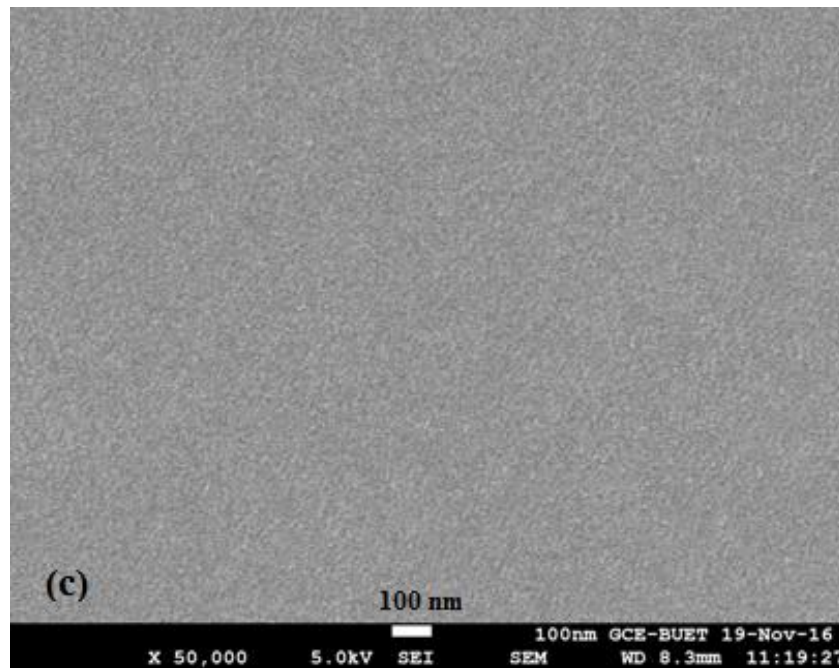
Fig. 4.4 FESEM micrograph of PPMA thin films of thickness(c) 290 nm with ×50 k.
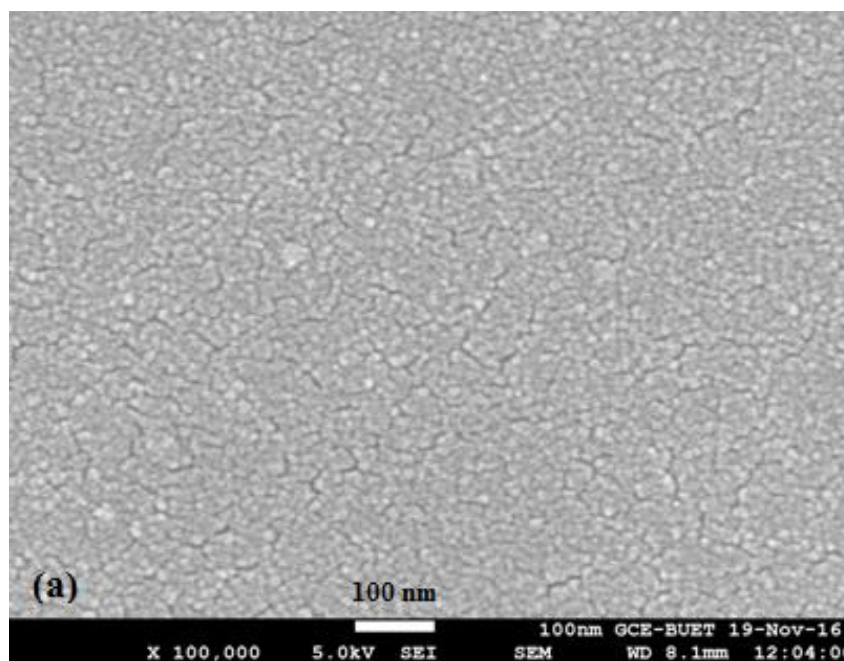
Fig. 4.5 FESEM micrograph of PPMA thin films of thickness (a) 170 nm with ×100 k
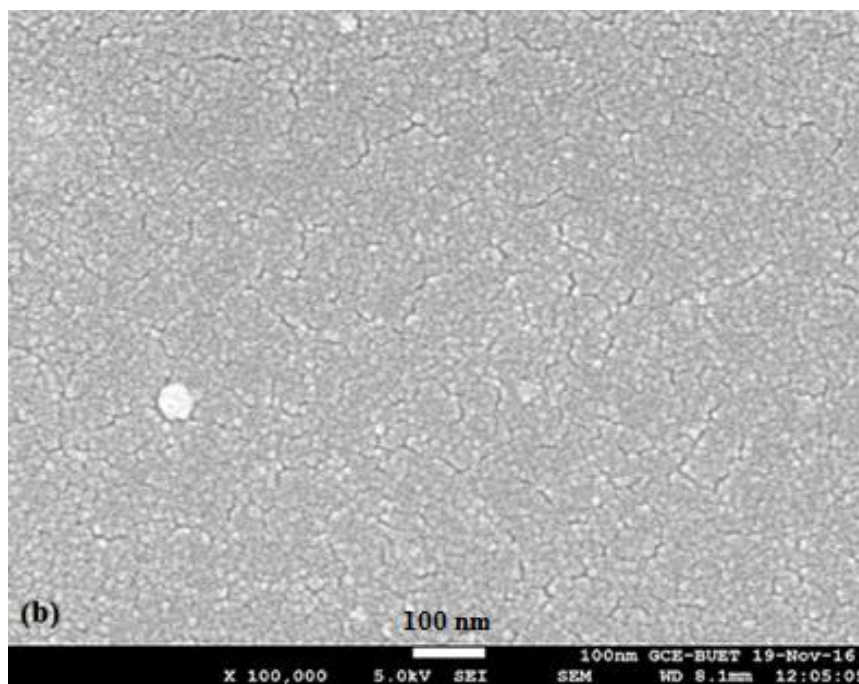
Fig. 4.5 FESEM micrograph of PPMA thin films of thickness (b) 220 nm with ×100 k
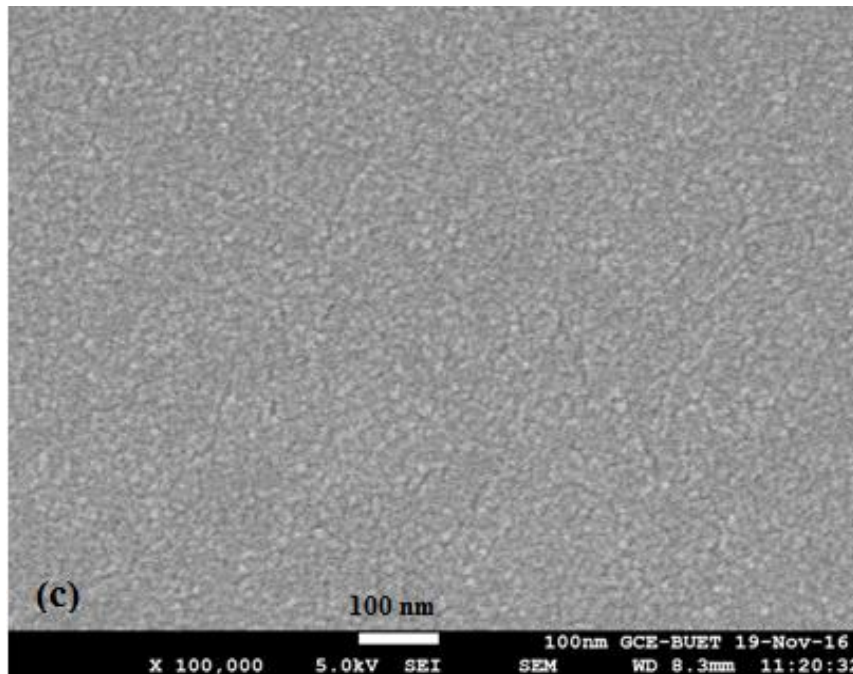
Fig. 4.5 FESEM micrograph of PPMA thin films of thickness(c) 290 nm with ×100 k
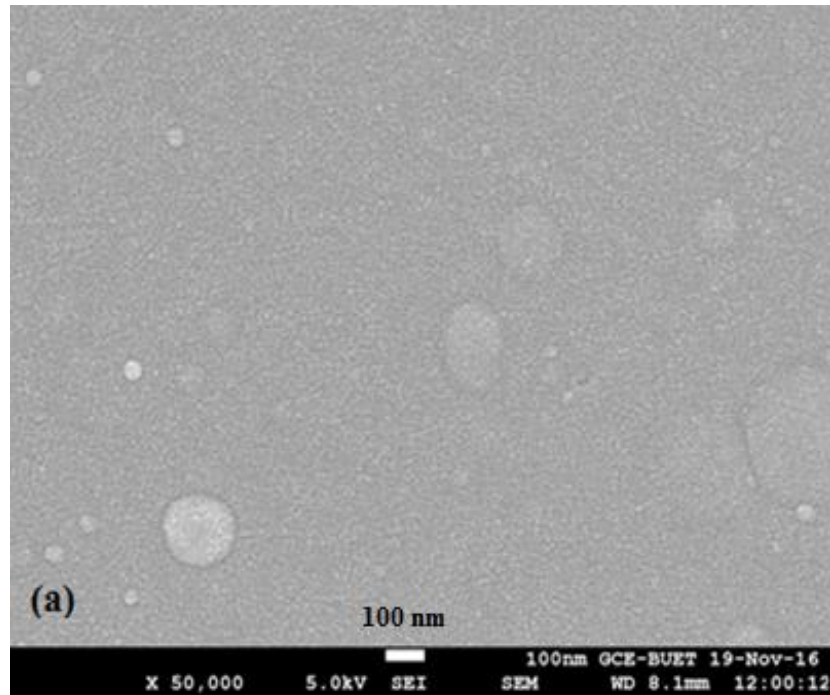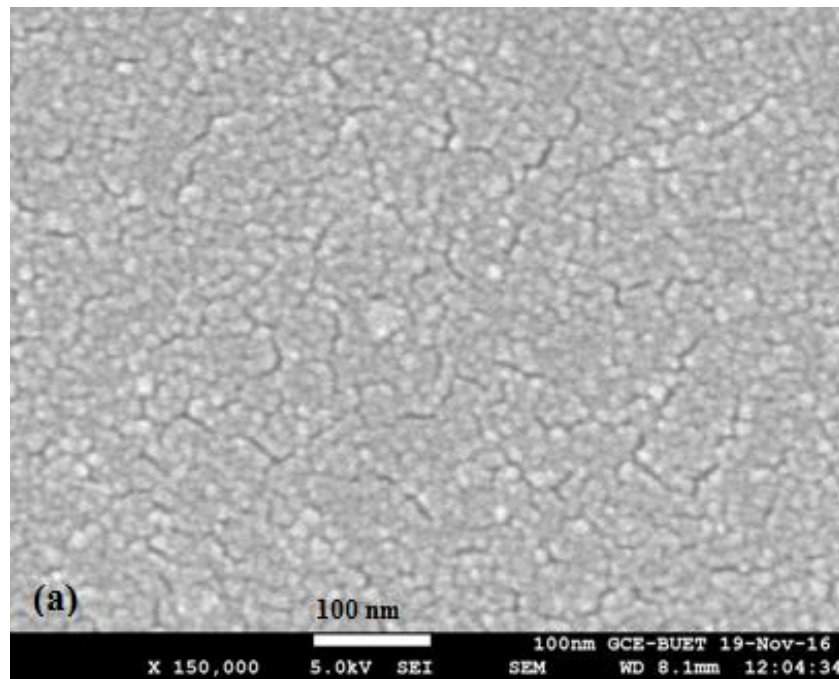
Fig. 4.6 FESEM micrograph of PPMA thin films of thickness (a) 170 nm with×150 k
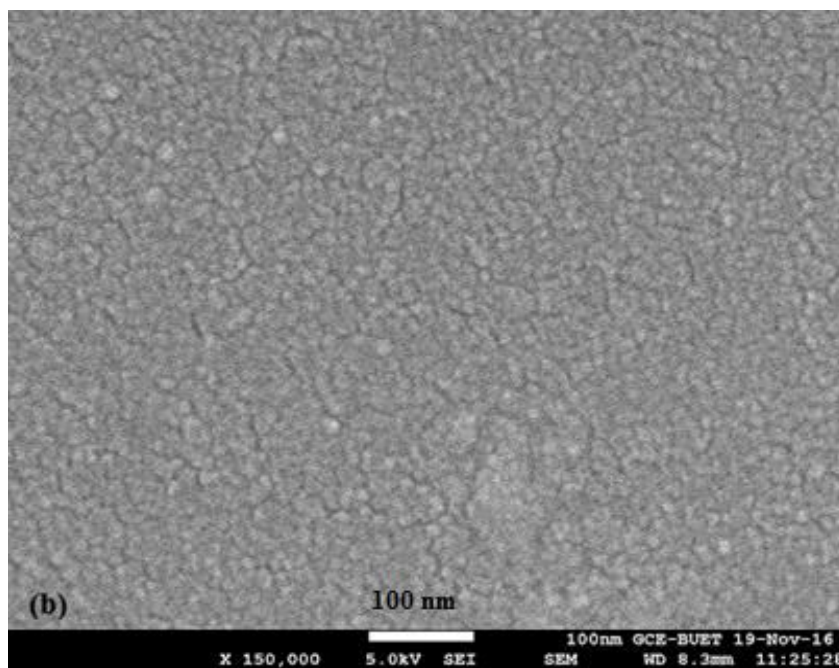
Fig. 4.6 FESEM micrograph of PPMA thin films of thickness (b) 220 nm with×150 k
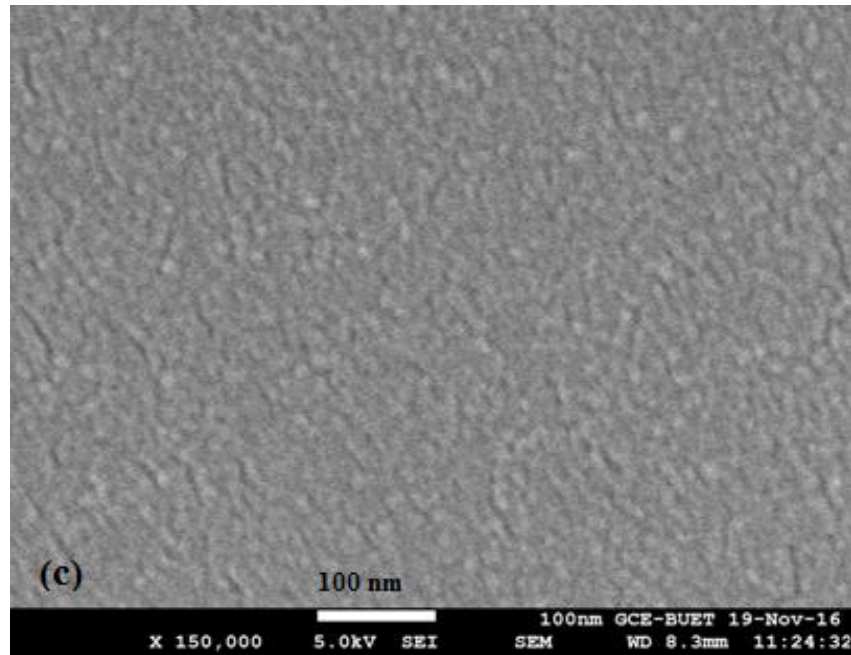
Fig. 4.6 FESEM micrograph of PPMA thin films of thickness (c) 290 nm with ×150 k

4.4 Energy Dispersive X-ray Spectroscopic Analyses

The compositional analysis was performed for the samples mentioned in Fig. 4.7 to Fig. 4.9 by EDX. The mass percentages (mass %) of MA (calculated) and PPMA thin films are shown in Table 4.2.
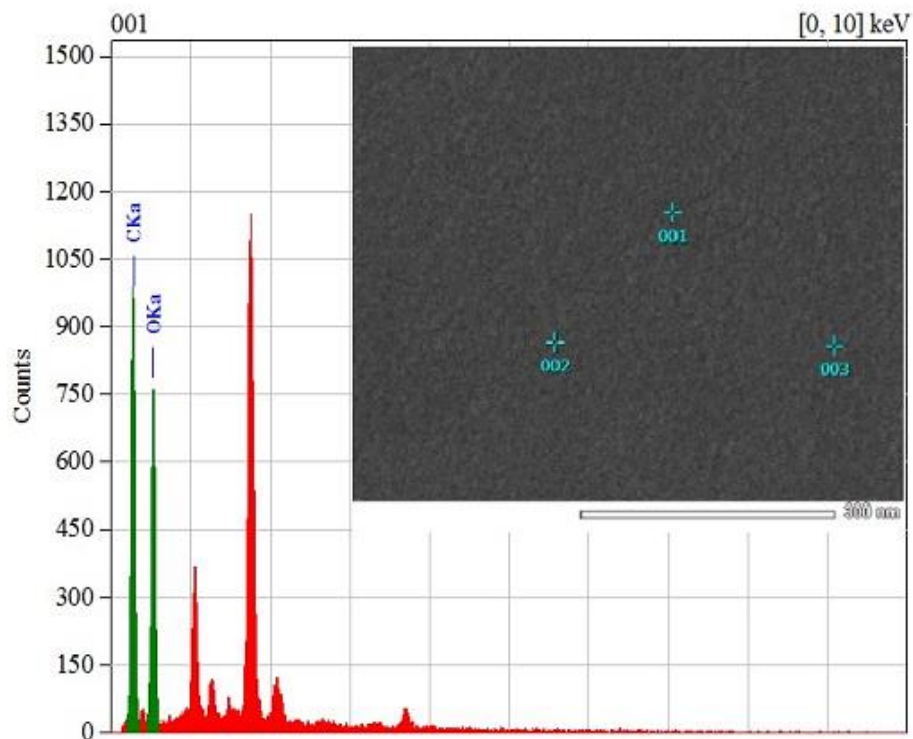
Fig. 4.7 EDX spectra of PPMA thin films of thickness 170 nm.
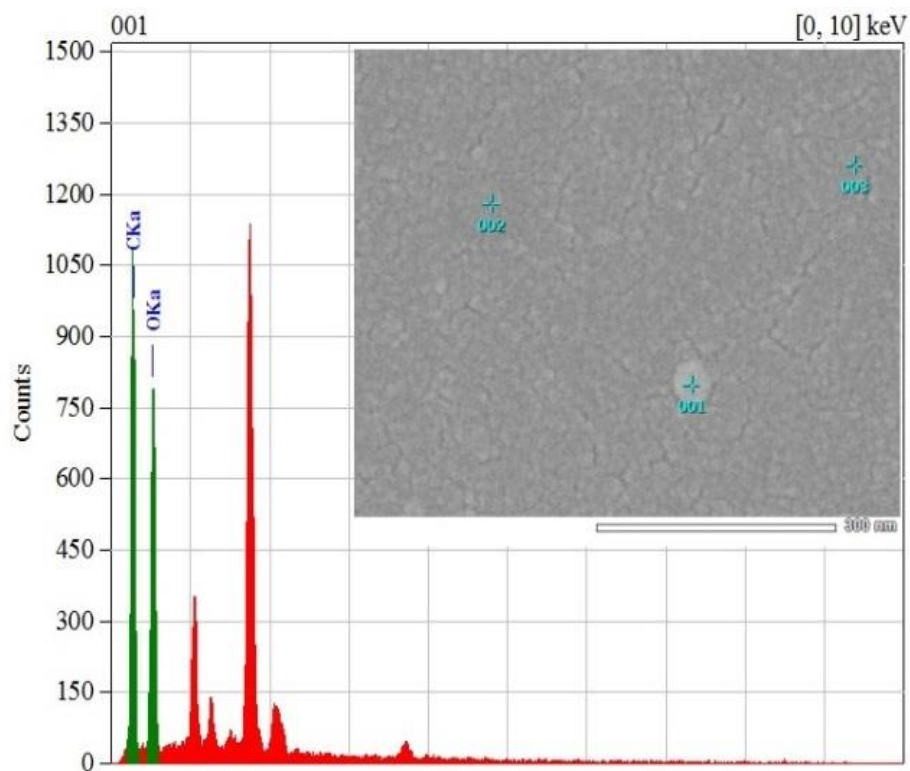
Fig. 4.8 EDX spectra of PPMA thin films of thickness 220 nm.
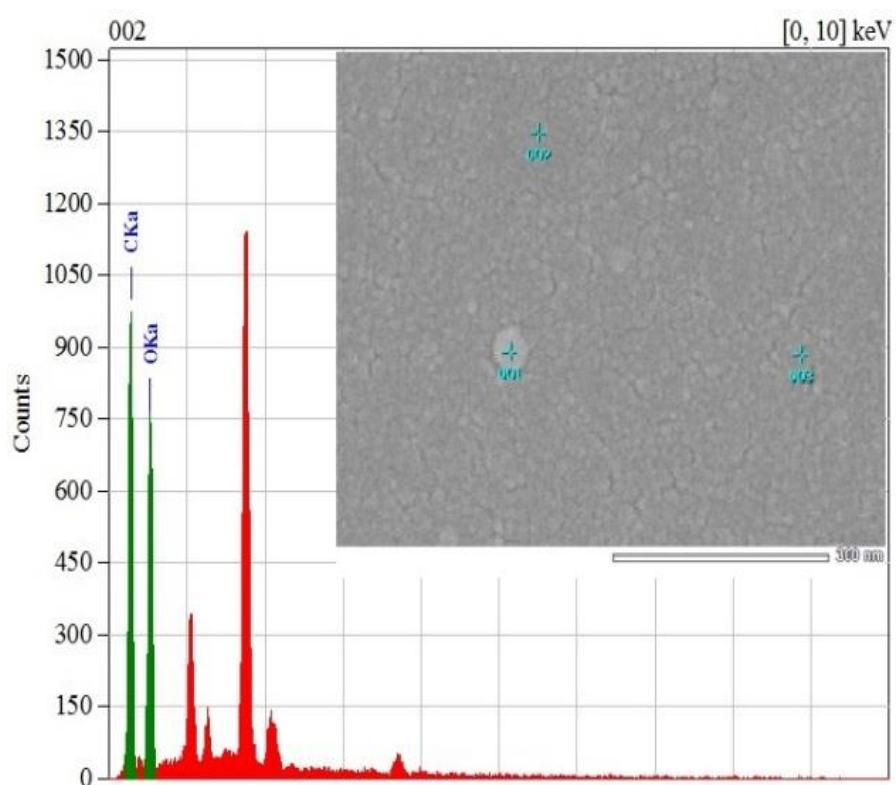
Fig. 4.9 EDX spectra of PPMA thin films of thickness 290 nm.

Table 4.2 Mass percentages of the elements for PPMA thin films of different thicknesses achieved by EDX analysis.

Elements detected	Monomer (MA) (Calculated)	PPMA thin films		
		Thickness		
		170 nm	220 nm	290 nm
	Mass (%)	Mass (%)	Mass (%)	Mass (%)
C	55.80	52.38	52.63	51.55
H	7.024	…….	…….	…….
O	37.17	47.62	47.31	48.45

The observation indicates the presence of Carbon (C) and Oxygen (O) in three types of PPMA thin films. Although methyl acrylate monomer is composed of carbon (C), Oxygen (O) and hydrogen (H) but hydrogen is not noted in Table 4.2, because the main obstacle of EDX is that it cannot detect the presence of H, He, etc., since EDX is related to K-shells which are not the valence shells. Again, oxygen is also present in higher mass % PPMA thin films because oxygen can be incorporated into PPMA during plasma deposition and/or exposure of PPMA thin films to the atmosphere [63, 64]. Additional peaks which are seen in Fig. 4.7 to Fig. 4.9 may be originated from the glass substrates. Quite similar data is observed for PPMA thin films of three different thicknesses.

4.5 Attenuated Total Reflectance - Fourier Transform Infrared Spectroscopic Analyses

The ATR-FTIR spectrum of MA monomer (liquid) and a representative ATR-FTIR spectrum of PPMA of 170 nm thick films are shown in Fig. 4.10.These spectra show that there are structural changes due to plasma polymerization and the structure of PPMA differs in respect of several chemical bands and relating intensity of the peaks from that of the monomer structure. It is detected from the ATR-FTIR spectrum of the PPMA that the intensity of the absorption bands decreased significantly compared to that of the monomer (MA) spectrum. This is an implication of reorganization of monomer molecule during plasma polymerization. To compare the position of

assignments for different absorption bands for MA and PPMA at a glance, the observations are summarized in Table 4.3.
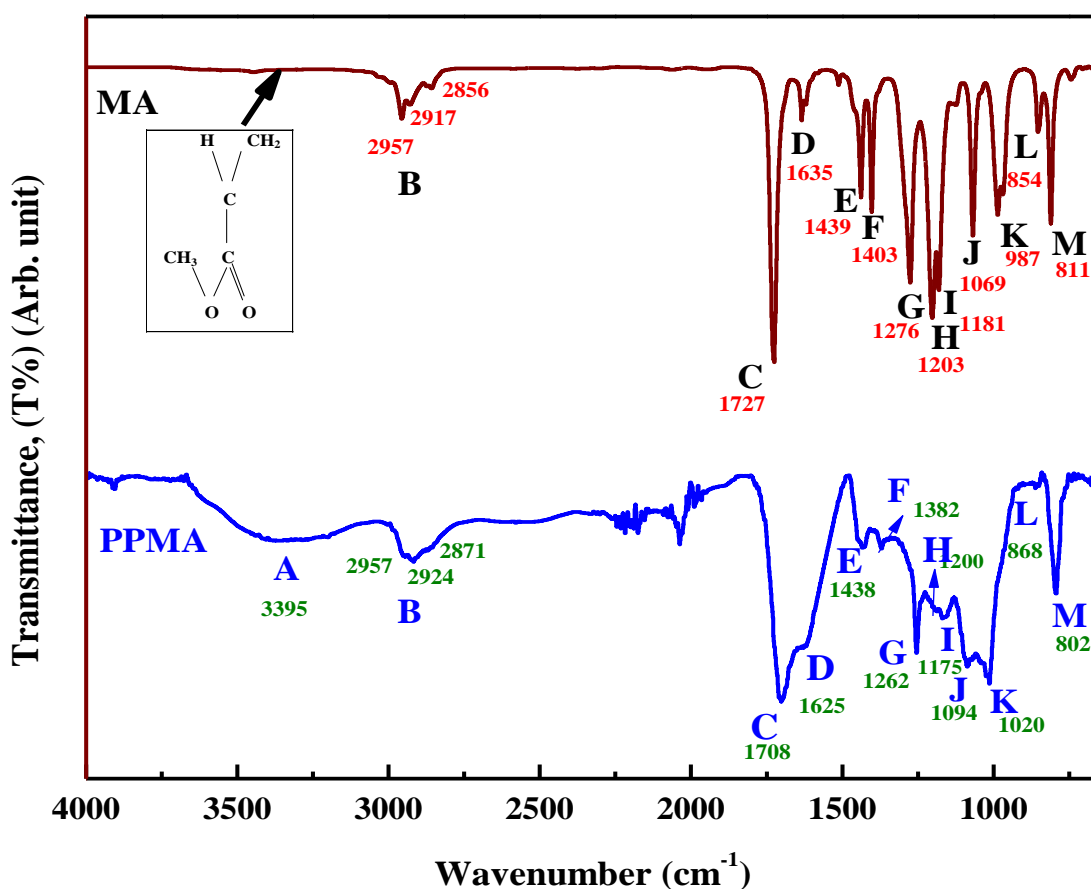
Fig. 4.10 The ATR-FTIR spectra of MA and PPMA.

In the spectrum for MA, no absorption band is appeared corresponding to absorption band at 3395 cm^{-1} (A) in the spectrum of PPMA indicating the presence of OH stretching. The hydroxyl group mainly dominates this region which giving rise to very characteristics band profiles. In spectrum for MA, the presence of CH$_3$, CH$_2$ and C-H stretching are observed at 2957 cm^{-1} (due to asymmetric stretching vibration of H atom), 2917 cm^{-1} (asymmetric vibration of H atom) and 2856 cm^{-1} respectively, which is similiar for PPMA but the absorption bands are (B) weaker than MA. In the spectrum for MA, the presence of absorption band for C=O is observed at 1727 cm^{-1} (C) whereas absorption band for C=O is observed at 1708 cm^{-1} in spectrum PPMA which proves the material as a carbonyl compound. The presence of conjugation i.e. C=C stretching is observed around 1635 cm^{-1} (D) in MA and 1625 cm^{-1} in PPMA. In the spectrum of MA, the absorption band is observed at 1439 cm^{-1} (E) and 1403 cm^{-1}

(F) indicates the presence of CH_3 and CH_2 groups which arises due to C–H bending, which is approximately equal for that of PPMA.

Table 4.3 Assignment of ATR-FTIR absorption bands for MA and PPMA.

Assignments	Absorption Bands	Wavenumber (cm^{-1})		Intensity band
		MA (Monomer)	PPMA	
OH stretching	A	----	3395	Broad peak
CH_3 stretching ,	B	2957	2957	Merged
CH_2 stretching,		2917	2924	
C-H stretching		2856	2871	
C=O stretching	C	1727	1708	Broad peak
C=C stretching	D	1635	1625	Very low
CH_3 bending	E	1439	1438	Merged
CH_2 bending	F	1403	1382	
C-O	G	1276	1262	Low
	H	1203	1200	Merged
	I	1181	1175	
	J	1069	1094	
C=C bending	K	987	1020	Broad peak
	L	854	868	Very low
	M	811	802	Similiar

The absorption band observed at 1300–1000 cm^{-1} (G to J) possibly arises due to C–O stretching, for the spectrum MA and PPMA. In the spectrum for MA, the presence of absorption band C=C bending is observed at 987 cm^{-1} (K) and absorption band is observed at 1020 cm^{-1} for spectrum. In the spectrum for MA, the presence of absorption band C=C bending are observed at 854 cm^{-1} (L) on the other hand absorption band is observed at 868 cm^{-1} in spectrum PPMA. In the spectrum for MA, the presence of absorption band C=C bending are observed at 811 cm^{-1} (M) whereas absorption band is observed at 802 cm^{-1} for spectrum PPMA. The C–H stretching

vibrations for methyl group are the most characteristic in terms of recognizing the compound as an organic compound. The bending vibrations help to tell more about the basic structure. From the above discussion it is clear that the presence of OH in the MA and PPMA arises due to the exposure of the monomer to the atmosphere. During plasma polymerization hydrogen loss occurs in CH_3 as a consequence CH_2 is observed in PPMA spectrum. The C=O absorption band shifts toward higher wavenumber region. It is found that the PPMA thin films have partially changed chemical structure owing to reorganization of methyl acrylate structure due to plasma polymerization.

4.6 Ultraviolet-Visible Optical Absorption Spectroscopic Analyses

The optical absorbance spectra were analyzed for the PPMA thin films of different thicknesses to investigate various optical parameters. Fig. 4.11 shows room temperature UV-Vis absorption spectra for PPMA thin films of different thicknesses. It is seen that the absorbance rise sharply in the low wavelength region, which rapidly decreases up to about 350 nm with a peak for all the PPMA thin films. Above 350 nm, absorbance decreases slowly. The absorbance increases with increasing thickness of the PPMA thin films which is due to scattering losses. The maximum wavelength (λ_{max}) and maximum absorbance values corresponding to the thickness of the PPMA thin films are tabulated in Table 4.4. It is observed from Table 4.4 that λ_{max} of the PPMA thin films are nearly equal for various thicknesses.
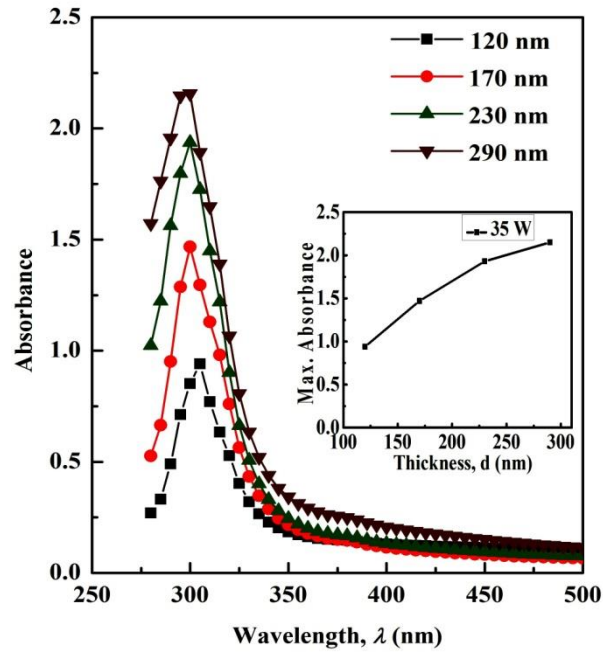
Fig. 4.11 Variation of absorbance with wavelength, for PPMA thin films of different thicknesses (Power: 35W).

Table 4.4 Maximum wavelength (λ_{max}) corresponding to maximum absorbance (A_{max}) with thickness.

Film thickness, d (nm)	λ_{max} (nm)	Max. absorbance
120	305	0.94
170	300	1.48
230	300	1.93
290	300	2.15

Fig. 4.12 shows a plot of absorption co-efficient, α, as a function of photon energy, $h\nu$ for PPMA thin films of different thicknesses. It is clear that the curves have different slopes indicating the presence of different optical transitions in the PPMA thin films. The optical transition regarded in the film can be determined on the basis of the dependence of α on $h\nu$ by taking help of the Tauc relation [55] $\alpha h\nu = B (h\nu - E_g)^n$ where, B is the proportionality factor, called Tauc parameter and n is the parameter connected to the distribution of the energy density of states. The index n equals 1/2 and 2 for allowed direct transition, $E_{g(d)}$ and indirect transition energy gaps, $E_{g(i)}$, respectively. Thus the E_g values can be obtained by extrapolating

the linear portion of the plots to the intercept in the x-axis. The plot of $(\alpha h\nu)^2$ as a function of $h\nu$ for $E_{g(d)}$ and plot of $(\alpha h\nu)^{1/2}$ as a function of $h\nu$ for $E_{g(i)}$ of the PPMA thin films of different thickness are shown in Fig. 4.13 and Fig. 4.14, respectively. The obtained $E_{g(d)}$ and $E_{g(i)}$ values are recorded in Table 4.5 .
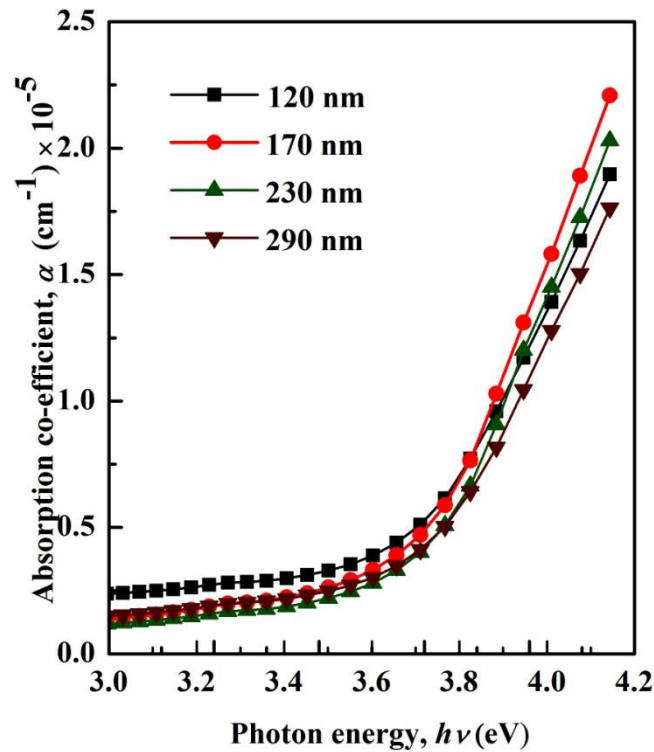
Fig. 4.12 Plots of absorption co-efficient, α, as a function of photon energy, $h\nu$ for PPMA thin films of different thicknesses.

The values of $E_{g(d)}$ varies from 3.77 to 3.83eV and that of $E_{g(i)}$ varies from 3.40 to 3.48eV, as the thickness varies from 120 to 290 nm for PPMA thin films. The increase of $E_{g(i)}$ values with the increasing thickness is due to the increase in fragmentation/cross-linking in the bulk of the material due to the impact of plasma on the surface of the thin films with plasma duration. In non-crystalline/ amorphous materials the physical processes that control the behavior of gap states are structural disorder responsible for the tail states and structural defects in deep states. The defects in polymer structure produces localized states in the band structure and consequently decreases E_g. The increase of $E_{g(i)}$ values of PPMA thin films with increasing thicknesses can be attributed to the reduction of structural defect states in the PPMA thin films with increasing thickness i.e. with plasma duration which is one of the plasma parameters. The Urbach energy was calculated from the reciprocal gradient of

the linear portion of these curves. The absorption edge in the spectral range of direct optical transitions has an exponential shape following the relationship [57] $\alpha = \alpha_0 \exp[h\nu/E_u]$, where α_0 is a constant, which is independent of temperature and E_u is the Urbach energy. The exponential dependence of α on energy may arise from the random fluctuations of the internal fields associated with the structural disorder in many amorphous materials [58]. The dependence of the optical α with $h\nu$ may also arise from electronic transitions between localized states. The density of these states falls off exponentially with energy, which is consistent with the theory of Tauc. The E_u can be evaluated as the width of the exponential absorption edge or as the width of the tails of the localized states, associated with the amorphous state, in the forbidden gap. The values of E_u were calculated from the slopes of these figures using the relationship, $E_u = [d(\ln\alpha)/d(h\nu)]$ and calculated values range from 0.29 to 0.35 eV which are given in Table 4.5. So the values of E_u increases with the variation of thickness due the increase of disorder in the PPMA thin films. The variation of extinction co-efficient, k with photon energy, $h\nu$ for PPMA thin films is shown in Fig. 4.16. The increase of k with the increase of $h\nu$ indicates the probability of electron transfer across the mobility gap rises with $h\nu$.

Fig. 4.13 $(\alpha h\nu)^2$ vs $h\nu$ curves for PPMA thin films of different thicknesses.
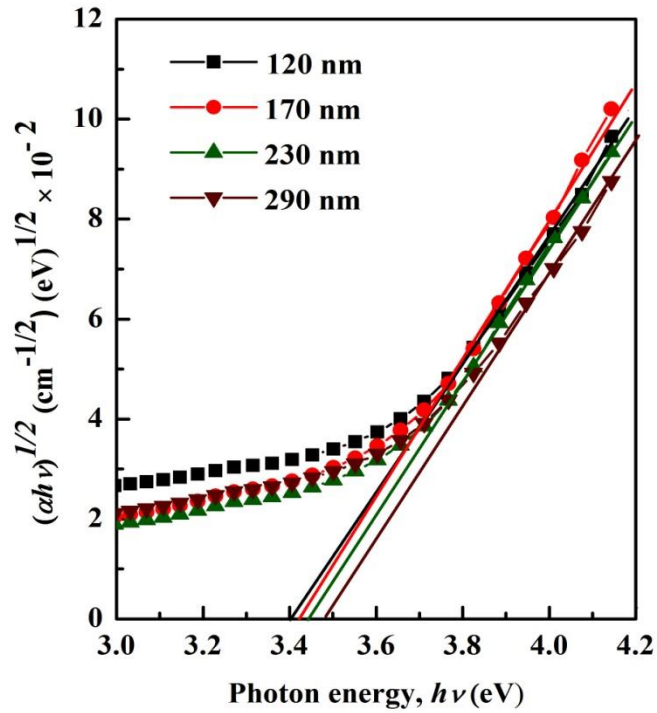
Fig. 4.14 $(\alpha h\nu)^{1/2}$ vs $h\nu$ curves for PPMA thin films of different thicknesses.
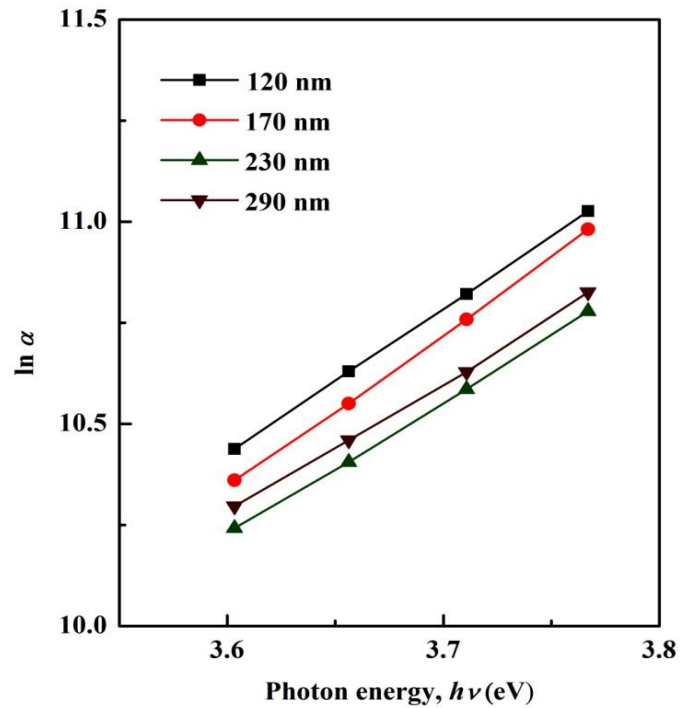
Fig. 4.15 The Urbach plots (ln α vs $h\nu$) for PPMA thin films of different thicknesses (α in cm^{-1}).

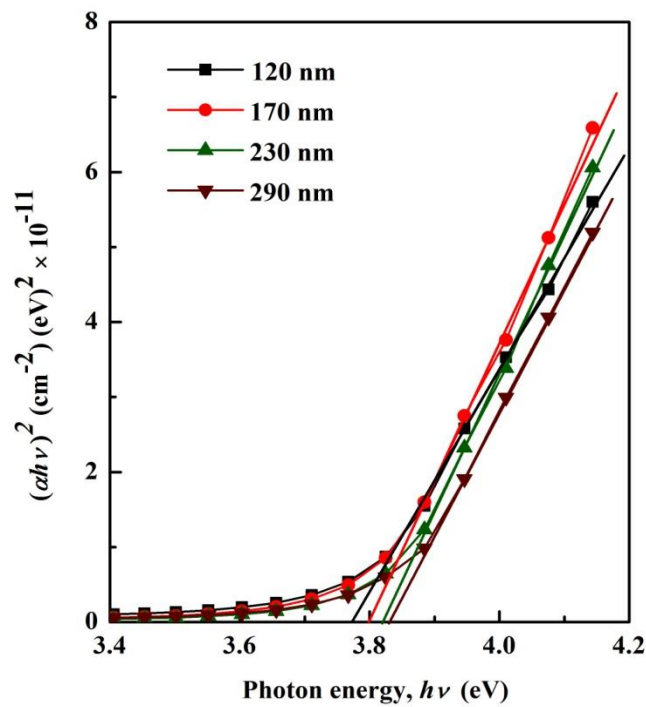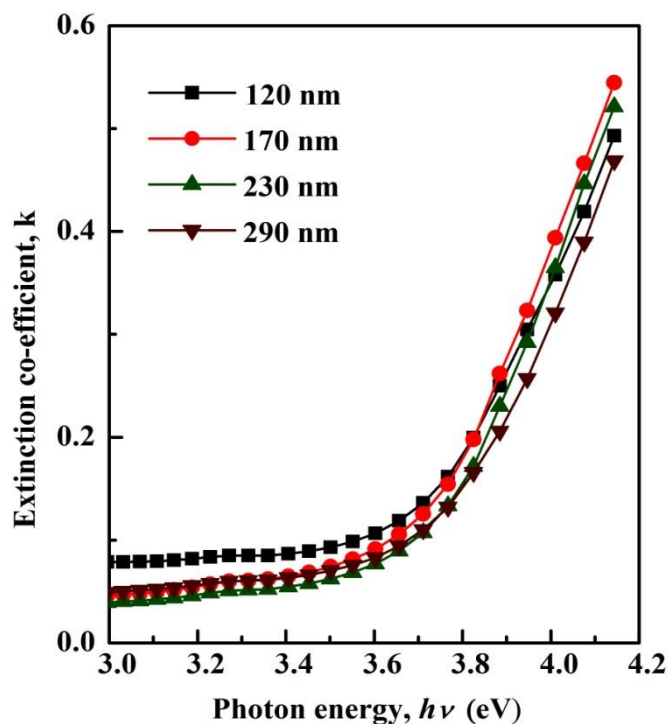Fig. 4.16 Plots of extinction co-efficient, k as a function of *hv* for PPMA thin films of different thicknesses.

Table 4.5 The optical parameters (direct, indirect transition energy gap and Urbach energy) of different thicknesses.

Film thickness d (nm)	Direct band gap $E_{g(d)}$ (eV)	Indirect band gap $E_{g(i)}$ (eV)	Urbach energy E_u(eV)
120	3.77	3.40	0.29
170	3.80	3.42	0.31
230	3.82	3.45	0.32
290	3.83	3.48	0.35

4.7 DC Electrical Properties of PPMA Thin Films

4.7.1 Current density-voltage characteristics

To elucidate the DC electrical conduction mechanism in PPMA, dependence of *J* have been observed on PPMA thin films of various thicknesses (115, 155, 170, 190, 220 nm) in the voltage range 0.1 to 75 V in the temperature of 298, 323, 348, 373 and 398 K. The *J-V* characteristics of PPMA thin films of different thicknesses at room

temperature are shown in Fig. 4.17. The observed *J-V* characteristics of the PPMA films of different thicknesses at various temperatures are presented in Fig. 4.18 to 4.22.
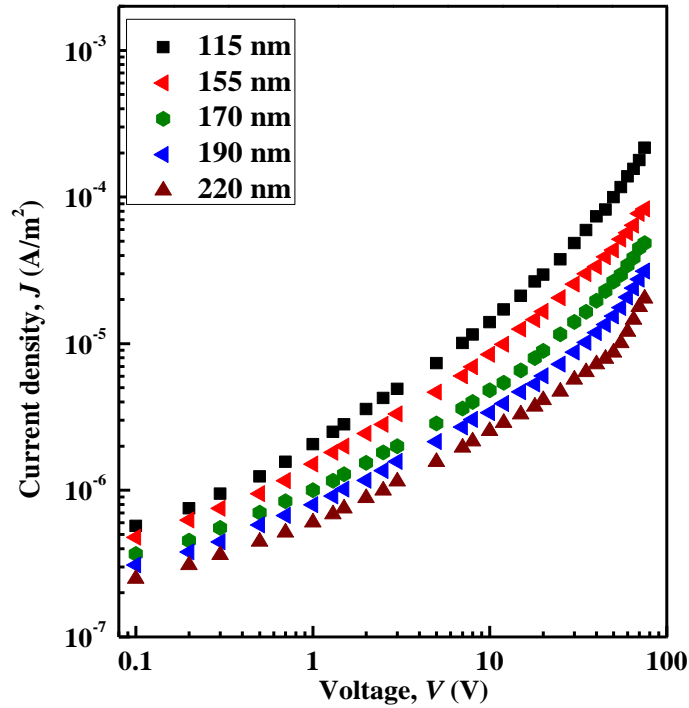
Fig. 4.17 *J-V* plots for PPMA thin films of different thicknesses at room temperature.

Fig. 4.18 *J-V* plots for PPMA thin films of 115 nm thickness at different temperatures.

Fig. 4.19 *J-V* plots for PPMA thin films of 155 nm thickness at different temperatures.

Fig. 4.20 *J-V* plots for PPMA thin films of 170 nm thickness at different temperatures.
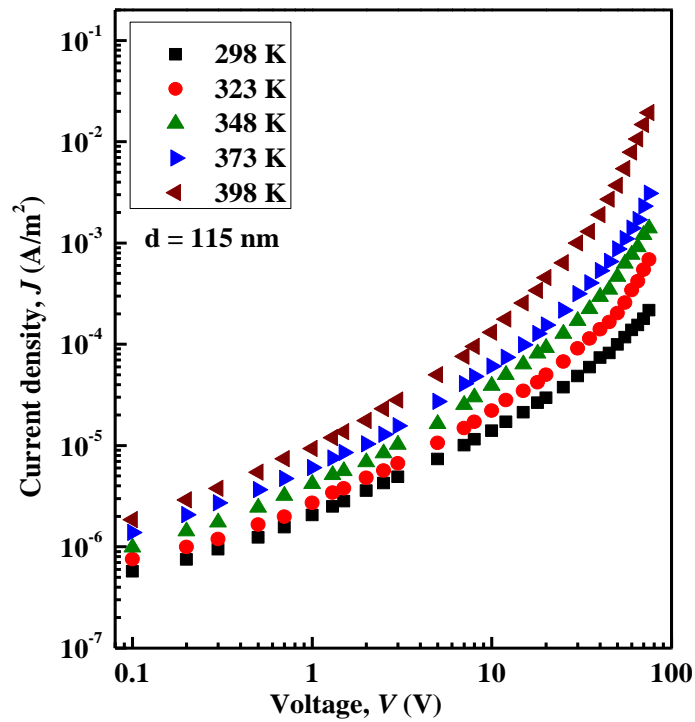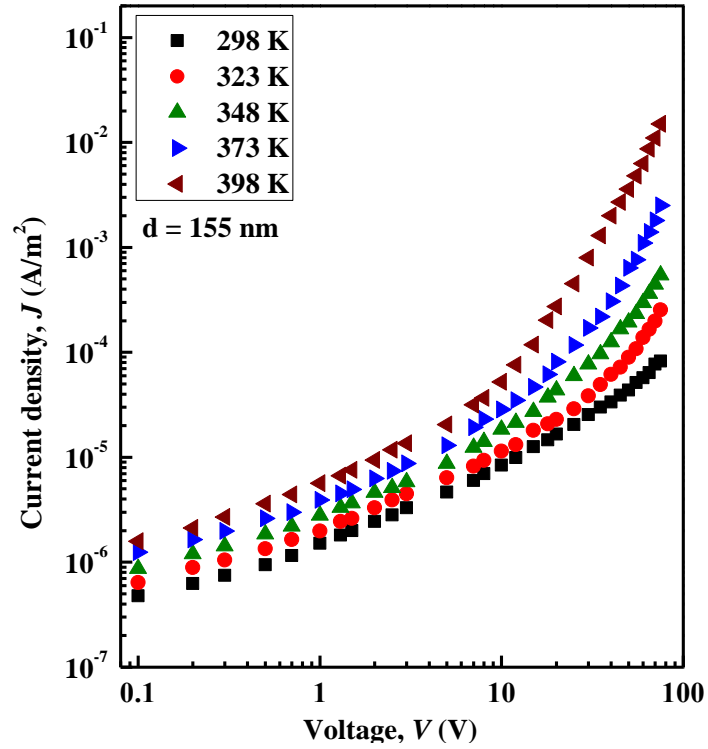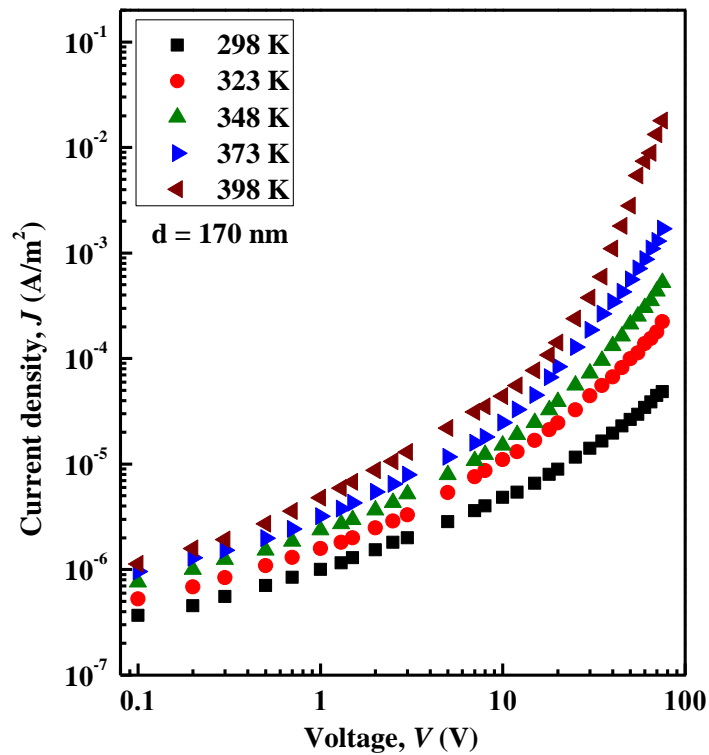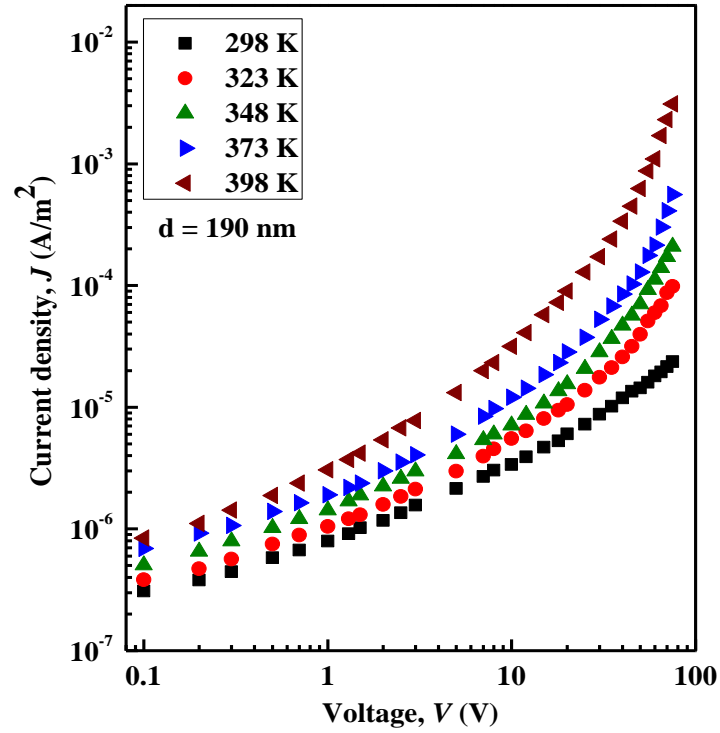
Fig. 4.21 *J-V* plots for PPMA thin films of 190 nm thickness at different temperatures.
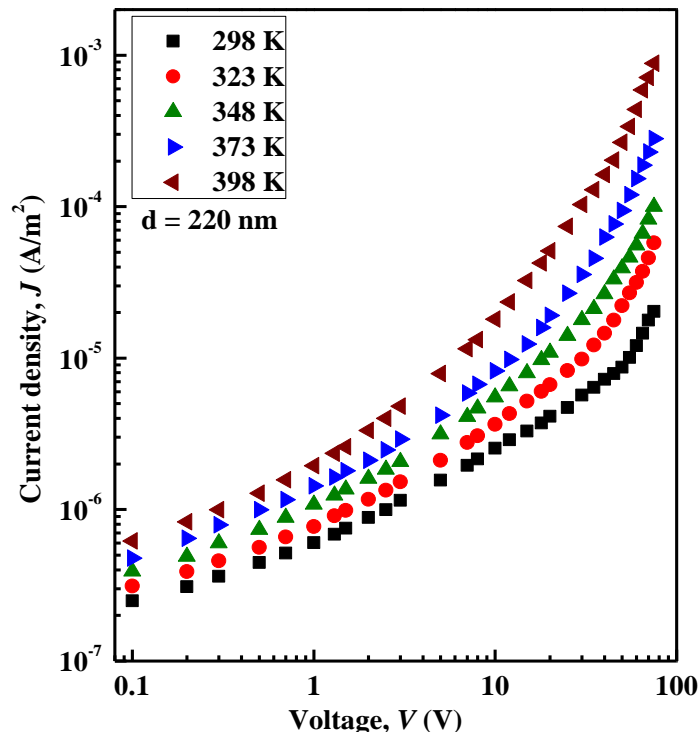
Fig. 4.22 *J-V* plots for PPMA thin films of 220 nm thickness at different temperatures.

It is observed that *J* increases with decreasing thickness (Fig. 4.17) and increasing with increasing temperature (Figs. 4.18 - 4.22) for PPMA thin films. Each *J-V* curve have approximately same shape having two different sections in the lower and higher voltage regions that implies two different conduction processes according to the power law of the form $J \propto V^n$, where *n* being power index. The values of the slopes are tabulated in Table 4.6. At lower voltages (0.1 ~ 10 Volts) the slope $0.61 \leq n \leq 1.01$ indicates approximate Ohmic region while at higher voltages (10 ~ 75 Volts) the value of the slope $1.46 \leq n \leq 4.40$ represents approximate non-Ohmic region. The voltage dependence of current density at the higher voltage region suggests that the current may be due to Schottky, PF or SCLC [65, 66] mechanisms in PPMA thin films. The thickness dependence of current follows the relation, $J \propto d^{-l}$ where *l* is a parameter depending upon the trap distribution. A slope $l < 3$ suggests the possibility of Schottky or Pool Frenkel (PF) mechanism and $l \geq 3$ indicates the possibility of SCLC mechanism. At the higher voltage of 60 V the dependence of *J* on PPMA thin films of different thicknesses is presented in Fig. 4.23. The linear slope derived from this plot has yielded negative a slope of about 4.28 for PPMA thin films, which is much higher than that corresponding to Schottky or PF. So, these observations do not signify the possibility of presence of Schottky or PF mechanism in PPMA thin films. Therefore, it may be inferred that the conduction mechanism of carrier transport operative in these films is space charge limited conduction type.
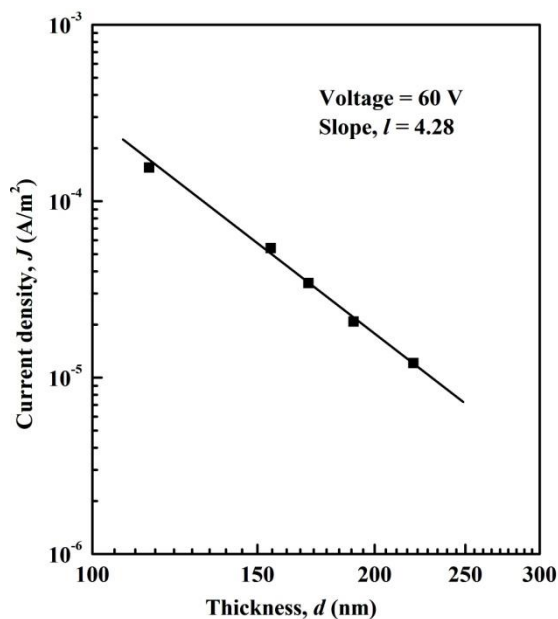
Fig. 4.23 *J* vs *d* plots for PPMA thin films in non-Ohmic region.

Table 4.6 The slopes in the lower and higher voltage regions at different temperatures for PPMA thin films of different thicknesses.

Thickness of PPMA thin films , d (nm)	Measurement temperature (K)	Values of slopes	
		Low voltage region (0.1~10 Volts) (Ohmic)	High voltage region (10 ~ 75 Volts) (Non-Ohmic)
115	298	0.73	1.46
	323	0.75	1.71
	348	0.76	2.15
	373	0.77	2.18
	398	0.81	2.78
155	298	0.72	1.54
	323	0.74	1.75
	348	0.72	2.23
	373	0.73	3.07
	398	0.80	3.41
170	298	1.00	1.48
	323	0.82	1.55
	348	0.78	2.04
	373	0.87	2.21
	398	0.83	4.40
190	298	0.66	1.85
	323	1.01	1.76
	348	0.68	1.94
	373	0.71	1.99
	398	0.85	2.69
220	298	0.62	2.09
	323	0.61	2.14
	348	0.67	2.49
	373	0.79	2.64
	398	0.90	2.90
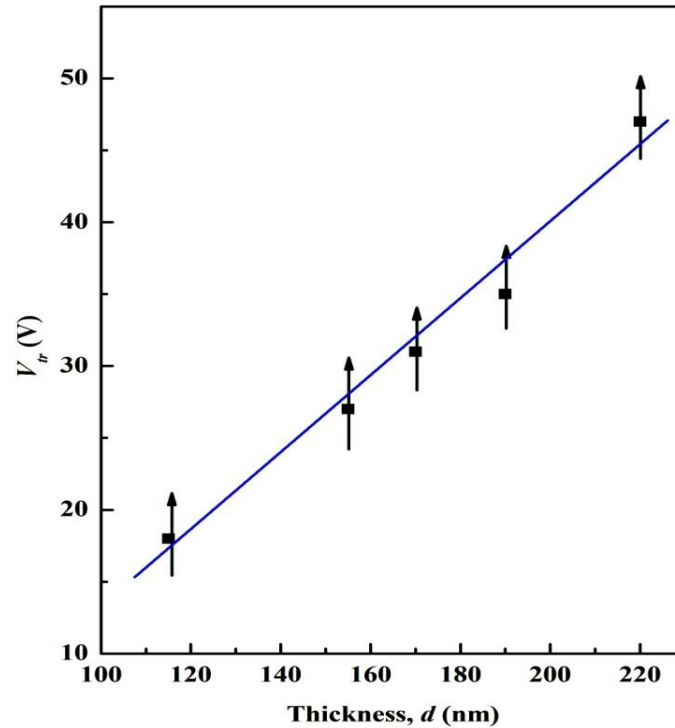
Fig. 4.24 Transition voltages (V_{tr}) vs thickness graph for the PPMA thin films.

From the Fig. 4.17, it is seen that current density turns out to be non-Ohmic and the systems of the conduction mechanism then switches to SCLC. The technique to extract V_{tr} is to draw to tangents one at lower voltage region and another at higher voltage region. Then V_{tr} is the voltage where two slopes intersects. The free carrier density, n_0 [67] can be calculated from the equation, $n_0 = \frac{9\varepsilon'\varepsilon_0 V_{tr}}{8ed^2}$, where V_{tr} is the voltage at which the transition from Ohmic to SCLC. The variation of V_{tr} with thickness, d is shown in Fig. 4.24, which shows that V_{tr} is higher for higher thickness.

4.7.2 Dependence of current density on temperature

The dependence of J on inverse absolute temperature, $1/T$, for PPMA thin films of different thicknesses, one in the Ohmic region with an applied voltage, 8 V and other in the SCLC region with an applied voltage, 60 V, are shown in Fig. 4.25 to 4.29. Each of the curves has two different slopes, one in the low temperature region and other in the higher temperature region. The activation energies calculated from the slopes of curves of Fig. 4.25 to 4.29 for all samples are tabulated in Table 4.7.
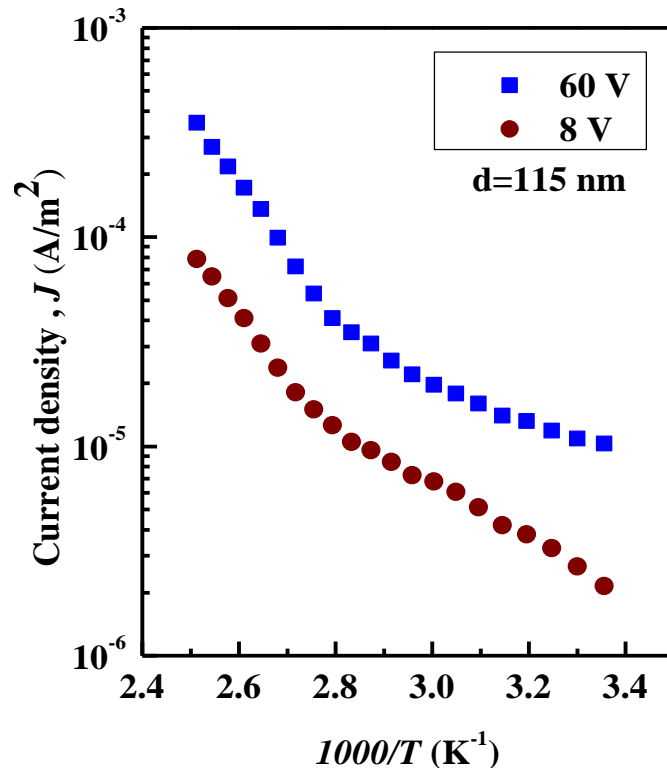
Fig. 4.25 Current density vs inverse of absolute temperature for PPMA thin films of 115 nm thickness.
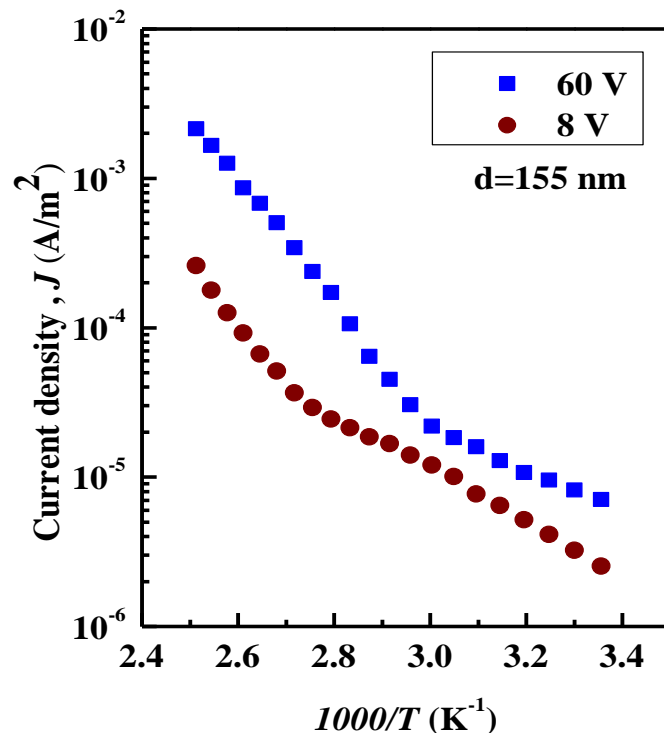
Fig. 4.26 Current density vs inverse of absolute temperature for PPMA thin films of 155 nm thickness.
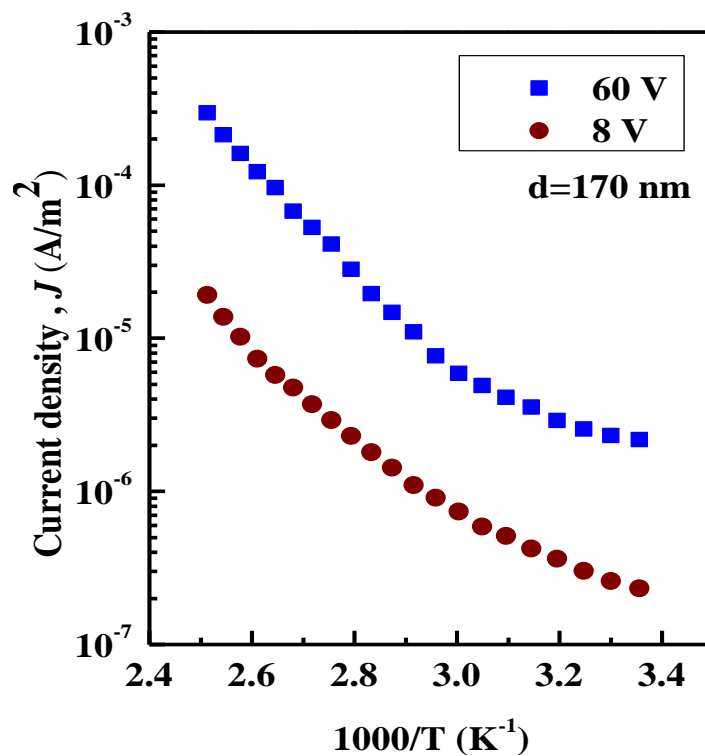
Fig. 4.27 Current density vs inverse of absolute temperature for PPMA thin films of 170 nm thickness.
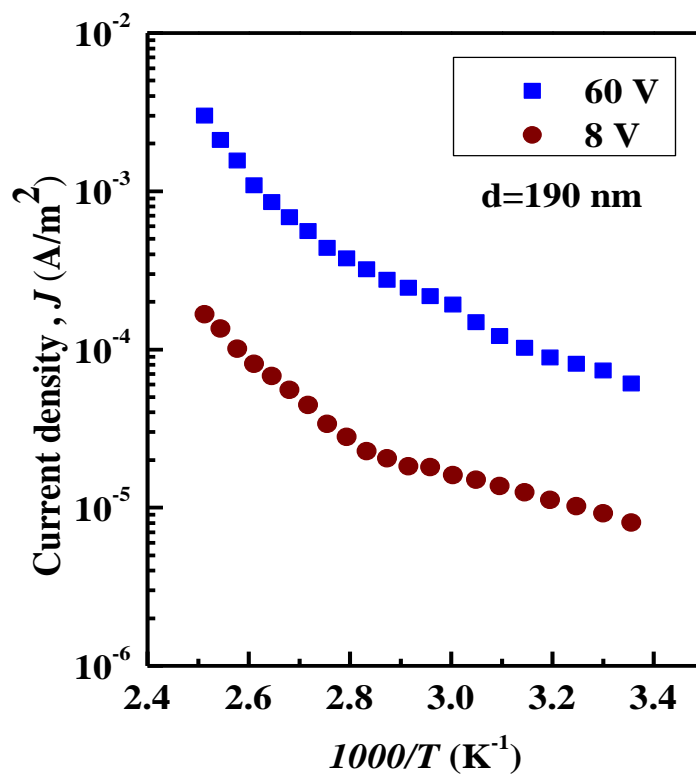
Fig. 4.28 Current density vs inverse of absolute temperature for PPMA thin films of 190 nm thickness.
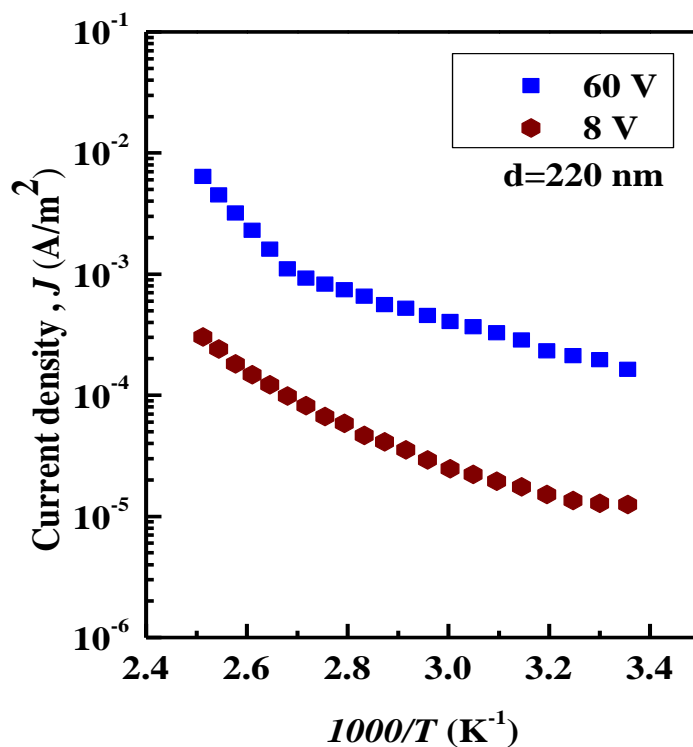
Fig. 4.29 Current density vs inverse of absolute temperature for PPMA thin films of 220 nm thickness.

Table 4.7 The values of activation energy ΔE (eV) for PPMA thin films of different thicknesses.

Thickness of PPMA thin films, d (nm)	Activation energies ΔE(eV)			
	8 V (Ohmic)		60 V (Non-Ohmic)	
	Temperature		Temperature	
	Lower	Higher	Lower	Higher
115	0.29	0.61	0.21	0.63
155	0.22	0.77	0.29	0.73
170	0.32	0.63	0.32	0.85
190	0.17	0.54	0.29	0.69
220	0.24	0.55	0.25	0.86

From table 4.7, the activation energy for applied voltage 8 V (Ohmic) is observed to be around an average value of 0.25 eV at lower temperature (308 ~ 318 K) region and that in the higher temperature (364 ~ 373 K) region is 0.62 eV. On the other hand for

60 V (Non-Ohmic) (SCLC region) applied voltage, the activation energy is observed to be around an average value of 0.27 eV at lower temperature (308 ~ 318 K) region and 0.75 eV at higher temperature (364 ~ 373 K) region.The lower activation energy, about 0.25 eV and 0.27 eV for 8 V and 60 V respectively, in the lower temperature (308 ~ 318 K) region and the higher activation energy, about 0.62 eV and 0.75 eV for 8 V and 60 V, respectively, in the higher temperature (308 ~ 318 K) region may be attributed to two different transition processes in the two different temperature regions. In the lower temperature region, low activation energy may be attributed to the transition between defects within the energy gaps and/or from the shallow defects levels to the conduction/ valence band. In the higher temperature region, the high activation energy may be responsible for the transition of careers between the bands and/or from the deep levels.

CHAPTER V

CONCLUSIONS

5.1 Conclusions

Plasma polymerized methyl acrylate thin films were deposited onto glass substrates using a capacitively coupled parallel plate glow discharge plasma reactor. The morphological, structural, thermal, optical and DC electrical properties of PPMA thin films of different thicknesses were investigated by different characterization techniques.. The followings are the outcomes of these studies.

The thermal analyses of PPMA thin films in air environment reveals that it is thermally stable up to about 534 K, whereas in N_2 environment it is about 543 K. It is observed that the weight loss decreased and thermal stability increased in N_2 environment than that of air. In air environment, two-stage degradation reaction might have taken place, which is represented by two exothermic peaks at the temperature 564 K and 650 K whereas in N_2 environment, one stage thermal decomposition is observed around 543 K.

FESEM micrographs reveal that the films are clusters/agglomeration like structure. The EDX analysis indicates the presence of prominent percentage of carbon and oxygen in PPMA thin films.

From the ATR-FTIR analyses, it is clear that the presence of OH stretching in the spectra of PPMA arises due to the exposure of the monomer to the atmosphere, which is absent in MA. During the plasma polymerization hydrogen loss occurs in CH_3 stretching, as a consequence CH_2 stretching is observed in the PPMA spectrum. So the PPMA thin films have partially changed chemical structure owing to reorganization of MA structure due to plasma polymerization.

From the UV-Vis spectral analyses, it is observed that $E_{g(i)}$ values are increasing with the increases thickness is due to the increase in fragmentation/cross-linking in the bulk of the material due to the impact of plasma on the surface of the thin films with plasma duration and $E_{g(d)}$ values are nearly equal. The Urbach energy varies from 0.29 to 0.35 eV. So the values of E_u increases with the variation of thickness due the increase of disorder in the PPMA thin films. The increase of extinction co-efficient, k with the increase of $h\nu$ indicates the probability of electron transfer across the mobility gap rises with $h\nu$. The *J-V* characteristics revealed that the dependence of *J* on *V* is Ohmic is the lower voltage region (8 V) and in higher voltage region (60 V), it

is non-Ohmic. *J–d* and *V_{tr}-d* curves confirmed a contact limited SCLC mechanism of PPMA thin films.

The activation energy (ΔE) for Ohmic region (8 V) is observed to be around an average value of 0.25 eV at lower temperature (308 ~ 318 K) region and that in the higher temperature (364 ~ 373 K) region is 0.62 eV whereas in non-Ohmic region (60 V), ΔE is observed to be around an average value of 0.27 eV at lower temperature (308 ~ 318 K) region and that in the higher temperature (364 ~ 373 K) region is 0.77 eV. In the lower temperature region, low activation energy may be attributed to the transition between defects within the energy gaps and/or from the shallow defects levels to the conduction/ valence band. In the higher temperature region, the high activation energy may be responsible for the transition of carriers between the bands and/or from the deep levels. The values of E_u increases with the variation of thickness due the increase of disorder in the PPMA thin films. The increase of k with the increase of *hv* indicates the probability of electron transfer across the mobility gap rises with *hv*. The results obtained in this work may help in finding potential applications in optical and electronic devices.

5.2 Suggestions for the Further Work

All the characterization done in the present study represents thermal, morphological, structural, optical and DC electrical properties of PPMA thin films. Beyond these characterizations some other can be done to establish the suitable applications areas for PPMA thin films. Some of them are stated below:

The atomic force microscopy (AFM) can be used to see the smoothness of the surface. The X-rays photoelectron spectroscopy (XPS) investigation should be carried out in order to see the bonding of different functionalities in the PPMA thin films. It also can provide quantitative information of the element present. Doping using other agents, in addition to iodine, need to be considered to see further modification of conductivity of PPMA thin films. The dielectric constant and loss factor, at different frequency and temperatures may be measured to find the dielectric application of the material. The AC measurement can be carried out on PPMA thin films. The PPMA thin films can be prepared in an asymmetric electrode configuration or inductively coupled, plasma polymerization set-up with rf power and can be characterized by the above mentioned techniques.

5.3 References

[1]   Stuart, M., "Dielectric properties of cross-linked polystyrene films formed in the glow discharge", Nature, Vol. 199, pp. 59-60, (1963).

[2]   White, M., "Vacuum evaporation of polythene", Vacuum, Vol. 15, pp. 449-450, (1965).

[3]   Jackson, G. N., "R.F. Sputtering", Thin Solid Films, Vol. 5, pp. 209-246, (1970).

[4]   Rastogi, A. C., Chopra, K. L., "Kinetics of growth of polyvinylchloride (PVC) films", Thin Solid Films, Vol. 18, pp. 187-200, (1973).

[5]   Yasuda, H., "Plasma polymerization", Academic Press, Inc., New York, (1985).

[6]   d'Agostino, R., "Plasma deposition, treatment and etching of polymers", Academic Press, Inc., Boston, (1990).

[7]   Hirvonen, James K., "Ion beam assisted thin film deposition", Mater. Sci. Rep., 6 (6), pp. 215-274, (1991).

[8]   Matin, R., Bhuiyan, A. H., "Electrical transport mechanism in plasma polymerized 2,6, diethylaniline thin films', Thin Solid Films, Vol. 519, pp. 3462-3467, (2011).

[9]   Shahjalal, A. B. M., Ahmed, S., Bhuiyan, A.H., Ibrahim, M., "On the conduction mechanism in plasma polymerized m-xylene thin films", Thin Solid Films, Vol. 295, pp. 125-130, (1997).

[10]   Zaman, M., Bhuiyan, A.H., "Direct current electrical conduction mechanism in plasma polymerized thin films of tetrathylorthosilicate', Thin Solid Films, Vol. 517, pp. 5431-5434, (2009).

[11]   Hu, X., Zhao X., Uddin, A., Lee, C. B., "Preparation, characterization and electronic and optical properties of plasma- polymerized nitriles", Thin Solid Films, Vol. 477, pp. 81-87, (2005).

[12]   Bae, I. S., Jung, C. K., Cho, S. J., Song, Y. H., Boo, J. H., "A comparative study of plasma polymerized organic thin films on their electrical and optical properties", J. Alloys Compd., Vol. 449, pp. 393-396, (2008).

[13]   Bazaka, K, Jacob, M. V., "Synthesis of radio frequency plasma polymerized non-synthetic Terpinen-4-ol thin films", Mater. Lett. Vol. 63, pp. 1594-1597, (2009).

[14]   Lim, J.S., Shin, P.K., Lee, B.J., Lee, S., "Plasma polymerized methyl methacrylate gate dielectric for organic thin-film transistors", Org. Electr., Vol. 11, pp. 951-954, (2010).

[15] Jumaili, A. J., Bazaka, K. Jacob, M.V., "Retention of antibacterial activity in germanium plasma polymer thin films", J. Nanomaterials, Vol. 7, p. 270, (2017).

[16] Majumder, S., Bhuiyan, A. H., "DC conduction mechanism in plasma polymerized vinylene carbonate thin films prepared by glow discharge technique", Polym. Sci., Ser. A, Vol. 53(1), pp. 85–91, (2011).

[17] Afroze, T., Bhuiyan, A. H., **"**Electrical conduction mechanism in plasma polymerized 2-(diethylamino) ethyl methacrylate thin films", Polym. Eng. Sci.**,** Vol. 55, pp. 2729-2734, (2015).

[18] Rahman, M. J., Bhuiyan A.H. "Structural and optical properties of plasma polymerized o-methoxyaniline thin films", Thin Solid Films, Vol. 534, pp. 132-136, (2013).

[19] Lim, J.S., Shin, P.K., Lee, B.J., "Organic thin film transistors with gate dielectrics of plasma polymerized styrene and vinyl acetate thin films", Trans. Electr. Electr. Mater., Vol. 16, No. 2, pp. 95-98, (2015).

[20] Ahmad, J., Bazaka, K., Vasilev, K., Jacob, M. V., "Electrical conduction in plasma polymerized thin films of γ-terpinene", J. Appl. Polym. Sci. pp. 42318, (2015).

[21] Bazaka, K, Destefani, R., Jacob, M. V., "Plant-derived cis-β-ocimene as a precursor for biocompatible, transparent, thermally-stable dielectric and encapsulating layers for organic electronics", Nat. Sci. Rep., V. 6, ID. 38571, (2016).

[22] Li, C., Hsieh J.H., Lee, Y.T., "Fabrication and structural characterization of plasma polymerized polypyrrole thin film", Surf. Coat. Tech., V. 320, pp. 206-212, (2017).

[23] Matin, R., Bhuiyan A.H., "Infrared and ultraviolet spectroscopic analyses of plasma polymerized 2, 6 diethylaniline thin films" Thin Solid Films, Vol. 534, pp. 100-106, (2013).

[24] Bazaka, K, Jacob, M. V., "Effects of iodine doping on optoelectronic and chemical properties of polyterpenol thin films", J. Nanomaterials, Vol. 7 (1), pp. 1-16, (2017).

[25] Kabir, H., Bhuiyan, A. H.,Rahman, M. M., "Understanding the charge carrier conduction mechanisms of plasma-polymerized 2-furaldehyde thin films via DC electrical studies", Thin Solid Films, Vol. 609, pp. 35–41, (2016).

[26] Shen, M., Bell, A.T., "Plasma polymerization", American Chemical Society, Washington, D. C., (1970).

[27] Krall, N.A., Trivelpiece, W. A., "Principles of Plasma Physics', Mcgraw-Hill Kogakhusha ltd., Tokyo, Japan, (1973).

[28] Fitzpatrick, R., "Plasma Physics", University of Texas, USA, (2012).

[29] Lieberman, M.A., Lichtenberg, A. J., "Principles of plasma discharges and materials processing', John Wiley and Son's, New York, (1994).

[30] Chen, F. F., "Plasma Physics and Controlled Fusion", Plenum Press, USA, (1984).

[31] Edbertho, L. Q., "Plasma processing of municipal solid waste", Brazilian J. Phy. , Vol. 34 (4B), p. 1587, (2004).

[32] Mamdouh, W., Li, Y., Shawky, S. M., Azzazy, H.M.E., Liu, C.J., "Influence of glow discharge plasma as an external stimulus on the self-assembly, morphology and binding affinity of gold nanoparticle-streptavidin conjugates", Int. J. Mol. Sci., Vol. 13(6), pp. 6534-6547, (2012).

[33] Bogaerts, A., Neyts, E., Gijbels, R., Mullen, J.V.D, "Gas discharge plasma and their applications", Spectrochimi. Acta Part B, Vol. 57, pp. 609-658, (2001).

[34] Uhm, H. S., "An analytical theory of corona discharge plasmas", Phys. Plasm. Vol. 4, p. 3117, (1997).

[35] Shi, F. F., "Developments in plasma-polymerized organic thin films with novel mechanical, electrical, and optical properties", Macromol. Chem. Phys., Vol. C36 (4), 795-826, (1996).

[36] Westwood, A.R., "Glow discharge polymerization-I. rates and mechanisms of polymer formation", Europ. Polym. J., Vol. **7** (4), pp. 363–375, (1971).

[37] Yasuda, H., Lamaze, C. E., "Polymerization of styrene in an electrodeless glow discharge", J. Appl. Polym. Sci., Vol. 15 (9), pp. 2277–2292, (1971).

[38] Yasuda, H., Marsh. H. C., Bumgarner, M. O. and Morosoff, N., "Polymerization of organic compounds in an electrodeless glow discharge. VI. Acetylene with unusual comonomers", J. Appl. Polym. Sci., Vol.19, pp. 2845-2858, (1975).

[39] Cowie, J. M. G., "Polymers: Chemistry and Physics of Modern Materials", Blackie Academic & Professionals, New York, (1993).

[40] Stevens, Malcolm P., "Polymer Chemistry: An Introduction", Oxford University Press, ISBN 0-19-512444-8, New York, (1999).

[41] Grill, A., "Cold Plasma in Materials Fabrication: From Fundamentals to Applications", IEEE Press, New York, (1994).

[42] Choi, C., Yeo, S., Shon, H. K., Kim, J.W., Moon, D.W., Jung,D., Lee, T.G., "Surface characterization of plasma polymerized cyclohexane thin films", J. Vac. Sci. Techno. Vol. A 25, p. 938, (2007).

[43] Bazaka, K., Ahmad, J., Oelgemöller, M., Uddin, A., Jacob, M. V., "Photostability of plasma polymerized γ-terpinene thin films for encapsulation of OPV" , Sci. Rep., Vol. 7, (2017).

[44] Dinescu, G., Satulu, V., Galca, A. C., Mitu, B., "Polythiophene thin films deposited in various RF plasma polymerization configurations", An international Symposium on Plasma Chemistry (ISPC), Vol. 19, Bochum, Germany, (2009).

[45] Biedermann, H., "Plasma Polymer Film", Imperial college press, London, (2004).

[46] Sayed, W. M., Salem T.A., "Preperation of polyaniline and studying its electrical conductivity", J. Appl. Sci., Vol. 77, pp. 1658-1665, (2000).

[47] Zhao, X. Y., "Opto-electronic polymer thin films deposited by glow discharge plasma technique: A review", Iran. Polym. J., Vol. 19 (11), pp. 823-841, (2010).

[48] Coats, A.W., Redfern, J.P., "Thermogravimetric analysis: A review", Analyst, Vol.88, pp. 906-924, (1963).

[49] Klančnik, G., Medved, J., Mrvar, P., "Differential thermal analysis (DTA) and differential scanning calorimetry (DSC) as a method of material investigation", RMZ- Materials and Geoenvironment, Vol. 57(1), pp. 127-142, (2010).

[50] Conley, R.T., "Infrared Spectroscopy", Allyn and Bacon, Inc., Boston, (1972).

[51] Griffiths, P. R., de Haseth, J.A., "Fourier Transform Infrared Spectroscopy", Wiley & Sons, Inc., New york, (1986).

[52] Coates, J., "Interpretation of infrared Spectra, a Practical Approach, in Encyclopedia of Analytical Chemistry", Mayers, R.A. (Ed.) John Wiley & Son's Ltd, pp. 10815-10837, (2000).

[53] Totolin, M., Neamţu, I., Filip, D., Stoica, I., Macocinschi, D., "An investigation of plasma polymer thin films deposition by low-pressure non-equilibrium plasma" Optoelectron. Adv. Mater., Vol. 2(5), pp. 309 – 314, (2008).

[54] Afroze, T., Bhuiyan, A.H., " Infrared and ultraviolet-visible spectroscopic studies of plasma polymerized 1,1,3,3-tetramethoxypropane thin films", Thin Solid Films , Vol. 519, pp. 1825-1830, (2011).

[55] Tauc J., "Amorphous and Liquid Semiconductors", J. Tauc (Ed) Plenum, London, (1974).

[56] Fox, M., "Optical Properties of Solids", Oxford Univ. Press, New York, (2001).

[57] Urbach, F., "The long-wavelength edge of photographic sensitivity and the electronic absorption of solid", Phys. Rev. Vol. 92, pp. 1324, (1953).

[58] Dow, J. D., Redfield, D., "Toward a unified theory of Urbach's rule and exponential edge", Phys. Rev. Vol. 5 , pp. 594 (1972).

[59] Simmons, J. G., "Conduction in thin dielectric films", J. Phys. D.: Appl. Phys., Vol. 4, pp. 613-657, (1971).

[60] Leon, I. M., Glang. R., "Handbook of Thin Films Technology", McGraw Hill Book Company, New York, (1970).

[61] John, R. K., Kumar, D. K., "Structural, electrical and optical studies of plasma polymerized and iodine doped polypyrrole", J. Appl. Polym. Sci., Vol. 83, pp. 1856-1859, (2002).

[62] Tolansky, S., "Multiple beam interferometry of surfaces and films", Clarendon Press, Oxford, (1948).

[63] Quan, Y.C., Yeo, S., Shim, C., Yang, J., Jung, D., " Significant improvement of electrical and thermal properties of low dielectric constant plasma polymerized paraxylene thin films by post decomposition of H_2+ He plasma treatment", J. Appl. Phys. Vol. 89, pp. 1402, (2001).

[64] Yang, J., Ju., Lee, S., Park, H., Jung, D., Chae H., " Characterization of low dielectric constant plasma polymer films deposited by plasma-enhanced chemical vapor deposition during decamethyl-cyclopentasiloxane and cyclohexane as the precursors", J. Vac. Sci. Technol. Vol. A 24, p. 165, (2006).

[65] Mott, N.F., Gurney, R.W., "Electronic Processes in Solids", Clarendon Press, Oxford, (1948).

[66] Anderson, L. J., Jacob, M. V., "Electrical characterization of plasma polymerized linalylacetate". Mater. Sci. Eng. B., Vol. 177, pp. 311-315, (2012).

[67] M.A. Lampert, P. Mark, "Current Injection in Solids, Academic Press, New York, (1970).